Gravitational Waves From the Kerr/CFT Correspondence

Gravitational waves from the Kerr/CFT correspondence

A dissertation presented
by

Achilleas Porfyriadis

to
The Department of Physics
in partial fulfillment of the requirements
for the degree of
Doctor of Philosophy
in the subject of

Physics

Harvard University
Cambridge, Massachusetts
May 2016

Thesis advisor

Andrew Strominger

Author

Achilleas Porfyriadis

Gravitational waves from the Kerr/CFT correspondence

Abstract

Astronomical observation suggests the existence of near-extreme Kerr black holes in the sky. Properties of diffeomorphisms imply that dynamics of the near-horizon region of near-extreme Kerr are governed by an infinite-dimensional conformal symmetry. This symmetry may be exploited to analytically, rather than numerically, compute a variety of potentially observable processes. In this thesis we compute the gravitational radiation emitted by a small compact object that orbits in the near-horizon region and plunges into the horizon of a large rapidly rotating black hole. We study the holographically dual processes in the context of the Kerr/CFT correspondence and find our conformal field theory (CFT) computations in perfect agreement with the gravity results.

We compute the radiation emitted by a particle on the innermost stable circular orbit (ISCO) of a rapidly spinning black hole. We confirm previous estimates of the overall scaling of the power radiated, but show that there are also small oscillations all the way to extremality. Furthermore, we reveal an intricate mode-by-mode structure in the flux to infinity, with only certain modes having the dominant scaling. The scaling of each mode is controlled by its conformal weight.

Massive objects in adiabatic quasi-circular inspiral towards a near-extreme Kerr black hole quickly plunge into the horizon after passing the ISCO. The post-ISCO plunge trajectory is shown to be related by a conformal map to a circular orbit.

Conformal symmetry of the near-horizon region is then used to compute analytically the gravitational radiation produced during the plunge phase.

Most extreme-mass-ratio-inspirals of small compact objects into supermassive black holes end with a fast plunge from an eccentric last stable orbit. We use conformal transformations to analytically solve for the radiation emitted from various fast plunges into extreme and near-extreme Kerr black holes.

Contents

Citations to Previously Published Work

Chapter 2 appeared in the following paper:

> [1] A. P. Porfyriadis and A. Strominger, "Gravity waves from the Kerr/CFT correspondence," Phys. Rev. D **90**, no. 4, 044038 (2014) `[arXiv:1401.3746 [hep-th]]`.

Chapter 3 appeared in the following paper:

> [2] S. E. Gralla, A. P. Porfyriadis and N. Warburton, "Particle on the Innermost Stable Circular Orbit of a Rapidly Spinning Black Hole," Phys. Rev. D **92**, no. 6, 064029 (2015) `[arXiv:1506.08496 [gr-qc]]`.

Chapter 4 appeared in the following paper:

> [3] S. Hadar, A. P. Porfyriadis and A. Strominger, "Gravity Waves from Extreme-Mass-Ratio Plunges into Kerr Black Holes," Phys. Rev. D **90**, no. 6, 064045 (2014) `[arXiv:1403.2797 [hep-th]]`.

Chapter 5 appeared in the following paper:

> [4] S. Hadar, A. P. Porfyriadis and A. Strominger, "Fast plunges into Kerr black holes," JHEP **1507**, 078 (2015) `[arXiv:1504.07650 [hep-th]]`.

Electronic preprints (shown in `typewriter font`) are available at the following address:

> `http://arXiv.org`

Acknowledgments

This thesis would not have been possible without the guidance and collaboration of Andy Storminger. An advisor who is inviting rather than intimidating and inclusive rather than exclusive, Andy has transformed the privilege and honor of working with him to one of the greatest pleasures of my life as a PhD student at Harvard.

It goes without saying that I am grateful to all my coauthors in publications that appear in this thesis and elsewhere, including Sam Gralla, Shahar Hadar, Temple He, Prahar Mitra, and Niels Warburton.

I would also like to thank Dan Jafferis, Avi Loeb, Chris Stubbs, Cumrun Vafa, and Xi Yin, for sharing their knowledge of physics and serving on various committees over the years. I remain forever indebted to Frank Wilczek for the crucial early endorsement and continuing support in my pursuit of theoretical physics.

I have benefited greatly from the lively and stimulating atmosphere of the High Energy Theory Group at Harvard and I extend my sincerest gratitude to all current and former members of the group with whom I have had the pleasure to interact and many of whom are also collaborators and friends.

Dedicated to my father Pavlos,
and my mother Maria.

Chapter 1

Introduction

The holographic principle represents a fundamental paradigm shift in modern theoretical physics. Holography introduced a new theoretical framework for addressing questions of strongly coupled states of matter on the one hand and gravitational physics on the other. While the first concrete realization of the holographic principle –the AdS/CFT correspondence– was discovered within string theory, in recent years holographic dualities have found significant applications that range from pure mathematics to condensed matter and nuclear physics to cosmology. The purpose of this thesis is to put holography on the astronomer's map too.

The Kerr/CFT correspondence is a much less understood cousin of AdS/CFT but it is one that pertains to *observed* regions in the sky. "Strong" Kerr/CFT is the conjecture that quantum gravity in the near-horizon region of a rapidly rotating Kerr black hole is equal to a warped two dimensional CFT. This conjecture is relevant for the study of quantum puzzles surrounding black holes. "Weak" Kerr/CFT is the *fact* that gravitational dynamics in the near-horizon region of a near-extreme Kerr

are constrained by an infinite-dimensional geometrical conformal symmetry. This fact follows from properties of diffeomorphisms in general relativity alone and so it suffices for addressing interesting questions in astrophysics. At the same time it enables powerful analytic techniques developed in the study of conformal field theories to be employed in the analysis of near-horizon gravitational dynamics.

One context in which to explore such ideas are the extreme mass ratio inspirals (EMRIs) of small compact objects, such as neutron stars or stellar mass black holes, into rotating supermassive black holes. EMRIs are primary sources of gravitational waves expected to be detected with the proposed evolved Laser Interferometer Space Antenna (eLISA). For a wide range of initial conditions, EMRIs consist of two stages: (i) a long adiabatic quasi-circular inspiral followed by (ii) a quick plunge into the black hole from the innermost stable circular orbit (ISCO; the edge of the accretion disk). For nearly extremal black holes, both near-ISCO circular orbits and the post-ISCO plunge take place deep in the near horizon region. Harnessing the power of the conformal symmetry present in this region, we compute in this thesis the exact spectrum of gravitational wave emission *analytically*.

In the remainder of this Chapter we review some necessary background on the geometry of the extreme Kerr throat and give a preview of the computations contained in the following chapters. In Chapter 2 we compute the gravitational radiation produced by a massive test object in a near-ISCO circular orbit of an extreme Kerr. Holographically, we see that the presence of the orbiting object in the bulk corresponds to a deformation of the dual CFT by a computable external driving source, and the gravitational radiation then follows from the application of Fermi's golden

rule to the deformed CFT. On the other hand, the action of the infinite-dimensional conformal group can relate extremal to near-extremal physics. Accordingly, in Chapter 3 we show that, to leading order in the deviation from extremality, the radiation emitted by a particle on the ISCO of a rapidly spinning Kerr may be obtained by a natural identification of parameters in the formulae previously derived in Chapter 2 for near-ISCO orbits in exactly extreme Kerr. This reveals an intricate mode-by-mode structure in the flux to infinity, with only certain modes (characterized by the conformal weight of the dual CFT operator) having the dominant scaling as we approach extremality. Our analysis also determines that the power radiated does not have a limit as there are small oscillations all the way to extremality. In Chapter 4 we find a conformal transformation that maps the near-ISCO circular orbit in extreme Kerr to the post-ISCO plunge in near-extreme Kerr. The holographic dual of the plunge problem has a richer dynamical evolution involving a quantum quench of the CFT that injects energy into the system which is subsequently thermalized and equilibrated. On the gravity side, the approach to equilibrium is marked by the explicit quasinormal mode ringing of our solution at late times. In Chapter 5 we use further conformal transformations that map the near-ISCO circular orbit in extreme Kerr to various fast plunges that spiral off an eccentric last stable orbit in extreme or near-extreme Kerr.

1.1 Extreme Kerr throat, NHEK, and near-NHEK

The metric of the Kerr black hole in Boyer-Lindquist coordinates is given by ($G = \hbar = c = 1$):

$$ds^2 = -\frac{\Delta}{\hat{\rho}^2}\left(d\hat{t} - a\sin^2\theta d\hat{\phi}\right)^2 + \frac{\sin^2\theta}{\hat{\rho}^2}\left((\hat{r}^2+a^2)d\hat{\phi} - ad\hat{t}\right)^2 + \frac{\hat{\rho}^2}{\Delta}d\hat{r}^2 + \hat{\rho}^2 d\theta^2\,,$$

$$\Delta = \hat{r}^2 - 2M\hat{r} + a^2\,, \quad \hat{\rho}^2 = \hat{r}^2 + a^2\cos^2\theta\,.$$

It is labeled by two parameters: the mass M and the angular momentum $J = aM$. The horizons are located at $r_\pm = M \pm \sqrt{M^2 - a^2}$. The Kerr/CFT correspondence pertains to Kerr black holes that are near extremality which is characterized by

$$J = M^2\,, \quad a = M\,.$$

In this case there is a very long throat to the horizon and one may derive two interesting decoupling metrics which we call NHEK and near-NHEK respectively:

$$ds^2 = 2M^2\Gamma(\theta)\left[-R^2dT^2 + \frac{dR^2}{R^2} + d\theta^2 + \Lambda(\theta)^2(d\Phi + RdT)^2\right]\,,$$

$$ds^2 = 2M^2\Gamma(\theta)\left[-r(r+2\kappa)dt^2 + \frac{dr^2}{r(r+2\kappa)} + d\theta^2 + \Lambda(\theta)^2(d\phi + (r+\kappa)dt)^2\right]\,,$$

where $\Gamma(\theta) = (1+\cos^2\theta)/2\,, \Lambda(\theta) = 2\sin\theta/(1+\cos^2\theta)$. These have an enhanced isometry group: $SL(2,\mathbb{R})_R \times U(1)_L$ (∂_t is in $SL(2,\mathbb{R})_R$ and ∂_ϕ is the $U(1)_L$). Moreover, the asymptotic symmetry group contains an entire Virasoro with a central charge that reproduces the Bekenstein-Hawking entropy of extreme Kerr.

There are two complementary ways to think about NHEK and near-NHEK. In this thesis we use both and exploit this complementarity to the maximum. The first way is to consider NHEK and near-NHEK as the corresponding patches in the global

extension of these spacetimes as shown in Fig 1.1. The advantage of this way of thinking is that we can then put overlapping NHEK and near-NHEK patches on the same diagram and find coordinate transformations that will map between them in overlapping regions. The second way is to consider NHEK and near-NHEK in relation

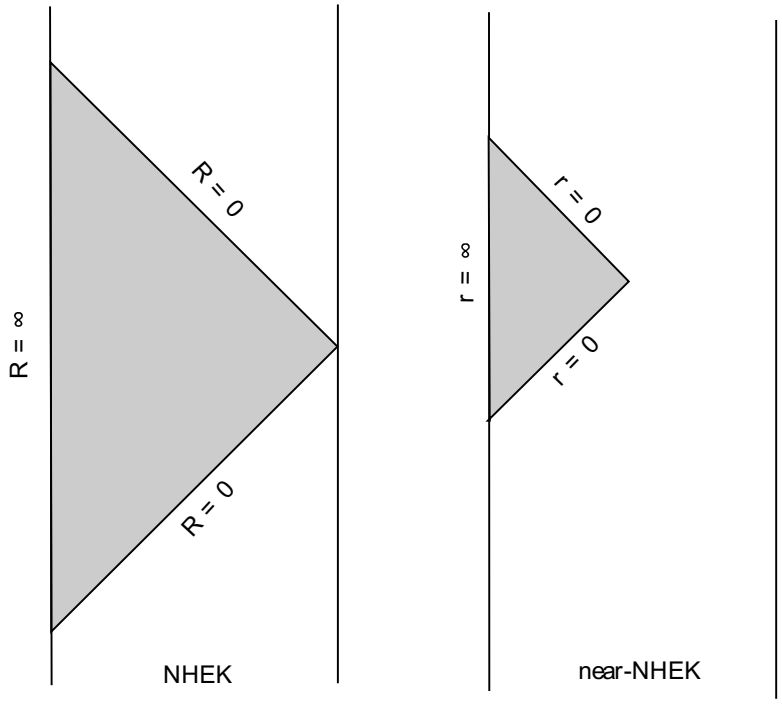

Figure 1.1: Penrose diagrams of the throat geometry. The large shaded wedge on the left diagram (bounded by $R = 0$ and $R = \infty$) is NHEK. The small shaded wedge on the right diagram (bounded by $r = 0$ and $r = \infty$) is near-NHEK.

to the full asymptotically flat Kerr geometry. Then they are approximate metrics in the appropriate regions of the throat that leads to the Kerr horizon as shown in Fig 1.2. The advantage of this way of thinking is that we can then use the method of matched asymptotic expansions to extend NHEK or near-NHEK solutions outside the throat all the way to asymptotically flat infinity.

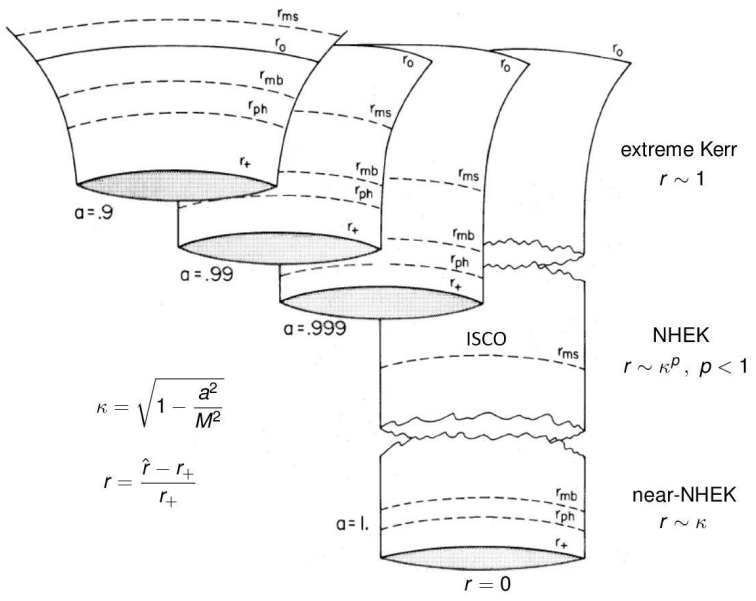

Figure 1.2: Embedding diagram of the throat as the black hole approaches extremality. Here κ measures deviation from extremality and r is a dimensionless radial coordinate that measures distance to the horizon. The very near horizon region where r is of the same order as κ is near-NHEK. The near horizon region where r is small but much larger than κ is NHEK.

1.2 The dual analyses

For each computation in this thesis we perform dual analyses from the gravity and CFT points of view and observe perfect agreement between the two. On the gravity side we solve the linearized Einstein equation with a source due to the orbiting or plunging star. From the gravity solution then we may compute for example the particle number flux flowing down the horizon of the black hole,

$$\mathcal{F}^{gravity} = \frac{dN}{dt} \,.$$

On the CFT side we identify the deformation of the action by the classical source that corresponds to the star and compute the induced transition rate out of the initial state,

$$\mathcal{R}^{CFT} = \frac{dP}{dt} \,.$$

When we compare these two quantities, using the dictionary of the Kerr/CFT correspondence, we observe that in all cases:

$$\mathcal{F}^{gravity} = \mathcal{R}^{CFT} \,.$$

Consider for example a geodesic point source on a circular equatorial orbit,

$$\begin{aligned} R(T) &= R_0 \,, \\ \Phi(T) &= -\frac{3}{4} R_0 \, T + \Phi_0 \,, \end{aligned}$$

in the NHEK geometry. If this source couples to a scalar field Ψ it will source the field according to the wave equation

$$\Box \, \Psi = g \, R_0 \delta(R - R_0) \delta(\theta - \pi/2) \delta(\Phi + \frac{3}{4} R_0 T) \,,$$

where g is the coupling constant. In the case of gravitational waves, studied in detail in Chapter 2, the linearized Einstein equation takes a similar form for the appropriate Teukolsky scalar. Using spheroidal harmonics and expanding the field according to

$$\Psi = \sum_{\ell,m} e^{im(\Phi+\frac{3}{4}R_0 T)} S_\ell(\theta) R_{\ell m}(R)\,,$$

the wave equation reduces to the following radial equation

$$\partial_R(R^2\partial_R R_{\ell m}) + \left(2m^2 - K_\ell + \frac{2\Omega m}{R} + \frac{\Omega^2}{R^2}\right) R_{\ell m} = \frac{M^2}{2\pi} g\, S_\ell(\pi/2)\, R_0 \delta(R-R_0)\,,$$

where $\Omega = -3mR_0/4$ and K_ℓ are separation constants. Being the radial equation associated with NHEK, rather than the entire Kerr, we can solve this equation analytically. The homogeneous solutions are given by confluent hypergeometric functions, such as the Whittaker functions $W_{im,h-1/2}(-2i\Omega/R)$ and $M_{im,h-1/2}(-2i\Omega/R)$, where

$$h \equiv \frac{1}{2} + \sqrt{\frac{1}{4} + K_\ell - 2m^2}\,.$$

Then, with ingoing boundary conditions at the horizon ($\sim R^{-im}e^{i\Omega/R}$) and Neumann at the boundary of NHEK ($\sim R^{-h}$), we find that, for real h, to leading order, the Klein-Gordon particle number flux down the horizon is given by ($m>0$):

$$\begin{aligned}\mathcal{F}^{gravity}_{\ell m} &= -\int \sqrt{-g}\, J^R_{KG}\, d\theta d\Phi \\ &= \frac{g^2 M^6}{12\pi^2} S_\ell(\pi/2)\, R_0\, m^{-1} e^{-\pi m} \frac{|\Gamma(h+im)|^2}{|\Gamma(2h)|^2} \left|M_{im,h-1/2}(3im/2)\right|^2\,.\end{aligned}$$

Holographically, the dual situation is a CFT which is driven at frequency Ω by an external classical source J that couples to an operator $\mathcal{O}$ dual to the scalar field Ψ:[1]

$$S = S_{CFT} + \sum_\ell \int d\Phi dT\, J_\ell(\Phi,T)\mathcal{O}_\ell(\Phi,T)\,,$$

[1]More precisely, with $\mathcal{O}_\ell(\Phi,T) = \sum_m \mathcal{O}_{\ell m}(T)e^{-im\Phi}$ the operators $\mathcal{O}_{\ell m}$ are the duals to the modes of the scalar field Ψ with separatation constant K_ℓ and angular momentum m.

with

$$J_\ell(\Phi,T)=\sum_m J_{\ell m}e^{im\left(\Phi+\frac{3}{4}R_0T\right)}\,.$$

According to the Kerr/CFT dictionary the operator $\mathcal{O}$ has conformal weight h. In a situation like the one we are considering here, where there is a classical source in the bulk of the spacetime, special care is required identifying the boundary sources $J_{\ell m}$. The solution for the scalar field with ingoing boundary conditions at the horizon and Neumann at the boundary takes the form

$$R_{\ell m}=X\Theta(R_0-R)R^{in}(R)+Z\Theta(R-R_0)R^{out}(R)\,,$$

where $R^{in}=W_{im,h-1/2}(-2i\Omega/R)\,,R^{out}=M_{im,h-1/2}(-2i\Omega/R)$ and the constants are $X\propto M_{im,h-1/2}(-2i\Omega/R_0)\,,Z\propto W_{im,h-1/2}(-2i\Omega/R_0)$. The boundary sources $J_{\ell m}$ are then read off from the Dirichlet modes of the *extension of the inner part* of the bulk solution all the way to the boundary:

$$R^{ext}_{\ell m}\equiv X\,R^{in}(R)\to J_{\ell m}\,R^{h-1}\,+\,\ldots\qquad R\to\infty\,.$$

Applying Fermi's Golden Rule, the transition rate out of the initial state $|i\rangle$ to any final state $|f\rangle$ is given by the Fourier transform of the two-point function of $\mathcal{O}$. Up to normalization of the operators, two-point functions are completely fixed by $SL(2,R)$ symmetry and so we have ($m>0$):

$$\begin{aligned}\mathcal{R}^{CFT}_{\ell m}&=2\pi|J_{\ell m}|^2\int d\Phi dT\,e^{-im\left(\Phi+\frac{3}{4}R_0T\right)}\langle\mathcal{O}^\dagger(\Phi,T)\mathcal{O}(0,0)\rangle\\&=\mathcal{C}^2_{\mathcal{O}}\frac{(2\pi)^2(3R_0/4)^{2h-1}}{\Gamma(2h)^2}|J_{\ell m}|^2m^{2h-1}e^{-\pi m}|\Gamma(h+im)|^2\,.\end{aligned}$$

Plugging in $J_{\ell m}$ and normalizing the operators with $\mathcal{C}_{\mathcal{O}}=2^{2h-1}(2h-1)M/2\pi$ we find:

$$\mathcal{R}^{CFT}_{\ell m}=\frac{g^2M^6}{12\pi^2}S_\ell(\pi/2)\,R_0\,m^{-1}e^{-\pi m}\frac{|\Gamma(h+im)|^2}{|\Gamma(2h)|^2}\left|M_{im,h-1/2}(3im/2)\right|^2=\mathcal{F}^{gravity}_{\ell m}\,.$$

1.3 Gluing back the asymptotically flat region

For each computation in this thesis we also obtain the signal observed far from the black hole. This means that near horizon solutions are extended all the way to asymptotically flat null infinity. For example, for the flux due to a star orbiting on a circular equatorial geodesic orbit in NHEK, we glue back the portion of the exterior of the extreme Kerr black hole that lies outside NHEK and extend the solution all the way to future null infinity $\mathcal{I}^+$, as shown in Fig 1.3. This is done using the method

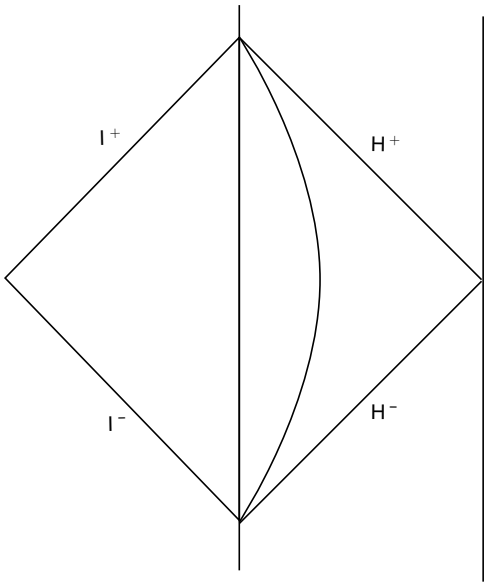

Figure 1.3: Penrose diagram showing NHEK with a star orbiting at constant radius in it. The asymptotically flat portion of the exterior of the extreme Kerr diamond that contains null infinity is attached. Radiation generated by the orbiting star will leak through the NHEK boundary to reach future null infinity $\mathcal{I}^+$.

of matched asymptotic expansions, which may be summarized as follows. Imagine we are given a differential equation with independent variable x and a suitable small

parameter $k \ll 1$ such that we know the exact solution to the 'near equation' obtained for $x \ll 1$ as well as the 'far equation' obtained for $x \gg k$. Then we can get an approximate solution to the differential equation for all x by matching asymptotic series of the two exact solutions in the overlap region $k \ll x \ll 1$.

Consider the wave equation in the entire extreme Kerr with a source orbiting on a circular geodesic lying near the horizon in the NHEK region. As shown in Chapter 2, in this case the small parameter is

$$k = 4M(\hat{\omega} - \frac{m}{2M}) = -\frac{3}{2}mR_0\,,$$

the 'near solution' is the NHEK solution, and for matching to the 'far solution' the frequency with respect to the asymptotic time needs to be very near the superradiant bound frequency $\hat{\omega} \approx m/(2M)$. In other words, the observed signal from processes in the NHEK region lies in a narrow frequency range around the superradiant bound frequency. Note also that matching to the 'far solution' with the boundary condition of purely outgoing radiation at null infinity implies that the full solution obeys "leaky boundary conditions" at the NHEK boundary. From the full solution everywhere we may calculate explicitly desired observables, such as the outgoing radiation flux at future null infinity:

$$\begin{aligned}\dot{\mathcal{E}}_\infty \;=\; & \frac{g^2M^4}{72\pi^2}S_\ell^2(\pi/2)\left|W_{im,h-\frac{1}{2}}(3im/2)\right|^2(3m^2R_0/2)^{2\mathrm{Re}[h]}m^{-2}e^{\pi|m|}\times \\ & \times\frac{|2h-1|^2|\Gamma(h-im)|^4/|\Gamma(2h)|^4}{\left|1-(3m^2R_0/2)^{2h-1}\frac{\Gamma(1-2h)^2}{\Gamma(2h-1)^2}\frac{\Gamma(h-im)^2}{\Gamma(1-h-im)^2}\right|^2}\,.\end{aligned}$$

1.4 The conformal group in action

Consider first the problem of radiation due to a small compact object on the ISCO of a near-extremal supermassive black hole. The location of the ISCO is given by

$$\frac{\hat{r} - r_+}{r_+} = 2^{1/3}\kappa^{2/3} + \mathcal{O}(\kappa)\,,$$

where $\kappa = \sqrt{1 - a^2/M^2}$. As shown in Chapter 3, to leading order in κ, the solution for this problem may be obtained simply by plugging in

$$R_0 = 2^{1/3}\kappa^{2/3}\,,$$

into the extremal formulae! Then the expression above for the radiation flux at future null infinity $\dot{\mathcal{E}}_\infty$ reveals a characteristic spectrum. We see for example that there is an intricate mode-by-mode structure in the flux to infinity which scales as $\kappa^{\frac{4}{3}\mathrm{Re}[h]}$ with only the modes corresponding to complex h having the dominant $\kappa^{2/3}$ scaling. Moreover, for the dominant modes we see that as $\kappa \to 0$ the flux $\dot{\mathcal{E}}_\infty$ displays small oscillations all the way to extremality, which means this particular observable does not have a good limit in the extremal case.

Conformal transformations may also be used to obtain solutions to plunge problems with minimal effort. Consider for example the slow equatorial plunge that spirals off ISCO

$$\begin{aligned} t(r) &= \frac{1}{2\kappa}\ln\frac{1}{r(r+2\kappa)} + t_0\,, \\ \phi(r) &= \frac{3r}{4\kappa} + \frac{1}{2}\ln\frac{r}{r+2\kappa} + \phi_0\,, \end{aligned}$$

and falls into the future horizon of the black hole in the near-NHEK metric. Direct analytical integration of the wave equation with this source is a formidable task.

However, the solution to this problem may be obtained very easily by mapping it to the circular geodesic in NHEK using the following bulk diffeomorphism on the gravity side:

$$\begin{aligned} T &= -e^{-\kappa t}\frac{r+\kappa}{\sqrt{r(r+2\kappa)}}\,, \\ R &= \frac{1}{\kappa}e^{\kappa t}\sqrt{r(r+2\kappa)}\,, \\ \Phi &= \phi - \frac{1}{2}\ln\frac{r}{r+2\kappa}\,, \end{aligned}$$

or, equivalently, the following boundary conformal transformation on the CFT side:

$$\begin{aligned} T &= -e^{-\kappa t}\,, \\ \Phi &= \phi\,. \end{aligned}$$

The computations are carried out in detail in Chapter 4 and Fig 4.1 illustrates how one is to obtain the above transformations. Similar transformations are employed in Chapter 5 to obtain the solutions for fast plunges that spiral off an eccentric last stable orbit (rather than the ISCO). The solutions to the plunges are very rich both on the gravity side, where they display characteristic quasimormal mode ringing, as well as on the CFT side, where they correspond to a quantum quench followed by thermalization.

Chapter 2

Gravity Waves from Kerr/CFT

2.1 Introduction

Astronomical observation suggests the existence of near-extreme Kerr black holes whose horizons spin at nearly the speed of light. Examples include the nearby stellar mass black holes GRS 1915+105 [5] and Cygnus X-1 [6], and the supermassive black hole at the center of the Seyfert-1.2 galaxy MCG-6-30-15 [7]. Indeed, measurements of black hole spin with X-ray reflection spectroscopy data from XMM-Newton and Suzaku suggest that a large fraction of supermassive black holes in active galactic nuclei are rapidly spinning [8, 9]. General relativity implies [10, 11] that the dynamics of the high-redshift near-horizon region of extreme Kerr, which includes the innermost-stable-circular-orbit (ISCO), is governed by an infinite-dimensional emergent conformal symmetry. Symmetries of physical systems in general may both usefully characterize and have striking consequences for observational data.

Precision black hole spectroscopy has advanced to the stage where we are be-

ginning to observe - with a variety of ingenious methods - the regions of spacetime governed by this conformal symmetry. A primary purpose of this thesis is to embark on an exploration of potential phenomenological consequences of the symmetry. In particular, we will study the gravitational radiation produced by a massive test object orbiting very near the horizon of an extreme Kerr black hole. The near-horizon approximation is valid, and the conformal symmetry relevant, for example for a compact stellar mass object orbiting within 10^{-2} au of the supermassive black hole in MCG-6-30-15. The resulting radiation is potentially observable at eLISA [12, 13, 14]. Such extreme-mass-ratio-inspirals (EMRIs) have been extensively studied with a variety of methods; see e.g. [15, 16, 17, 18, 19, 20, 21, 22] for recent progress and [23, 24, 25] for recent reviews. Previous computations of the gravitational waveform typically employ either the post-Newtonian expansion or numerical methods, both of which face important challenges in the interesting case of extreme Kerr. Here, we exploit the conformal symmetry and develop a complementary analytic approach. One hopes that the greatly enhanced symmetry will enable an analytic treatment of a variety of astrophysical phenomena in the near-horizon region of extreme Kerr, such as self-force [26, 27] or transient resonances [28].

In this chapter we consider only the case of an extreme Kerr black hole. The near-extreme case is treated, to leading order in the deviation from extremality, in the following chapters. Massive objects orbiting a near-extreme Kerr black hole quickly plunge into the horizon after passing the ISCO. Computing the radiation production during the plunge phase appears much more difficult, but the plunge is still soluble because it is related by a conformal transformation to the circular orbits of this

chapter. In the plunge context the utility of the conformal symmetry comes into full play.

The emergence of conformal symmetry at large redshifts near an extreme Kerr horizon is mathematically similar to the more familiar emergence of conformal symmetry at low energies in condensed matter systems near a critical point. This leads to many striking observed phenomena: for example critical opalescence at the liquid-gas transition of carbon dioxide. In the astrophysical setting, it also resembles the emergence of conformal symmetry at large cosmological redshifts posited in the theory of inflation. This implies the observed scale invariance of the CMB spectrum. Although we do not propose a candidate smoking gun for the conformal symmetry of extreme Kerr herein, we hope that future investigations will produce one.

In a second motivation, the present work also bears on ongoing investigations in quantum gravity. The extreme Kerr horizon bears similarities to that of certain supersymmetric string theoretic black holes, for which it is known [29, 30, 31, 32] that, at low energies and large redshifts, the near horizon dynamics has a completely equivalent "dual" description as a two-dimensional conformal field theory (CFT). In this case the near-horizon geometry has an anti-deSitter (AdS) factor, and this equivalence is an early example of the AdS/CFT correspondence. The close resemblance of the stringy and Kerr horizons motivated the "Kerr/CFT conjecture" which posits that quantum gravity near the extreme Kerr horizon is also dual to a two-dimensional boundary CFT [11] (see [33, 34] for reviews). A secondary purpose of this thesis is to both test and illuminate the Kerr/CFT conjecture through explicit computation. We shall see that the presence of an orbiting star induces a computable deformation of

the CFT, and the gravitational radiation then follows from the application of Fermi's golden rule to the deformed CFT. The perfect and detailed agreement[1] between the bulk gravity and boundary CFT computations of the radiation rate found herein provide new evidence for the conjecture. Although mathematically far less understood than the AdS/CFT conjecture, the Kerr/CFT conjecture pertains to observable regions of our universe. The classical conformal symmetry on which it is based may, with future advances in both theory and observation, ultimately be directly observed.

This chapter is organized as follows. Section 2.2 contains a telegraphic review of the Kerr metric, the extreme and near-horizon limits, the decoupled Near-Horizon Extreme Kerr - or NHEK - geometry and Kerr/CFT. In section 2.3 we introduce, as a warmup, a scalar field coupled to the orbiting star. Scalar radiation is computed for both the decoupled NHEK and the full asymptotically flat case. The NHEK computation is shown to agree with the dual computation for the boundary CFT. In section 2.4 we adopt the Newman-Penrose formalism and compute gravitational radiation for both the asymptotically flat and the NHEK case. Agreement is again found with the application of Fermi's golden rule to a deformation of the boundary CFT.

2.2 Review of Kerr, NHEK and Kerr/CFT

This section contains a lightning review of Kerr, its NHEK limit, and the Kerr/CFT correspondence.

The metric of the Kerr black hole in Boyer-Lindquist coordinates is ($G = \hbar = c =$

[1]Perhaps even better than expected, see section 2.3.3 for discussion.

1):

$$ds^2 = -\frac{\Delta}{\hat{\rho}^2}\left(d\hat{t} - a\sin^2\theta d\hat{\phi}\right)^2 + \frac{\sin^2\theta}{\hat{\rho}^2}\left((\hat{r}^2+a^2)d\hat{\phi} - ad\hat{t}\right)^2 + \frac{\hat{\rho}^2}{\Delta}d\hat{r}^2 + \hat{\rho}^2 d\theta^2\,, \quad (2.1)$$

$$\Delta = \hat{r}^2 - 2M\hat{r} + a^2\,, \quad \hat{\rho}^2 = \hat{r}^2 + a^2\cos^2\theta\,.$$

It is labeled by two parameters: the mass M and angular momentum $J = aM$. We consider the extreme limit in which

$$J = M^2\,, \quad a = M\,. \quad (2.2)$$

The horizon is then at $\hat{r} = M$ and the proper spatial distance to it is infinite, which, as shown by Bardeen and Horowitz [10], allows us to zoom in on the near horizon region and treat it as its own spacetime. We may take the near horizon limit by defining

$$t = \frac{\hat{t}}{2M}\,, \quad r = \frac{\hat{r}-M}{M}\,, \quad \phi = \hat{\phi} - \frac{\hat{t}}{2M}\,, \quad (2.3)$$

and considering the small r limit. The resulting NHEK geometry is:

$$ds^2 = 2M^2\Gamma(\theta)\left(-r^2dt^2 + \frac{dr^2}{r^2} + d\theta^2 + \Lambda(\theta)^2(d\phi + rdt)^2\right)\,, \quad (2.4)$$

where

$$\Gamma(\theta) = \frac{1+\cos^2\theta}{2}\,, \quad \Lambda(\theta) = \frac{2\sin\theta}{1+\cos^2\theta}\,, \quad (2.5)$$

and $\phi \sim \phi + 2\pi\,, 0 \le \theta \le \pi$. The entrance to the throat, where the near horizon region glues onto the full asymptotically flat Kerr geometry, corresponds to the boundary of NHEK at $r = \infty$. NHEK has an enhanced isometry group,

$$U(1)_L \times SL(2,\mathbb{R})_R\,, \quad (2.6)$$

generated by the Killing vectors:

$$\begin{aligned} Q_0 &= -\partial_\phi \,, \\ H_{-1} &= \partial_t \,, \\ H_0 &= t\partial_t - r\partial_r \,, \\ H_1 &= \frac{1}{2r^2}\partial_t + \frac{t^2}{2}\partial_t - tr\partial_r - \frac{1}{r}\partial_\phi \,. \end{aligned} \tag{2.7}$$

Excitations of NHEK carry the associated charges. These isometries govern the dynamics of NHEK in the sense that all processes must lie in representations of $U(1)_L \times SL(2,\mathbb{R})_R$. However, it is often the case in general relativity [35, 36] that the diffeomorphisms which act nontrivially and govern the physical dynamics - known as the asymptotic symmetry group or ASG - are comprised of more than the isometries. In [11] it was shown, for a certain choice of boundary conditions enforcing $M^2 = J$, that the ASG contains a full Virasoro symmetry whose zero mode is the angular momentum $Q_0 = -\partial_\phi$. Non-extremal excitations with $M^2 - J > 0$ correspond to non-zero charges under $SL(2,\mathbb{R})_R$. Boundary conditions allowing for such excitations were introduced in [37, 38, 39] and found to lead to a second Virasoro in the ASG whose zero mode is the energy.

The appearance of Virasoro symmetries in the classically computed ASG, together with the analogy to $\mathrm{AdS}_3/\mathrm{CFT}_2$ [35, 29, 30, 31, 32] motivates the conjecture that bulk quantum gravity on the NHEK region of Kerr is dual to a two-dimensional boundary CFT.[2] Reviews can be found in [33, 34]. From the first law of black hole thermodynamics one concludes that the CFT must be at the left-moving temperature

[2]The CFT duals to NHEK are expected to be more exotic than their AdS_3 counterparts, possibly involving non-local or warped behavior and reflecting the superradiant instabilities [40, 41, 42, 43, 44, 45].

(conjugate to Q_0) $T_L = 1/2\pi$. Conformal symmetry can be used to derive a dictionary relating bulk gravity quantities to their CFT counterparts. The conjecture predicts that all processes in NHEK can be mapped to and computed as a process in the dual finite-temperature two-dimensional CFT. We shall verify herein that this is indeed the case for gravity wave production by an orbiting star. We wish to stress that the Kerr/CFT conjecture goes beyond the existence of classical conformal symmetries, whose consequences are the primary focus of this thesis.

2.3 Scalar radiation from a star orbiting near the horizon

In this section we consider a test particle - or "star" - in an eternal (relative to asymptotic time) circular orbit in the NHEK geometry. We couple it to a massless scalar field and compute and compare the resulting scalar radiation at the horizon from the bulk gravity and boundary CFT perspectives. We then attach the asymptotically flat region back and compute the radiation flux at future null infinity as well.

2.3.1 Gravity analysis in NHEK

Consider a star orbiting at radius r_0 in the NHEK geometry (A.8). We may parameterize the corresponding geodesic $x^\mu_*(t)$ with the NHEK time t:

$$\begin{aligned} x^t_*(t) &= t\,, \\ x^\phi_*(t) &= \phi_0 - \frac{3}{4} r_0\, t\,, \end{aligned}$$

$$\begin{aligned} x_*^r(t) &= r_0\,, \\ x_*^\theta(t) &= \frac{\pi}{2}\,. \end{aligned} \tag{2.8}$$

This has NHEK energy and angular momentum (per unit rest mass)

$$E = -g_{t\mu}\partial_\tau x_*^\mu = 0\,, \quad L = g_{\phi\mu}\partial_\tau x_*^\mu = \frac{2M}{\sqrt{3}}\,, \tag{2.9}$$

where τ is the proper time.

We couple the star to a massless scalar field Ψ with the interaction

$$S_I = 4\pi\lambda \int d\tau\, \Psi(x_*(\tau))\,, \tag{2.10}$$

where λ is a coupling constant. The scalar wave equation in the presence of the star is then:

$$\Box\, \Psi = 4\pi \mathcal{T}\,, \tag{2.11}$$

where (setting $\phi_0 = 0$)

$$\mathcal{T} = -\frac{\sqrt{3}\lambda r_0}{4M^3}\delta(r - r_0)\delta(\theta - \frac{\pi}{2})\delta(\phi + \frac{3}{4}r_0 t)\,. \tag{2.12}$$

The scalar source preserves one Killing symmetry:

$$\chi = \partial_t - \frac{3}{4}r_0\,\partial_\phi\,. \tag{2.13}$$

A χ-invariant solution to the wave equation may be constructed using the mode expansion

$$\Psi = \sum_{\ell,m} e^{im(\phi + 3r_0 t/4)} S_\ell(\theta) R_{\ell m}(r)\,, \tag{2.14}$$

$$\mathcal{T} = \frac{1}{8\pi M^2 \Gamma(\theta)} \sum_{\ell,m} e^{im(\phi + 3r_0 t/4)} S_\ell(\theta) T_{\ell m}(r)\,, \tag{2.15}$$

where S_ℓ are the spheroidal harmonics obeying

$$\frac{1}{\sin\theta}\partial_\theta(\sin\theta\,\partial_\theta S_\ell) + \left(K_\ell - \frac{m^2}{\sin^2\theta} - \frac{m^2}{4}\sin^2\theta\right) S_\ell = 0\,, \tag{2.16}$$

with K_ℓ a separation constant, $\ell \geq 0\,, -\ell \leq m \leq \ell$. S_ℓ and K_ℓ depend on both m and ℓ but we write only their primary label ℓ to avoid index clutter. The spheroidal harmonics are normalized as:

$$\int_0^\pi \sin\theta d\theta\, S_\ell(\theta) S_{\ell'}(\theta) = \delta_{\ell\ell'}\,. \tag{2.17}$$

The expansion coefficients for $\mathcal{T}$ are

$$\begin{aligned} T_{\ell m}(r) &= 4M^2 \int d\left(\phi + 3r_0 t/4\right)\, \sin\theta d\theta\, e^{-im(\phi+3r_0\, t/4)} S_\ell(\theta)\Gamma(\theta)\,\mathcal{T} \\ &= -\frac{\sqrt{3}\lambda r_0}{2M} S_\ell(\pi/2)\delta(r-r_0)\,. \end{aligned} \tag{2.18}$$

The separated radial equation becomes

$$\partial_r(r^2\partial_r R_{\ell m}) + \left(2m^2 - K_\ell + \frac{2\omega m}{r} + \frac{\omega^2}{r^2}\right) R_{\ell m} = T_{\ell m}\,, \tag{2.19}$$

where

$$\omega = -\frac{3}{4} m r_0\,. \tag{2.20}$$

The radial equation is a Sturm-Liouville problem that may be solved, for given boundary conditions, via standard Green function methods as follows. Two linearly independent solutions to the homogeneous radial equation ($T_{\ell m} = 0$) are given by the Whittaker (i.e. confluent hypergeometric) functions [46]:

$$M_{im,h-\frac{1}{2}}\left(-2i\omega/r\right)\,, \quad W_{im,h-\frac{1}{2}}\left(-2i\omega/r\right)\,, \tag{2.21}$$

where

$$h \equiv \frac{1}{2} + \sqrt{1/4 + K_\ell - 2m^2}\,. \tag{2.22}$$

In this chapter, we will only consider the case

$$\mathrm{Re}[h] < 1\,. \tag{2.23}$$

Then the Whittaker functions have the following asymptotic behaviors:

$$\begin{aligned} M_{im,h-\frac{1}{2}}\left(-2i\omega/r\right) &\rightarrow A\, r^{-im} e^{i\omega/r} + B\, r^{im} e^{-i\omega/r} && \text{for } r \to 0\,, \\ &\rightarrow (-2i\omega)^h\, r^{-h} && \text{for } r \to \infty\,, \end{aligned} \tag{2.24}$$

$$\begin{aligned} W_{im,h-\frac{1}{2}}\left(-2i\omega/r\right) &\rightarrow (-2i\omega)^{im}\, r^{-im} e^{i\omega/r} && \text{for } r \to 0\,, \\ &\rightarrow C\, r^{h-1} + D\, r^{-h} && \text{for } r \to \infty\,, \end{aligned} \tag{2.25}$$

where

$$A = (2i\omega)^{im} \frac{(-i\omega)^h}{(i\omega)^h} \frac{\Gamma(2h)}{\Gamma(h+im)}\,, \qquad B = (-2i\omega)^{-im} \frac{\Gamma(2h)}{\Gamma(h-im)}\,, \tag{2.26}$$

$$C = (-2i\omega)^{1-h} \frac{\Gamma(2h-1)}{\Gamma(h-im)}\,, \qquad D = (-2i\omega)^{h} \frac{\Gamma(1-2h)}{\Gamma(1-h-im)}\,. \tag{2.27}$$

Note that $W_{im,h-\frac{1}{2}}\left(-2i\omega/r\right)$ is purely ingoing at the horizon, but has both falloffs at infinity. $M_{im,h-\frac{1}{2}}\left(-2i\omega/r\right)$ on the other hand has both incoming and outgoing modes at the horizon but only one falloff, r^{-h}, at infinity, which we will refer to as the Neumann boundary condition.

To go further we must specify boundary conditions on the solution. We consider the solution of (2.19) that is purely ingoing at the horizon and obeys Neumann boundary conditions at $r = \infty$. This is given by:

$$R_{\ell m}(r) = \frac{1}{W}\left[X\,\Theta(r_0 - r) W_{im,h-\frac{1}{2}}\left(-2i\omega/r\right) + Z\,\Theta(r - r_0) M_{im,h-\frac{1}{2}}\left(-2i\omega/r\right)\right] \tag{2.28}$$

where W is the r-independent Wronskian,

$$W = r^2 \left[W_{im,h-\frac{1}{2}}\left(-2i\omega/r\right) \partial_r M_{im,h-\frac{1}{2}}\left(-2i\omega/r\right) - (W \leftrightarrow M) \right] = 2i\omega \frac{\Gamma(2h)}{\Gamma(h-im)} \,, \tag{2.29}$$

and

$$X = -\frac{\sqrt{3}\lambda r_0}{2M} S_\ell(\pi/2) M_{im,h-\frac{1}{2}}\left(3im/2\right) \,, \quad Z = -\frac{\sqrt{3}\lambda r_0}{2M} S_\ell(\pi/2) W_{im,h-\frac{1}{2}}\left(3im/2\right) \,. \tag{2.30}$$

Putting everything together we have:

$$\Psi(r \to 0) = \sum_{\ell,m} e^{im(\phi + 3r_0 t/4)} \, S_\ell(\theta) \, \frac{X}{W} (-2i\omega)^{im} \, r^{-im} e^{-3imr_0/4r} \,, \tag{2.31}$$

$$\Psi(r \to \infty) = \sum_{\ell,m} e^{im(\phi + 3r_0 t/4)} \, S_\ell(\theta) \, \frac{Z}{W} (-2i\omega)^{h} \, r^{-h} \,. \tag{2.32}$$

The Klein-Gordon particle number flux,

$$\mathcal{F} = -\int \sqrt{-g} J^r d\theta d\phi \,, \quad J^\mu = \frac{i}{8\pi} (\Psi^* \nabla^\mu \Psi - \Psi \nabla^\mu \Psi^*) \,, \quad \nabla_\mu J^\mu = \mathrm{Im}[\Psi \mathcal{T}] \,, \tag{2.33}$$

vanishes at infinity for real h, while at the horizon we have:

$$\mathcal{F}_{\ell m} = \frac{\lambda^2}{4} r_0 m^{-1} e^{-\pi m} S_\ell^2(\pi/2) \frac{|\Gamma(h+im)|^2}{|\Gamma(2h)|^2} \left| M_{im,h-\frac{1}{2}}\left(3im/2\right) \right|^2 \,, \tag{2.34}$$

for $m > 0$.

To summarize, the orbiting star emits scalar radiation. This radiation is reflected off of the NHEK boundary with Neumann boundary conditions, and falls into the black hole. The particle number flux across the future horizon is given by (2.34).

2.3.2 CFT analysis

Let us now consider the dual description of the scalar emission by an orbiting star as a process in the two-dimensional boundary CFT. Analogous types of dualities

have been analyzed in the context of AdS/CFT [47, 48, 49]. The effect of the star at fixed radius r_0 in NHEK may be compared to that of, e.g., adding a static D_3 brane in AdS_5 with flux N at fixed radius r_0 in Poincare coordinates while maintaining the asymptotic boundary conditions. In the AdS_5 case the resulting geometry is unaffected for $r > r_0$ but corresponds to flux $N-1$ for $r < r_0$. The radius r_0 is identified with a scale in the dual $N = 4$ $U(N)$ gauge theory. Processes above this scale, or outside the D-brane, are governed by $U(N)$ gauge theory, while those at low scales inside the D-brane are governed by $U(N-1)$ gauge theory.

In our example the orbiting star should lead to a deformed CFT at scales corresponding to $r < r_0$. To find that CFT, we extend the solution in the region $r < r_0$ all the way out to the boundary at $r = \infty$ ignoring the discontinuity produced by the star. This extended solution will contain both Neumann and Dirichlet modes at infinity. The CFT deformation is then read off of the coefficients of the Dirichlet modes.[3]

To be explicit, we write the action of the deformed CFT as

$$S = S_{CFT} + \sum_\ell \int dt^+ dt^- J_\ell(t^+, t^-) \mathcal{O}_\ell(t^+, t^-) \,. \tag{2.35}$$

Here S_{CFT} is the original CFT action and J_ℓ are to-be-determined c-number source functions, and $\mathcal{O}_\ell(t^+, t^-) \equiv \sum_m \mathcal{O}_{\ell m}(t^-) e^{-imt^+}$. The operators $\mathcal{O}_{\ell m}$ are the boundary duals to the mode of the bulk scalar with separation constant K_ℓ and angular momentum m. According to the Kerr/CFT dictionary (see e.g. [51]) these have left

[3] One may alternately, for $\mathrm{Re}[h] < 1$, define the deformation in terms of the Neumann modes: this would be dual to the gravity problem with Dirichlet boundary conditions [50].

and right conformal weight:

$$h_L = h_R = h\,. \tag{2.36}$$

In this subsection, we consider only real h. The bulk isometries ∂_ϕ and ∂_t are identified, up to a scale, with left and right translations in the 2D CFT, which implies

$$t^+ = \phi\,, \quad t^- = t\,. \tag{2.37}$$

It follows from the symmetry (2.13) that $J_\ell(t^+, t^-)$ can only depend on the combination $t^+ + 3r_0 t^-/4$. We accordingly Fourier expand:

$$J_\ell(t^+, t^-) = \sum_m J_{\ell m} e^{im(t^+ + 3r_0 t^-/4)}\,. \tag{2.38}$$

ϕ-periodicity implies that m is an integer. As discussed above, the coefficients $J_{\ell m}$ are then read off the extension $R^{ext}_{\ell m}$ of the small r behavior of the radial solution $R_{\ell m}$ in (4.23),

$$R^{ext}_{\ell m}(r) = \frac{X}{W} W_{im,h-\frac{1}{2}}\left(-2i\omega/r\right)\,, \tag{2.39}$$

to large r. Using the asymptotic behavior in (3.44) one finds:

$$R^{ext}_{\ell m}(r) \to \frac{X}{W}\left(C\, r^{h-1} + D\, r^{-h}\right) \qquad \text{for } r \to \infty\,. \tag{2.40}$$

It follows that

$$J_{\ell m} = \frac{X}{W}\, C\,, \tag{2.41}$$

and the perturbed action may be written as

$$S = S_{CFT} + \sum_{\ell,m} \int dt^+ dt^- J_{\ell m} e^{im(t^+ + 3r_0 t^-/4)} \mathcal{O}_\ell(t^+, t^-)\,. \tag{2.42}$$

This perturbation will induce transitions out of or 'decays' of the vacuum state. Fermi's golden rule then gives the transition rate [31, 52]:

$$\mathcal{R} = 2\pi \sum_{\ell,m} |J_{\ell m}|^2 \int dt^+ dt^- e^{-imt^+ - im3r_0 t^-/4} G(t^+, t^-)\,. \tag{2.43}$$

Here $G(t^+, t^-) = \langle \mathcal{O}^\dagger(t^+, t^-)\mathcal{O}(0,0)\rangle_{T_L}$ is the two point function of the dual two-dimensional conformal field theory, which has a finite left-moving temperature $T_L = 1/2\pi$ and angular potential. Such two point functions are fixed up to an overall normalization $C_{\mathcal{O}}^2$ by conformal invariance. Precisely these two point functions were studied in the context of superradiant scalar scattering in [51], to which we refer the reader for details. One finds, with the appropriate $i\epsilon$ prescription, the general formula:

$$\begin{aligned}&\int dt^+ dt^- e^{-i\omega_L t^+ - i\omega_R t^-} G(t^+, t^-) \\ &\qquad = C_{\mathcal{O}}^2 \frac{(2\pi T_L)^{2h_L-1}}{\Gamma(2h_L)} e^{-\omega_L/2T_L} \left|\Gamma\left(h_L + i\frac{\omega_L}{2\pi T_L}\right)\right|^2 \frac{2\pi}{\Gamma(2h_R)} \omega_R^{2h_R-1}\,. \end{aligned} \tag{2.44}$$

Substitution into (4.45) then gives:

$$\mathcal{R}_{\ell m} = C_{\mathcal{O}}^2 \, \frac{(2\pi)^2 (3r_0/4)^{2h-1}}{\Gamma(2h)^2} \, |J_{\ell m}|^2 \, m^{2h-1} e^{-\pi m} |\Gamma(h + im)|^2 \,, \tag{2.45}$$

for $m > 0$.

2.3.3 Comparison

The holographic dictionary predicts that the vacuum decay rate in the CFT equals the particle flux across the horizon. Indeed we see that for the normalization

$$C_{\mathcal{O}} = \frac{2^{h-1}(2h-1)}{2\pi} M\,, \tag{2.46}$$

we have exactly:

$$\mathcal{R}_{\ell m} = \frac{\lambda^2}{4} r_0 m^{-1} e^{-\pi m} S_\ell^2(\pi/2) \frac{|\Gamma(h+im)|^2}{\Gamma(2h)^2} \left| M_{im,h-\frac{1}{2}}(3im/2) \right|^2 = \mathcal{F}_{\ell m} \,. \tag{2.47}$$

Hence, up to the normalization (4.48), we find agreement between the gravity and CFT computations.

Recent investigations of Kerr/CFT suggest that the dual CFT may have some exotic features such as nonlocality [41, 42, 53] or a single Virasoro-Kac-Moody in place of two Virasoros [44, 54]. Given this one may wonder why the very detailed agreement found here, which rests on the standard CFT formulae for correlators and deformations, works so well. One possibility is simply that the standard CFT formulae are highly universal and remain valid for the exotic variations under consideration. We leave this to future investigations.

2.3.4 Reattaching the asymptotically flat region

In this subsection we reattach the asymptotically flat region, and compute the flux of scalar radiation at future null infinity generated by a star on the orbit (4.13) coupled to a scalar via the interaction (2.10). Expanding the scalar field in modes

$$\Psi_{\ell m\hat{\omega}} = e^{-i\hat{\omega}\hat{t}} e^{im\hat{\phi}} \hat{S}_\ell(\theta) \hat{R}_{\ell m\hat{\omega}}(\hat{r}) \,, \tag{2.48}$$

the wave equation in the full extreme Kerr separates into

$$\frac{d}{d\hat{r}}\left(\Delta \frac{d\hat{R}_{\ell m\hat{\omega}}}{d\hat{r}}\right) + \left(\frac{H^2}{\Delta} + 2Mm\hat{\omega} - \hat{K}_\ell\right) \hat{R}_{\ell m\hat{\omega}} = \hat{T}_{\ell m\hat{\omega}} \,, \tag{2.49}$$

$$\frac{1}{\sin\theta}\partial_\theta(\sin\theta\, \partial_\theta \hat{S}_\ell) + \left(\hat{K}_\ell - \frac{m^2}{\sin^2\theta} - M^2\hat{\omega}^2 \sin^2\theta\right) \hat{S}_\ell = 0 \,, \tag{2.50}$$

where $H = (\hat{r}^2 + M^2)\hat{\omega} - Mm$, and $\hat{T}_{\ell m\hat{\omega}}$ is the source term for the orbiting star.

In the coordinates (2.3) the radial equation (2.49) becomes

$$\partial_r(r^2\partial_r\hat{R}_{\ell m\hat{\omega}}) + V\hat{R}_{\ell m\hat{\omega}} = \hat{T}_{\ell m\hat{\omega}}\,, \tag{2.51}$$

with

$$V = \left(\frac{M\hat{\omega}r^2 + 2M\hat{\omega}r + k/2}{r}\right)^2 + 2Mm\hat{\omega} - \hat{K}_\ell\,, \qquad k = 4M(\hat{\omega} - \frac{m}{2M})\,. \tag{2.52}$$

The orbiting star sources the scalar deep in the NHEK region at small r. Generic modes do not penetrate into this region because the potential V diverges like $1/r$. However when the frequency is near the superradiant bound, i.e. when

$$k \equiv 2\omega = -\frac{3}{2}mr_0\,, \quad \text{with} \quad r_0 \ll 1\,, \tag{2.53}$$

the divergence is absent and the modes penetrate. We then have to leading order:

$$2M\hat{\omega} = m\,, \quad \hat{K}_\ell = K_\ell\,, \quad \hat{S}_\ell = S_\ell\,, \quad 2M\hat{\omega} - m = k/2\,. \tag{2.54}$$

In the near region $r \ll 1$ the modes (2.48) agree with the ones in (2.14) and equation (4.52) becomes the NHEK equation (2.19) whose solutions were studied in section 2.3.1. In the far region $r \gg k$ equation (4.52) becomes

$$\partial_r(r^2\partial_r\hat{R}_{\ell m\hat{\omega}}) + \left[\frac{m^2}{4}(r+2)^2 + m^2 - K_\ell\right]\hat{R}_{\ell m\hat{\omega}} = 0\,. \tag{2.55}$$

The solution of this with no incoming flux at past null infinity is

$$\hat{R}^{far}_{\ell m\hat{\omega}}(r) = P\,r^{h-1}e^{-imr/2}{}_1F_1\left(h + im\,, 2h\,, imr\right) + Q\left(h \to 1-h\right), \tag{2.56}$$

where

$$\frac{P}{Q} = -(-im)^{2h-1}\frac{\Gamma(2-2h)}{\Gamma(2h)}\frac{\Gamma(h-im)}{\Gamma(1-h-im)}\,. \tag{2.57}$$

The asymptotic behaviors are:

$$\hat{R}^{far}_{\ell m\hat{\omega}}(r\to\infty) = Q\,\frac{\Gamma(2-2h)}{\Gamma(1-h+im)}(im)^{h-1+im}\times \tag{2.58}$$
$$\times\left[1-\frac{(-im)^{2h-1}}{(im)^{2h-1}}\frac{\sin\pi(h+im)}{\sin\pi(h-im)}\right]r^{-1+im}e^{imr/2}\,,$$
$$\hat{R}^{far}_{\ell m\hat{\omega}}(r\to 0) = P\,r^{h-1}+Q\,r^{-h}\,. \tag{2.59}$$

The demand of no incoming flux from null infinity does not fix the overall magnitude of the solution. This is fixed by matching it with a solution of (2.19), which includes the near-region source, with no incoming flux at the past horizon. We use the method of matched asymptotic expansions as in [51, 55], matching the small r behavior of $\hat{R}^{far}_{\ell m\hat{\omega}}$ above with the large r behavior of a solution of (2.19) from section 2.3.1. This specifies the magnitude of the solution in terms of the source according to:

$$Q=\frac{Z}{W}(-2i\omega)^h\left[1-(3r_0/2)^{2h-1}|m|^{4h-2}\frac{\Gamma(1-2h)^2}{\Gamma(2h-1)^2}\frac{\Gamma(h-im)^2}{\Gamma(1-h-im)^2}\right]^{-1}\,. \tag{2.60}$$

Putting this all together we have finally the outgoing radiation flux at future null infinity:

$$\frac{d\hat{E}}{d\hat{t}} = \frac{\lambda^2}{24M^2}S^2_\ell(\pi/2)\left|W_{im,h-\frac{1}{2}}(3im/2)\right|^2(3r_0/2)^{2\mathrm{Re}[h]}m^{4\mathrm{Re}[h]-2}e^{\pi m}\times \tag{2.61}$$
$$\times\frac{|2h-1|^2|\Gamma(h-im)|^4/|\Gamma(2h)|^4}{\left|1-(3r_0/2)^{2h-1}m^{4h-2}\frac{\Gamma(1-2h)^2}{\Gamma(2h-1)^2}\frac{\Gamma(h-im)^2}{\Gamma(1-h-im)^2}\right|^2}\,,$$

for $m>0$.

Although we shall not attempt to do so here, the above result should also be obtainable from a yet-more-refined CFT analysis. Imposing Dirichlet or Neumann conditions for real h at the NHEK boundary ensures there is no energy flux through

the boundary and decouples the CFT from the far region. When the far region is attached, we of course want to allow flux to leak out of the NHEK region, but in a very specific way that gives only outgoing flux at null infinity. This requires "leaky" boundary conditions in which the fast and slow modes - or sources and vevs in the CFT - are related in amplitude by the ratio P/Q in equation (4.60). P and Q are determined by the physics of the far region and cannot be determined either by a bulk NHEK or boundary CFT calculation. An alternate approach to a CFT analysis would be to compute amplitudes directly rather than the probabilities given by their squares. The problem then becomes linear in the modes and the bulk result will just be a linear sum of CFT amplitudes with Dirichlet/Neumann boundary conditions weighted by P and Q.

2.4 Gravitational radiation from a star orbiting near the horizon

In this section we generalize the previous scalar analysis to the gravity case.

2.4.1 Gravity computation in NHEK

Gravity waves are most efficiently analyzed in the Newman-Penrose formalism [56] which involves the null tetrad $(l, n, m, \bar{m})$. Teukolsky showed [57, 58] that the perturbation of the Weyl scalar

$$\psi_4 = C_{\alpha\beta\gamma\delta} n^\alpha \bar{m}^\beta n^\gamma \bar{m}^\delta \,, \tag{2.62}$$

in any Type D background obeys:

$$[(\Delta+3\gamma-\bar{\gamma}+4\mu+\bar{\mu})(D+4\epsilon-\rho)-(\bar{\delta}-\bar{\tau}+\bar{\beta}+3\alpha+4\pi)(\delta-\tau+4\beta)-3\psi_2]\delta\psi_4 = 4\pi T_4\,, \tag{2.63}$$

where,

$$\begin{aligned} T_4 &= (\Delta+3\gamma-\bar{\gamma}+4\mu+\bar{\mu})[(\bar{\delta}-2\bar{\tau}+2\alpha)T_{n\bar{m}}-(\Delta+2\gamma-2\bar{\gamma}-\bar{\mu})T_{\bar{m}\bar{m}}] \\ &+ (\bar{\delta}-\bar{\tau}+\bar{\beta}+3\alpha+4\pi)[(\Delta+2\gamma+2\bar{\mu})T_{n\bar{m}}-(\bar{\delta}-\bar{\tau}+2\bar{\beta}+2\alpha)T_{nn}] \end{aligned} \tag{2.64}$$

Here $D = l^\mu\partial_\mu\,, \Delta = n^\mu\partial_\mu\,, \delta = m^\mu\partial_\mu\,, \bar{\delta} = \bar{m}^\mu\partial_\mu$ and $T_{n\bar{m}} = T_{\mu\nu}n^\mu\bar{m}^\nu$, etc. For NHEK we choose the Kinnersley tetrad ($l\cdot n = -m\cdot\bar{m} = -1$):

$$\begin{aligned} l^\mu &= \left(\frac{1}{r^2}, 1, 0, -\frac{1}{r}\right)\,, \\ n^\mu &= \frac{1}{2M^2(1+\cos^2\theta)}\left(1, -r^2, 0, -r\right)\,, \\ m^\mu &= \frac{1}{\sqrt{2}M(1+i\cos\theta)}\left(0, 0, 1, \frac{i(1+\cos^2\theta)}{2\sin\theta}\right)\,, \end{aligned} \tag{2.65}$$

so that the nonzero spin coefficients are:

$$\begin{gathered} \tau = -\frac{i\eta\bar{\eta}\sin\theta}{\sqrt{2}M}\,, \quad \pi = \frac{i\eta^2\sin\theta}{\sqrt{2}M}\,, \quad \beta = -\frac{\bar{\eta}\cot\theta}{2\sqrt{2}M}\,, \\ \alpha = \pi - \bar{\beta}\,, \quad \gamma = \frac{\eta\bar{\eta}r}{2M^2}\,, \end{gathered} \tag{2.66}$$

where,

$$\eta \equiv -\frac{1}{1-i\cos\theta}\,, \tag{2.67}$$

and the Weyl scalars are: $\psi_0 = \psi_1 = \psi_3 = \psi_4 = 0\,, \psi_2 = \eta^3/M^2$. The energy-momentum tensor for a point particle of rest mass m_0 on a geodesic $x^\alpha_*(\tau)$ is given by

$$T^{\mu\nu} = m_0\int d\tau(-g)^{-1/2}\frac{dx^\mu}{d\tau}\frac{dx^\nu}{d\tau}\delta^{(4)}(x^\alpha - x^\alpha_*(\tau))\,, \tag{2.68}$$

which for our simple geodesic (4.13) in NHEK has only one non-vanishing component (setting $\phi_0 = 0$):

$$T_{\phi\phi} = \frac{m_0 r_0}{\sqrt{3}M}\delta(r-r_0)\delta(\theta-\frac{\pi}{2})\delta(\phi+\frac{3}{4}r_0 t)\,. \tag{2.69}$$

Then from (2.64) we find:

$$\begin{aligned} T_4 \;=\; & \frac{m_0 r_0^3}{64\sqrt{3}M^7}\Big[144\,\delta(r-r_0)\delta(\theta-\tfrac{\pi}{2})\delta(\phi+\tfrac{3}{4}r_0 t) \\ & +16\,r_0\delta'(r-r_0)\delta(\theta-\tfrac{\pi}{2})\delta(\phi+\tfrac{3}{4}r_0 t) - 48i\,\delta(r-r_0)\delta'(\theta-\tfrac{\pi}{2})\delta(\phi+\tfrac{3}{4}r_0 t) \\ & -21\,\delta(r-r_0)\delta(\theta-\tfrac{\pi}{2})\delta'(\phi+\tfrac{3}{4}r_0 t) - 8i\,r_0\delta'(r-r_0)\delta'(\theta-\tfrac{\pi}{2})\delta(\phi+\tfrac{3}{4}r_0 t) \\ & -3\,r_0\delta'(r-r_0)\delta(\theta-\tfrac{\pi}{2})\delta'(\phi+\tfrac{3}{4}r_0 t) + 6i\,\delta(r-r_0)\delta'(\theta-\tfrac{\pi}{2})\delta'(\phi+\tfrac{3}{4}r_0 t) \\ & +2\,r_0^2\delta''(r-r_0)\delta(\theta-\tfrac{\pi}{2})\delta(\phi+\tfrac{3}{4}r_0 t) - 8\,\delta(r-r_0)\delta''(\theta-\tfrac{\pi}{2})\delta(\phi+\tfrac{3}{4}r_0 t) \\ & +\frac{9}{8}\,\delta(r-r_0)\delta(\theta-\tfrac{\pi}{2})\delta''(\phi+\tfrac{3}{4}r_0 t)\Big]\,. \end{aligned} \tag{2.70}$$

Equation (2.63) separates in NHEK for the variable:

$$\psi^{(-2)} \equiv \eta^{-4}\delta\psi_4\,. \tag{2.71}$$

As in the scalar case, we respect the symmetry (2.13) and construct a solution using the expansion

$$\psi^{(-2)} \;=\; \sum_{\ell,m} e^{im(\phi+3r_0 t/4)}S_\ell(\theta)R_{\ell m}(r)\,, \tag{2.72}$$

$$4\pi\mathcal{T} \;=\; \eta\bar{\eta}\sum_{\ell,m} e^{im(\phi+3r_0 t/4)}S_\ell(\theta)T_{\ell m}(r)\,, \tag{2.73}$$

where $\mathcal{T} \equiv 2M^2\eta^{-4}T_4$ and S_ℓ are now the spin-weighted spheroidal harmonics obeying

$$\frac{1}{\sin\theta}\partial_\theta(\sin\theta\,\partial_\theta S_\ell) + \left(K_\ell - \frac{m^2+s^2+2ms\cos\theta}{\sin^2\theta} - \frac{m^2}{4}\sin^2\theta - ms\cos\theta\right)S_\ell = 0\,, \tag{2.74}$$

with K_ℓ a separation constant, $\ell \geq |s|\,, -\ell \leq m \leq \ell$. In general, for gravity waves we have $s = \pm 2$ but in particular, since we have chosen to work with the Weyl scalar ψ_4, for us:

$$s = -2\,. \tag{2.75}$$

However, for convenience and because some (though not all) of the formulae that follow apply to more general spin we often leave s in the equations. As before, S_ℓ and K_ℓ depend on m and s as well but we write only their primary index ℓ to avoid clutter. We also assume the same normalization (2.17). The expansion coefficients for $\mathcal{T}$ are

$$T_{\ell m}(r) \;=\; a_0\delta(r-r_0) + a_1 r_0\delta'(r-r_0) + a_2 r_0^2\delta''(r-r_0)\,, \tag{2.76}$$

where

$$\begin{aligned} a_0 &= \frac{m_0 r_0^3}{16\sqrt{3}M^5}\left(40S + 3imS - \frac{9}{8}m^2 S + 6mS' - 16iS' - 8S''\right)\,, \\ a_1 &= \frac{m_0 r_0^3}{16\sqrt{3}M^5}\left(8iS' - 3imS - 16S\right)\,, \\ a_2 &= \frac{m_0 r_0^3}{16\sqrt{3}M^5} 2S\,, \end{aligned} \tag{2.77}$$

and S, S', S'' are $S_\ell(\pi/2), S'_\ell(\pi/2), S''_\ell(\pi/2)$ respectively. The separated radial equation becomes:

$$r^{-2s}\partial_r(r^{2s+2}\partial_r R_{\ell m}) + V_s R_{\ell m} = T_{\ell m}\,, \tag{2.78}$$

where ω is given in (2.20) and

$$V_s(r) = 2m^2 - K_\ell + s(s+1) + \frac{2\omega(m-is)}{r} + \frac{\omega^2}{r^2}\,. \tag{2.79}$$

This radial equation is again a Sturm-Liouville problem that is solved, for given

boundary conditions, via standard Green's function methods. Two linearly independent solutions to the homogeneous radial equation ($T_{\ell m} = 0$) are given by [46]:

$$\mathcal{M}(r) \equiv r^{-s}\, M_{im+s,h-\frac{1}{2}}\,(-2i\omega/r)\ , \quad \mathcal{W}(r) \equiv r^{-s}\, W_{im+s,h-\frac{1}{2}}\,(-2i\omega/r)\ , \tag{2.80}$$

where h is given by (2.22). These have simple behaviors at infinity and the horizon respectively:

$$\mathcal{M}(r) \ \to\ (-2i\omega)^h r^{-h-s} \qquad \text{for } r\to\infty\,, \tag{2.81}$$

$$\mathcal{W}(r) \ \to\ (-2i\omega)^{im+s} r^{-im-2s} e^{i\omega/r} \qquad \text{for } r\to 0\,. \tag{2.82}$$

The corresponding solution of the radial equation (2.78) is given by:

$$R_{\ell m}(r) = \frac{1}{r_0^{-2s} W}\left[\mathcal{X}\,\Theta(r_0-r)\mathcal{W}(r) + \mathcal{Z}\,\Theta(r-r_0)\mathcal{M}(r)\right] + a_2\delta(r-r_0)\,, \tag{2.83}$$

where W is the r-independent Wronskian of the two solutions (2.80),

$$W = 2i\omega\frac{\Gamma(2h)}{\Gamma(h-im-s)}\,, \tag{2.84}$$

and

$$\begin{aligned}\mathcal{X} &= r_0\mathcal{M}'(r_0)(2sa_2 - a_1 - 2a_2) + \mathcal{M}(r_0)(a_0 - 2sa_1 - 2sa_2 + 4s^2a_2 - a_2V_s(r_0))\,,\\ \mathcal{Z} &= \mathcal{X}(\mathcal{M}\to\mathcal{W})\,.\end{aligned} \tag{2.85}$$

Putting everything together we have:

$$\psi^{(-2)}(r\to 0) = \sum_{\ell,m} e^{im(\phi+3r_0t/4)}\, S_\ell(\theta)\,\frac{\mathcal{X}}{r_0^4 W}(-2i\omega)^{im-2}\, r^{-im+4} e^{-3imr_0/4r} \tag{2.86}$$

$$\psi^{(-2)}(r\to\infty) = \sum_{\ell,m} e^{im(\phi+3r_0t/4)}\, S_\ell(\theta)\,\frac{\mathcal{Z}}{r_0^4 W}(-2i\omega)^{h}\, r^{-h+2}\,. \tag{2.87}$$

The graviton number flux at the horizon is given by:

$$\begin{aligned} \mathcal{F}_{\ell m} &= \frac{12M^{10}r_0}{|\mathcal{C}|^2} m e^{-\pi m} \left| \frac{\mathcal{X}}{r_0^4 W} \right|^2 , \\ |\mathcal{C}|^2 &\equiv \left((K_\ell - m^2)^2 + m^2\right)\left((K_\ell - m^2 - 2)^2 + 9m^2\right) , \end{aligned} \tag{2.88}$$

for $m > 0$.

2.4.2 Matching with CFT analysis

The matching of the bulk gravity wave analysis with the boundary CFT analysis proceeds as in the scalar case with two minor differences. Again, in this subsection we assume h is real.

The first difference arises because the perturbation $\delta\psi_4$ studied involves the second derivative of the metric, while the sources of the dual CFT are related to the falloff coefficients of the metric perturbation itself. The latter (in ingoing radiation gauge) is obtained from a Hertz potential Ψ_H as follows [59, 60, 61, 62]:

$$h_{\mu\nu} = \Theta_{\mu\nu}\Psi_H , \tag{2.89}$$

where

$$\begin{aligned} \Theta_{\mu\nu} &= -l_\mu l_\nu(\bar{\delta} + \alpha + 3\bar{\beta} - \bar{\tau})(\bar{\delta} + 4\bar{\beta} + 3\bar{\tau}) - \bar{m}_\mu \bar{m}_\nu (D - \bar{\rho})(D + 3\bar{\rho}) \\ &+ l_{(\mu}\bar{m}_{\nu)}\left[(D + \rho - \bar{\rho})(\bar{\delta} + 4\bar{\beta} + 3\bar{\tau}) + (\bar{\delta} + 3\bar{\beta} - \alpha - \pi - \bar{\tau})(D + 3\bar{\rho})\right] \end{aligned} \tag{2.90}$$

The Hertz potential itself solves the $s = -2$ vacuum Teukolsky equation and is given by:

$$\Psi_H = \frac{4}{\mathcal{C}} R^{(-2)}(r) S^{(+2)}(\theta) e^{-i\omega t + im\phi} , \tag{2.91}$$

where

$$R^{(-2)}(r) = \frac{\mathcal{X}}{r_0^{-2s}W}\mathcal{W}(r) \tag{2.92}$$
$$\to \frac{\mathcal{X}}{r_0^{-2s}W}\left[\frac{(-2i\omega)^{1-h}\Gamma(2h-1)}{\Gamma(h-im-s)}r^{h-1-s} + \frac{(-2i\omega)^{h}\Gamma(1-2h)}{\Gamma(1-h-im-s)}r^{-h-s}\right] \quad \text{for } r\to\infty\,.$$

Reading off the CFT source from the leading term of the Hertz potential at the boundary we get:

$$J_{\ell m} = \frac{4}{\mathcal{C}}\frac{\mathcal{X}}{r_0^{-2s}W}\frac{(-2i\omega)^{1-h}\Gamma(2h-1)}{\Gamma(h-im-s)}\,. \tag{2.93}$$

The second difference is that instead of $h_L = h_R = h$, the Kerr CFT dictionary [62] implies:

$$h_R = h\,, \quad h_L = h - s\,. \tag{2.94}$$

Normalizing the operators with

$$C_{\mathcal{O}} = \frac{2^{h-1}M^5}{2\pi}\frac{\sqrt{\Gamma(2h+4)\Gamma(2h)}}{\Gamma(2h-1)}\,, \tag{2.95}$$

we again find agreement between the bulk and boundary computations.

2.4.3 Reattaching the asymptotically flat region

In this subsection we compute the flux of gravitational radiation out to future null infinity sourced by a star in a near horizon orbit in extreme Kerr. As in the scalar case, the radiation is dominated by near-superradiant modes, because the effective potential prohibits other modes from penetrating to the source. Using the near-superradiant relations (2.54), in the near region $r \ll 1$ the full spin-two Teukolsky equation for $\hat{\psi}^{(-2)} \equiv (\hat{r} - iM\cos\theta)^4\delta\hat{\psi}_4$ reduces to the NHEK equation (2.78) and in

the far region $r \gg k$ it becomes

$$r^{-2s}\partial_r(r^{2s+2}\partial_r\hat{R}_{\ell m\hat{\omega}})+\left[\frac{m^2}{4}(r+2)^2+ismr+m^2+s(s+1)-K_\ell\right]\hat{R}_{\ell m\hat{\omega}}=0\,. \quad (2.96)$$

The solution of this that is purely outgoing at null infinity (i.e. behaves as $r^{-1+im-2s}e^{imr/2}$ for large r) is given by:

$$\hat{R}^{far}_{\ell m\hat{\omega}}(r)=P\,r^{h-1-s}e^{-imr/2}{}_1F_1\left(h+im-s\,,2h\,,imr\right)+Q\left(h\to 1-h\right), \quad (2.97)$$

with,

$$\frac{P}{Q}=-(-im)^{2h-1}\frac{\Gamma(2-2h)}{\Gamma(2h)}\frac{\Gamma(h-im+s)}{\Gamma(1-h-im+s)}\,. \quad (2.98)$$

Asymptotically:

$$\begin{aligned}\hat{R}^{far}_{\ell m\hat{\omega}}(r\to\infty) &= Q\,\frac{\Gamma(2-2h)}{\Gamma(1-h+im-s)}(im)^{h-1+im-s}\times \quad (2.99)\\ &\quad\times\left[1-\frac{(-im)^{2h-1}}{(im)^{2h-1}}\frac{\sin\pi(h+im)}{\sin\pi(h-im)}\right]r^{-1+im-2s}e^{imr/2}\,,\\ \hat{R}^{far}_{\ell m\hat{\omega}}(r\to 0) &= P\,r^{h-1-s}+Q\,r^{-h-s}\,. \quad (2.100)\end{aligned}$$

Q is again fixed by matching with a solution of (2.78) which is purely ingoing at the horizon. One thereby finds (note that $\hat{\psi}^{(-2)}=M^6\psi^{(-2)}$):

$$\begin{aligned}Q &= M^6\frac{\mathcal{Z}}{r_0^{-2s}W}(-2i\omega)^h\times \quad (2.101)\\ &\quad\times\left[1-(3r_0/2)^{2h-1}|m|^{4h-2}\frac{\Gamma(1-2h)^2}{\Gamma(2h-1)^2}\frac{\Gamma(h-im-s)\Gamma(h-im+s)}{\Gamma(1-h-im-s)\Gamma(1-h-im+s)}\right]^{-1}.\end{aligned}$$

Finally this implies the outgoing energy flux at future null infinity, for $m>0$, is:

$$\begin{aligned}\frac{d\hat{E}}{d\hat{t}} &= \frac{m_0^2}{2^5 3^3 M^2}|\gamma_{\ell m}|^2(3r_0/2)^{2\mathrm{Re}[h]}m^{4\mathrm{Re}[h]-2}e^{\pi m}\times\\ &\quad\times\frac{|2h-1|^2|\Gamma(h+2-im)|^2|\Gamma(h-2-im)|^2/|\Gamma(2h)|^4}{\left|1-(3r_0/2)^{2h-1}m^{4h-2}\frac{\Gamma(1-2h)^2}{\Gamma(2h-1)^2}\frac{\Gamma(h-im-s)\Gamma(h-im+s)}{\Gamma(1-h-im-s)\Gamma(1-h-im+s)}\right|^2}\,, \quad (2.102)\end{aligned}$$

where

$$\begin{aligned}\gamma_{\ell m} &= 2\left[(h^2-h+6-im)S+4(2i+m)S'-4S''\right]W_{im-2,h-\frac{1}{2}}(3im/2)\\ &\quad+\left[(4+3im)S-8iS'\right]W_{im-1,h-\frac{1}{2}}(3im/2)\,.\end{aligned}\tag{2.103}$$

For example, it is expected [63] that an important contribution comes from the $\ell = m = 2$ mode. For this mode the eigenvalue K_ℓ has been computed numerically to good accuracy in [64] and corresponds to $h = 0.5+2.05i$. The eigenfunction $S_\ell(\theta)$ can then be computed numerically to good accuracy as well using Leaver's series solution as described in [65, 66]. We find:

$$\frac{d\hat{E}}{d\hat{t}} = 0.10\,\frac{m_0^2}{M^2}r_0\,.\tag{2.104}$$

Chapter 3

Particle on the ISCO of near-extreme Kerr black holes

3.1 Introduction

Unlike its simple Newtonian counter-part, the general relativistic two-body problem is a sprawling collection of different regimes, each with its own special techniques, where it becomes possible to precisely define and solve the problem. In recent years this two-body landscape has been explored in impressive detail, driven primarily by the need for accurate theoretical models of gravitational-wave sources. Well-separated masses are treated with high-order post-Newtonian expansions, large mass-ratio cases are treated with point particle perturbation theory, and close orbits of comparable mass systems are handled with numerical simulations. Non-trivial checks in overlapping domains of validity [67] give confidence that these diverse efforts are converging towards what could be called a complete solution of the relativistic two-body problem.

One corner just beginning to be filled in [1, 3, 4] is that of a particle orbiting in the near-horizon region of a near-extreme Kerr black hole. From a theoretical perspective, this is one of the most interesting regimes since it enjoys an enhanced isometry group as well as an infinite-dimensional asymptotic symmetry group [10, 11]. For practical purposes, calculations at extremes of parameter space can provide useful calibration points for approximation schemes, such as the effective one-body formalism [68], aiming to be uniform over parameter space. Finally, thought experiments showing naive violation of the cosmic censorship conjecture by throwing particles into a near-extreme black hole [69, 70] provide additional motivation to study near-horizon, near-extreme orbits.

In this article we compute the radiation from a particle on the innermost stable circular orbit (ISCO) of a rapidly spinning Kerr black hole. This radiation plays an important role in the transition from inspiral to plunge [71, 72] and also informs studies of the validity of the cosmic censorship conjecture [73, 74, 75]. Previous work [76, 72, 75] has estimated the scaling near extremality to be $p = 2/3$, where the total energy radiated per unit time is expressed as

$$\dot{\mathcal{E}} = C\epsilon^p, \qquad \epsilon \equiv \sqrt{1 - a^2/M^2}, \tag{3.1}$$

with M and Ma the mass and spin of the black hole.

Our calculations confirm $p = 2/3$ but also reveal some interesting details. First, the coefficient C is not a constant, and instead exhibits oscillations in ϵ about its mean value. Second, there is an intricate structure in the ℓ, m angular modes of the radiation. While all modes have $p = 2/3$ for the flux down the horizon, the same is not true for the flux at infinity. Instead, the exponent for the power at infinity is

given by

$$p_\infty = \frac{4}{3}\mathrm{Re}[h], \tag{3.2}$$

where h is the *conformal weight* of the mode, given in terms of the angular eigenvalues $\{K, m\}$ (spheroidal and azimuthal) by

$$h \equiv \frac{1}{2} + \sqrt{K - 2m^2 + \frac{1}{4}}. \tag{3.3}$$

The notion of a conformal weight arises in the representation theory of the near-horizon symmetry group (App. A.4) and is a key entry in the Kerr/CFT dictionary. The weight h should be thought of as fundamental, with the formula (3.3) depending on conventional choices like the definition of K. The appearance of the conformal weight in the radiation at infinity can be interpreted as a far-field signature of the near-field symmetry enhancement.

The conformal weight controls the character of each mode. Modes with complex weight ($K-2m^2+1/4 < 0$) have $\mathrm{Re}[h] = 1/2$ and hence the dominant scaling $p = 2/3$, while modes with real weight ($K - 2m^2 + 1/4 > 0$) have $\mathrm{Re}[h] > 1/2$ and hence subdominant scaling $p > 2/3$.[1] Only the dominant modes display the oscillations in the prefactor C. At each ℓ, modes with higher values of $|m|$ are dominant (Fig. 3.1). The transition is increasingly sharp as extremality is approached, and (e.g.) already at $\epsilon = 0.1$ ($a = 0.995M$), the 2-2 mode dominates the 2-1 mode by four orders of magnitude (Fig. 3.3). An observation of a huge difference in power between the 2-2 and 2-1 modes would signal the presence of a near-extreme black hole.[2]

[1] An analogous mode structure was previously observed in the study of near-extremal quasi-normal modes [77, 78].

[2] A detector at a fixed position cannot probe angular dependence, but for a circular orbit the difference between $m = 1$ and $m = 2$ is visible in the associated time-dependence $e^{im\Omega t}$.

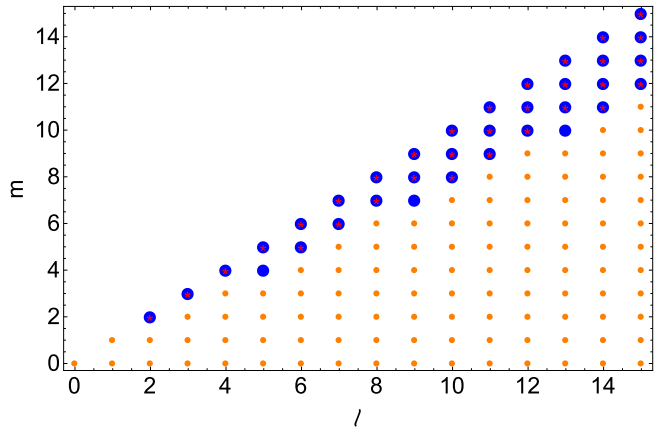

Figure 3.1: Diagram indicating the scaling (3.1) of energy radiated to infinity for each mode. Blue dots indicate the dominant scaling $p = 2/3$ in the gravitational case, while red stars indicate the dominant scaling $p = 2/3$ in the scalar case. Yellow dots indicate subdominant scaling $p > 2/3$. The flux down the horizon always has dominant scaling $p = 2/3$.

We compute the radiation both analytically (to leading order in ϵ) and numerically (at small, finite ϵ). Comparing the results, we begin seeing agreement (to about 10%) at $\epsilon = 0.01$ ($a = 0.99995M$) and we achieve eight digits of accuracy by the time we reach $\epsilon = 10^{-13}$, the smallest value we simulate. Historically, the near-extremal region of parameter space has been difficult to access numerically. Our new codes mark a substantial improvement over previous work and can accurately calculate the radiated fluxes for spins as high as $a = 0.99999999999999999999999995M$.

Our analytic solution of the Teukolsky equation uses the method of matched asymptotic expansions, a technique used in [79, 80, 55] and many times since. Our consideration of a particle on the ISCO complicates matters because this orbit is in a sense intermediate between the near-horizon and far regions (Fig. 3.2). The proper

way to think of the extremal ISCO has been the subject of some discussion over the years, and our calculations afford an opportunity to chime in. The fate of the ISCO is discussed in Sec. 3.2 and App. A.

In Chapter 2 we considered the physically distinct problem of a particle on a circular orbit in the near-horizon region of an exactly extremal Kerr black hole, working to leading order in the deviation from the horizon. After performing the calculation in the case of a scalar charge in this chapter, we find that the power radiated is *identical* to that of Chapter 2 with parameters identified in the natural way. The agreement is not completely surprising since the geometry in the vicinity of the near-extremal ISCO is the same as the near-horizon geometry of exactly extremal Kerr (the "NHEK" geometry, App. A.3). On the other hand, the agreement is highly nontrivial since the near-extremal Kerr throat contains an entire near-horizon region with a curved geometry, which is absent in extremal Kerr. (This region is the bottom section of Fig. 3.2 and is described by the "near-NHEK" metric, App. A.4.)

One can expect the analogous agreement to hold in the gravitational case. We therefore do not repeat the detailed calculation of the scalar case but instead rely on the gravitational results of Chapter 2.[3] Identifying the two problems in the same manner as before produces analytic expressions for the power radiated by a particle on the ISCO. We confirm these expressions numerically. We have not identified the precise reason for the agreement (in this particular observable) between the two different problems, but we think it is a manifestation of the action of the infinite-dimensional conformal group, which can relate extremal to near-extremal physics

[3]Only the flux at infinity was presented in Chapter 2. We compute the horizon flux using expressions given therein.

[3, 4].

In Sec. 3.2 we give an overview of near-extremal physics and establish notation. In Sec. 3.3 we perform the analytic calculation in the scalar case. In Sec. 3.4 we present analytic results for the gravitational case. In Sec. 3.5 we present the new numerical codes and compare the results with the analytic expressions. An appendix reviews near-horizon limits, placing our computation in the context of this rich structure. Our metric has signature $-+++$ and we use units with $G = c = 1$.

3.2 Near-Extremal Physics

The non-extremal Kerr black hole is invariantly characterized by two parameters a and M satisfying $M > 0$ and $a < M$. We will work with $M > 0$ and $\epsilon > 0$, where ϵ is the near-extremality parameter defined in Eq. (3.1). It is also useful to introduce $r_\pm = M \pm \sqrt{M^2 - a^2}$, the Boyer-Lindquist (BL) coordinate radii of the horizons, and the (outer) horizon angular frequency $\Omega_H = a/(r_+^2 + a^2)$. We restrict attention to $r > r_+$, which we call the Kerr exterior.

One may now ask the question: "What is the extremal ($\epsilon \to 0$) limit of the Kerr exterior?" Fixing Boyer-Lindquist (BL) coordinates, one obtains the spacetime conventionally called extreme Kerr. On the other hand, fixing alternative coordinates adapted to the near-horizon region (App. A.2) gives a different spacetime, normally called NHEK (for near-horizon extremal Kerr). There is yet a *third* limit adapted to the ISCO, which gives a different patch of the maximally extended NHEK spacetime (App. A.3). The first limit leaves asymptotic infinity intact but replaces the non-degenerate horizon by a degenerate one. The second and third limits replace

asymptotic null infinity with a timelike boundary. The answer to the question is thus "not enough information". There are multiple limits and none is preferred on any fundamental grounds.

The existence of the various limits is a signal that near-extremal physics falls into the class of what are generally called *singular perturbation* problems. In our ISCO calculation, the singular nature appears as the impossibility of imposing all the boundary conditions of the differential equation in a single small-ϵ approximation. Instead we must make a far-zone approximation where we can satisfy the far boundary conditions (no incoming radiation from past null infinity), a near-zone approximation where we can satisfy the near boundary conditions (no incoming radiation from the past horizon), and match the two in their region of overlap.

3.2.1 Circular Orbits and the ISCO

We consider a non-extremal ($\epsilon > 0$) Kerr black hole and work with the dimensionless radial coordinate x defined by

$$x = \frac{r - r_+}{r_+}, \tag{3.4}$$

which places the event horizon at $x = 0$. The exterior of a non-extremal black hole has three important circular equatorial geodesics picked out by geometric considerations [81]: the ISCO (the marginally stable orbit), the innermost bound circular orbit (the marginally bound orbit) and the photon orbit or light ring. As noted by [81], the (BL or x) coordinate radii of these orbits approach that of the horizon as $\epsilon \to 0$. The marginally bound and photon orbits go like $x \sim \epsilon$, while the ISCO approaches more

slowly, being given to leading order in ϵ by

$$x_0 = 2^{1/3}\epsilon^{2/3}. \tag{3.5}$$

Fig. 3.2 illustrates the properties of these orbits, and a formal discussion of their $\epsilon \to 0$ limits is given in App. A. While our focus is on the ISCO, our analysis holds for any orbit going like $x_0 \sim \epsilon^k$ with $0 < k < 1$. Except where explicitly noted, all later formulae in this chapter hold for such orbits.

Two other useful properties of a circular orbit are its angular velocity Ω and "redshift factor" $g = e - \Omega l$ (where e and l are the particle's conserved energy and angular momentum per unit rest mass). To leading order we have

$$\frac{\Omega - \Omega_H}{\Omega_H} = -\frac{3}{4}x_0, \quad g = \frac{\sqrt{3}}{4}x_0. \tag{3.6}$$

The physical significance of g is that a photon emitted by the particle with energy $\mathcal{E}$ is observed on the symmetry axis at infinity to have energy $g\mathcal{E}$. This thought experiment illustrates how signals from the near-horizon region are redshifted away; in the case of the ISCO the observed energy vanishes as $x_0 \sim \epsilon^{2/3}$ as extremality is reached. This is the same scaling as the radiation from the particle orbit, our focus in this chapter.

Note that as $\epsilon \to 0$ the horizon angular velocity and BL horizon radii go as

$$\Omega_H = \frac{1}{2M}\left(1 - \epsilon\right). \tag{3.7}$$

$$r_\pm = M\left(1 \pm \epsilon\right). \tag{3.8}$$

Since $\Omega_H \to 1/(2M)$ like ϵ, one may replace Ω_H with $1/(2M)$ in Eq. (3.6).

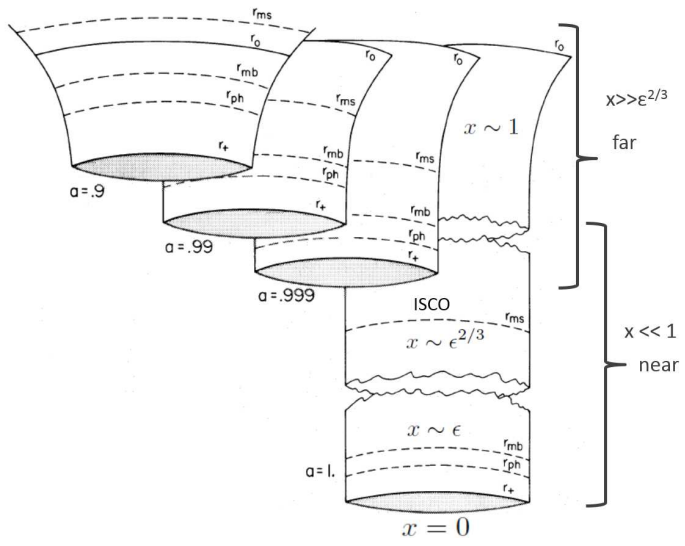

Figure 3.2: The well-known diagram of [81] overlaid with corresponding regions of the dimensionless coordinate x that we consider. The dashed lines illustrate the BL radii of the ISCO $r_{\rm ms}$, the marginally bound orbit $r_{\rm mb}$, and the photon orbit $r_{\rm ph}$. Also shown are the horizon r_+ and a constant (ϵ-independent) BL radius r_0. (Note that we use the notation x_0 for the ISCO radius in the main body.) The "cracks" in the throat illustrate infinite proper radial distance on a BL slice in the extremal limit. They can also be interpreted as signaling the presence of three physically distinct extremal limits (App. A).

3.3 Scalar Calculation

We first define the problem at finite $\epsilon > 0$. We consider the scalar wave equation,

$$g^{ab}\nabla_a\nabla_b\Phi = -4\pi T, \tag{3.9}$$

with source

$$T = \frac{qg}{r_0^2}\delta(r-r_0)\delta(\theta-\pi/2)\delta(\phi-\Omega t). \tag{3.10}$$

Here q is a constant called the scalar charge, g is the redshift factor (3.6), r_0 is the BL coordinate radius of the ISCO, and Ω is its angular velocity. The source has a mode expansion,

$$T = \frac{qg}{r_0^2}\sum_{\ell,m}\delta(r-r_0)S_{\ell m}(\pi/2)S_{\ell m}(\theta)e^{im(\phi-\Omega t)}, \tag{3.11}$$

where ℓ ranges from 0 to ∞ and m ranges from $-\ell$ to ℓ. Only these modes will be excited in the field, which we similarly decompose as

$$\Phi = \sum_{\ell,m}\Phi_{\ell m} = \sum_{\ell,m}R_{\ell m}(r)S_{\ell m}(\theta)e^{im(\phi-\Omega t)}. \tag{3.12}$$

The $S_{\ell m}$ satisfy the spheroidal harmonic differential equation,

$$\left[\frac{\partial_\theta(\sin\theta\partial_\theta)}{\sin\theta} + K_{\ell m} - \frac{m^2}{\sin^2\theta} - a^2m^2\Omega^2\sin^2\theta\right]S_{\ell m} = 0. \tag{3.13}$$

Solutions regular at the poles are labeled by ℓ and m with an associated eigenvalue $K_{\ell m}$. We normalize them so that $\int \sin\theta d\theta S^2 = 1$.

In terms of the dimensionless coordinate x (3.4), the radial functions satisfy

$$\begin{aligned} x(x+\sigma)R''(x)+(2x+\sigma)R'(x) + VR(x) = \\ \frac{-2qg}{r_+}S_{\ell m}(\pi/2)\delta(x-x_0), \end{aligned} \tag{3.14}$$

with

$$V = \frac{(r_+ m\Omega x(x+2) + n\sigma/2)^2}{x(x+\sigma)} + 2am^2\Omega - K, \tag{3.15}$$

where we have introduced

$$\sigma = \frac{r_+ - r_-}{r_+}, \quad n = 4mM\frac{\Omega - \Omega_H}{\sigma}. \tag{3.16}$$

We have dropped the mode labels ℓ and m. Eq. (3.14) is also the spin-zero Teukolsky equation [58] with angular frequency $\omega = m\Omega$.

For the non-radiative $m = 0$ modes, Eq. (3.14) can be solved exactly for any value of spin [82]. We focus on the radiative case, and for the remainder of the chapter we assume $m \neq 0$. In this case, the solutions to (3.14) have asymptotic behaviors given by

$$\begin{aligned} R(x) \to{}& C^\infty e^{im\Omega r_+ x} x^{-1+im\Omega r_+\sigma/\epsilon} \\ &+ D^\infty e^{-im\Omega r_+ x} x^{-1-im\Omega r_+\sigma/\epsilon}, \qquad x \to \infty \end{aligned} \tag{3.17}$$

$$\begin{aligned} R(x) \to{}& C^H x^{-inr_+\sigma/(4M\epsilon)} \\ &+ D^H x^{inr_+\sigma/(4M\epsilon)}, \qquad x \to 0, \end{aligned} \tag{3.18}$$

where C^∞, D^∞, C^H, and D^H are (complex) constants. We impose no incoming radiation from the past horizon or past null infinity,

$$D^\infty = D^H = 0. \tag{3.19}$$

From the properties of the differential equation (3.14), it is clear that this uniquely fixes the solution. The observables we are interested in are the power radiated to

infinity and down the event horizon. These are given for each mode by

$$\dot{\mathcal{E}}_\infty = \frac{1}{2} r_+^2 m^2 \Omega^2 |C^\infty|^2 \tag{3.20}$$

$$\dot{\mathcal{E}}_H = M r_+ m^2 \Omega (\Omega - \Omega_H) |C^H|^2. \tag{3.21}$$

This defines the problem for every $\epsilon > 0$.

The need for a matched expansion to study the $\epsilon \to 0$ limit can be seen at the level of the differential equation. Naively setting $\epsilon = 0$ in (3.14) and solving, one finds that the solutions go as x^{h-1} and x^{-h} near $x = 0$, rather than the oscillatory behavior (3.18) of the finite-ϵ equation. Thus the $\epsilon = 0$ equation cannot satisfy the boundary conditions of the problem, the hallmark of a singular perturbation problem.

3.3.1 Near-extremal Simplification

We first make some simplifications using $\epsilon \ll 1$. The angular equation (3.13) becomes

$$\left[\frac{\partial_\theta (\sin\theta \partial_\theta)}{\sin\theta} + K - m^2 \left(\frac{1}{\sin^2\theta} + \frac{1}{4} \sin^2\theta \right) \right] S = 0, \tag{3.22}$$

which is independent of the frequency Ω and hence independent of ϵ. To leading order Eq. (3.16) becomes

$$\sigma = 2\epsilon \tag{3.23}$$

$$n = -\frac{3}{4} m x_0 \epsilon^{-1}, \tag{3.24}$$

where we have used Eq. (3.6) to get the second relation. For the ISCO we see that n diverges as $n \sim \epsilon^{-1/3}$. In App. A n is related to the frequency conjugate to the time of the near-horizon metric. The radial equation (3.14) becomes

$$x(x + 2\epsilon) R'' + 2(x + \epsilon) R' + \hat{V} R = N x_0 \delta(x - x_0), \tag{3.25}$$

where we introduce

$$N = -\frac{\sqrt{3}}{2}\frac{q}{M}S_{\ell m}(\pi/2) \tag{3.26}$$

and

$$\hat{V} = \frac{(\frac{1}{2}mx(x+2) - n\epsilon)^2}{x(x+2\epsilon)} + m^2 - K. \tag{3.27}$$

We can also simplify (3.20), (3.21) using (3.6),

$$\dot{\mathcal{E}}_\infty = \frac{1}{8}m^2|C^\infty|^2 \tag{3.28}$$

$$\dot{\mathcal{E}}_H = -\frac{3}{16}x_0 m^2|C^H|^2. \tag{3.29}$$

Notice that $\dot{\mathcal{E}}_H < 0$, indicating that these modes are superradiant.

3.3.2 Matched Asymptotic Expansions Overview

For $x \gg x_0$, Eq. (3.25) becomes

$$x^2R'' + 2xR' + [m^2(2 + x + x^2/4) - K]R = 0. \tag{3.30}$$

(Note that $x_0 \sim n\epsilon$ by (3.24).) This is the "far" equation and its solutions will carry the label "far". For $x \ll 1$ Eq. (3.25) instead becomes

$$\begin{aligned} &x(x+2\epsilon)R'' + 2(x+\epsilon)R' \\ &\quad + \left[\frac{(mx+n\epsilon)^2}{x(x+2\epsilon)} + m^2 - K\right]R = Nx_0\delta(x-x_0). \end{aligned} \tag{3.31}$$

Eq. (3.31) is the "near" equation and its solutions will carry the label "near". The equations agree when $x_0 \ll x \ll 1$, becoming

$$x^2R'' + 2xR' + [2m^2 - K]R = 0. \tag{3.32}$$

This is the "region of overlap" and the solutions are

$$R^{\text{overlap}} = Px^{h-1} + Qx^{-h} \tag{3.33}$$

for constants P and Q, where h is given in (3.3). This region corresponds to the $x \to 0$ behavior of solutions of the far equation (3.30) and the $x \to \infty$ behavior of solutions to the near equation (3.31). Thus each solution of (3.30) or (3.31) is characterized by values of P and Q obtained by looking at the appropriate asymptotic region. A pair of solutions approximates a single smooth solution to Eq. (3.25) (and hence (3.14)) when the solutions have the same P and Q.

3.3.3 Far Solutions

The far equation (3.30) is a confluent hypergeometric equation and its solutions can be written in a number of equivalent ways. We parameterize the general solution by P and Q,

$$\begin{aligned} R^{\text{far}} = {} & Px^{h-1}e^{-imx/2}{}_1F_1\left(h+im; 2h; imx\right) \\ & + Qx^{-h}e^{-imx/2}{}_1F_1\left(1-h+im; 2(1-h); imx\right). \end{aligned} \tag{3.34}$$

That is, at small x we have

$$R^{\text{far}} \to Px^{h-1} + Qx^{-h}, \quad x \to 0. \tag{3.35}$$

Notice that the two solutions are related by $h \to 1-h$. For large x the asymptotic behavior is

$$\begin{aligned} R^{\text{far}} \to {} & C^{\infty}e^{imx/2}x^{-1+im} \\ & + D^{\infty}e^{-imx/2}x^{-1-im}, \qquad x \to \infty. \end{aligned} \tag{3.36}$$

with

$$C^\infty = P\frac{(im)^{-h+im}\Gamma(2h)}{\Gamma(h+im)} + Q\frac{(im)^{h-1+im}\Gamma(2(1-h))}{\Gamma(1-h+im)}$$
$$D^\infty = P\frac{(-im)^{-h-im}\Gamma(2h)}{\Gamma(h-im)} + Q\frac{(-im)^{h-1-im}\Gamma(2(1-h))}{\Gamma(1-h-im)}$$

To be outgoing at infinity we must have $D^\infty = 0$ or

$$P/Q = (-im)^{2h-1}\frac{\Gamma(1-2h)\Gamma(h-im)}{\Gamma(2h-1)\Gamma(1-h-im)}. \tag{3.37}$$

In this case the coefficient C^∞ is given by

$$\begin{aligned} C^\infty &= Q\,\frac{\Gamma(2-2h)}{\Gamma(1-h+im)}(im)^{h-1+im} \\ &\quad\times\left[1-\frac{(-im)^{2h-1}}{(im)^{2h-1}}\frac{\sin[\pi(h+im)]}{\sin[\pi(h-im)]}\right] \\ &= -Q\,(-1)^{-\mathrm{sign}(m)\,h}\frac{\Gamma(h-im)}{\Gamma(2h-1)}e^{\pi|m|}(im)^{h-1+im}. \end{aligned} \tag{3.38}$$

3.3.4 Near Solutions

The near equation (3.31) is a hypergeometric equation. We will work with the following two linearly independent homogeneous solutions,[4]

$$\begin{aligned} R^{\rm near}_{\rm in} &= x^{-\frac{in}{2}}\left(\frac{x}{2\epsilon}+1\right)^{i\left(\frac{n}{2}-m\right)} \\ &\quad\times {}_2F_1\left(h-im,1-h-im;1-in;-\frac{x}{2\epsilon}\right) \end{aligned} \tag{3.39}$$

$$\begin{aligned} R^{\rm near}_{\rm N} &= x^{-h}\left(\frac{2\epsilon}{x}+1\right)^{i\left(\frac{n}{2}-m\right)} \\ &\quad\times {}_2F_1\left(h-im,h+i(n-m);2h;-\frac{2\epsilon}{x}\right) \end{aligned} \tag{3.40}$$

[4]This choice expedites writing the answer for the horizon flux in a form that makes manifest the scaling for small ϵ.

The asymptotic behaviors are

$$R_{\rm in}^{\rm near} \to x^{-in/2} \qquad \text{for } x \to 0\,, \tag{3.41}$$

$$\to A\,x^{h-1} + B\,x^{-h} \qquad \text{for } x \to \infty\,, \tag{3.42}$$

$$R_{\rm N}^{\rm near} \to C\,x^{-in/2} + D\,x^{in/2} \qquad \text{for } x \to 0\,, \tag{3.43}$$

$$\to x^{-h} \qquad \text{for } x \to \infty\,, \tag{3.44}$$

where

$$A = \frac{\Gamma(2h-1)\Gamma(1-in)}{\Gamma(h-im)\Gamma(h-i(n-m))}(2\epsilon)^{1-h-\frac{in}{2}}\,, \tag{3.45}$$

$$B = \frac{\Gamma(1-2h)\Gamma(1-in)}{\Gamma(1-h-im)\Gamma(1-h-i(n-m))}(2\epsilon)^{h-\frac{in}{2}}\,, \tag{3.46}$$

$$C = \frac{\Gamma(2h)\Gamma(in)}{\Gamma(h+im)\Gamma(h+i(n-m))}(2\epsilon)^{-h+\frac{in}{2}}\,, \tag{3.47}$$

$$D = \frac{\Gamma(2h)\Gamma(-in)}{\Gamma(h-im)\Gamma(h-i(n-m))}(2\epsilon)^{-h-\frac{in}{2}}\,. \tag{3.48}$$

The "in" solution is purely ingoing at the horizon, while the "N" solution has only the x^{-h} falloff at large x. Here "N" stands for Neumann, which is the terminology used in Chapter 2.[5] The Wronskian W is given by

$$x(x+2\epsilon)W(R_{\rm in}^{\rm near}, R_{\rm N}^{\rm near}) = (1-2h)A. \tag{3.49}$$

From the properties of the differential equation, the combination on the LHS above is known to be independent of x and may therefore be easily computed at large x.

[5]The reason for this terminology is that for real h the falloff x^{-h} is subdominant compared to x^{1-h}.

3.3.5 Up solution

We now consider the solution with pure outgoing radiation at infinity, conventionally called the "up" solution. The normalization is arbitrary and we will choose

$$R^{\rm near}_{\rm up} = R^{\rm near}_{\rm in} + \alpha R^{\rm near}_{\rm N} \tag{3.50}$$

in the near zone. At large x we have $R^{\rm near}_{\rm up} = Ax^{h-1} + (B+\alpha)x^{-h}$. Matching to (3.35), we have $P = A$ and $Q = B + \alpha$. We can thus write

$$\alpha = B\left(\frac{A}{B}\frac{Q}{P} - 1\right) = B(1/b - 1), \tag{3.51}$$

where B is given in (3.46), and from (3.37), (3.45), and (3.46) we can compute $b \equiv (B/A)(P/Q)$ to be

$$\begin{aligned} b = (-im)^{2h-1}&\frac{\Gamma(1-2h)^2\Gamma(h-im)^2}{\Gamma(2h-1)^2\Gamma(1-h-im)^2} \\ &\times \frac{\Gamma(h+i(m-n))}{\Gamma(1-h+i(m-n))}(2\epsilon)^{2h-1}. \end{aligned} \tag{3.52}$$

The up solution in the far zone is given by Eq. (3.34) with

$$P = A, \qquad Q = B + \alpha = B/b. \tag{3.53}$$

The behavior near infinity (which controls the outgoing radiation) is given by plugging $Q = B/b$ into (3.38). We thus have

$$C^{\infty}_{\rm up} = -\frac{B}{b}(-1)^{-{\rm sign}(m)\,h}\frac{\Gamma(h-im)}{\Gamma(2h-1)}e^{\pi|m|}(im)^{h-1+im}. \tag{3.54}$$

3.3.6 Retarded Solution

To construct the retarded solution we demand pure ingoing at the horizon, pure outgoing at infinity, and the proper match at the delta-function source at $x = x_0$ in

Eq. (3.31). This is given by

$$R^{\rm near}_{\rm ret}(x) = Nx_0 \frac{R^{\rm near}_{\rm in}(x_<)R^{\rm near}_{\rm up}(x_>)}{x(x+2\epsilon)W[R^{\rm near}_{\rm in}(x), R^{\rm near}_{\rm up}(x)]}$$
$$= \frac{Nx_0}{\alpha A(1-2h)} R^{\rm near}_{\rm in}(x_<)R^{\rm near}_{\rm up}(x_>), \tag{3.55}$$

where $x_<$ and $x_>$ are the lesser and greater of x and x_0, respectively. We have used (3.50) and (3.49) to evaluate the Wronskian.

3.3.7 Large-n Asymptotics

Thus far we have considered exact solutions of the near equation (3.31), where ϵ (and hence x_0 and n) is treated as finite.We now simplify further using the smallness of ϵ, which by (3.24) corresponds to large n.

We first simplify the expressions for A, B, α, and b. For this we need the following asymptotic approximation,

$$\frac{\Gamma(p+z)}{\Gamma(q+z)} = z^{p-q}, \quad z \to \infty, \tag{3.56}$$

which holds for any complex p, q, z. From (3.45) and (3.46) we have

$$A = \frac{\Gamma(2h-1)}{\Gamma(h-im)}(-in)^{-im}(2\epsilon)^{-in/2}\left(\tfrac{3}{2}imx_0\right)^{1-h} \tag{3.57}$$
$$B = \frac{\Gamma(1-2h)}{\Gamma(1-h-im)}(-in)^{-im}(2\epsilon)^{-in/2}\left(\tfrac{3}{2}imx_0\right)^{h}, \tag{3.58}$$

and from (3.51) and (3.52) we have

$$\alpha = B(1/b-1) \tag{3.59}$$
$$b = \frac{\Gamma(1-2h)^2}{\Gamma(2h-1)^2}\frac{\Gamma(h-im)^2}{\Gamma(1-h-im)^2}(3m^2x_0/2)^{2h-1}. \tag{3.60}$$

(We repeat Eq. (3.51) for convenience.) In obtaining these equations we have used that $n\epsilon = -3mx_0/4$ from Eq. (3.24).

When the radial functions are evaluated at $x = x_0$, the ${}_2F_1$ hypergeometrics in Eqs. (3.39) and (3.40) reduce to Whittaker W and M functions via the confluence identities:

$$W_{\nu,\mu}(z) = \lim_{c\to\infty} {}_2F_1(\mu-\nu+\tfrac{1}{2}, -\mu-\nu+\tfrac{1}{2}; c; 1-\tfrac{c}{z}) \times e^{-z/2} z^{\nu} \tag{3.61}$$

$$M_{\nu,\mu}(z) = \lim_{b\to\infty} {}_2F_1(\mu-\nu+\tfrac{1}{2}, b; 1+2\mu; \frac{z}{b}) \times e^{-z/2} z^{\mu+\frac{1}{2}}. \tag{3.62}$$

Specifically, we have

$$R^{\rm near}_{\rm in}(x_0) = x_0^{-\frac{in}{2}} \left(\frac{x_0}{2\epsilon}+1\right)^{i\left(\frac{n}{2}-m\right)} \times e^{3im/4}(3im/2)^{-im} W_{im,h-\frac{1}{2}}(3im/2) \tag{3.63}$$

$$R^{\rm near}_{\rm N}(x_0) = (3imx_0/2)^{-h} \left(\frac{2\epsilon}{x_0}+1\right)^{i\left(\frac{n}{2}-m\right)} \times e^{3im/4} M_{im,h-\frac{1}{2}}(3im/2), \tag{3.64}$$

where we have again used that $n\epsilon = -3mx_0/4$.

3.3.8 Horizon flux

To compute the power radiated down the event horizon we need to examine the $x \to 0$ behavior of our solution and extract the coefficient C^H defined in (3.18). For $x < x_0$ the solution is given by

$$R^{\rm near}_{\rm ret}(x) = \frac{Nx_0}{\alpha A(1-2h)} R^{\rm near}_{\rm in}(x) R^{\rm near}_{\rm up}(x_0). \tag{3.65}$$

Thus the horizon coefficient is

$$C^{\rm H}_{\rm ret} = \frac{N x_0}{\alpha A(1-2h)} C^{\rm H}_{\rm in} R^{\rm near}_{\rm up}(x_0), \tag{3.66}$$

where $C^{\rm H}_{\rm in}$ is the horizon coefficient for the in solution. However, from (3.41) we have simply $C^{\rm H}_{\rm in} = 1$. Using Eqs. (3.50) and (3.59), a more convenient expression is

$$C^{\rm H}_{\rm ret} = \frac{N x_0}{AB(1-2h)} \left(B R^{\rm near}_{\rm N}(x_0) + \frac{b}{1-b} R^{\rm near}_{\rm in}(x_0) \right). \tag{3.67}$$

Using Eqs. (3.26), (3.57), (3.58), (3.60), (3.63), and (3.64) and simplifying, we find

$$\begin{aligned} C^{\rm H}_{\rm ret} = {} & N \frac{2i}{3m} e^{3im/4} (-in)^{im} (2\epsilon)^{in/2} \left(1 + \frac{2\epsilon}{x_0}\right)^{i\left(\frac{n}{2}-m\right)} \\ & \times \frac{\Gamma(h-im)}{\Gamma(2h)} \left(\mathscr{M} + \frac{b}{1-b} \frac{\Gamma(1-h-im)}{\Gamma(1-2h)} \mathscr{W} \right), \end{aligned} \tag{3.68}$$

where we introduce

$$\mathscr{M} = M_{im,h-\frac{1}{2}}\left(\frac{3im}{2}\right), \quad \mathscr{W} = W_{im,h-\frac{1}{2}}\left(\frac{3im}{2}\right). \tag{3.69}$$

Squaring and plugging into (3.29) gives the power radiated,

$$\begin{aligned} \dot{\mathcal{E}}_H = {} & -\frac{q^2}{16M^2} x_0 \, e^{-\pi|m|} S\left(\tfrac{\pi}{2}\right)^2 \left| \frac{\Gamma(h-im)}{\Gamma(2h)} \right|^2 \\ & \times \left| \mathscr{M} + \frac{b}{1-b} \frac{\Gamma(1-h-im)}{\Gamma(1-2h)} \mathscr{W} \right|^2. \end{aligned} \tag{3.70}$$

The energy flux down the horizon scales as x_0, so that for the ISCO it scales as $\epsilon^{2/3}$. The formula for b was given in Eq. (3.60). When h has an imaginary part, b is order unity and oscillatory in ϵ, causing $\dot{\mathcal{E}}_H$ to have small oscillations. When h is real, $b \ll 1$ and the entire term proportional to $\mathscr{W}$ drops out at the leading order, making there be no oscillations.

3.3.9 Infinity flux

For $x > x_0$ the solution is given in the near-zone by

$$R^{\rm near}_{\rm ret}(x) = \frac{N x_0}{\alpha A(1-2h)} R^{\rm near}_{\rm in}(x_0) R^{\rm near}_{\rm up}(x). \tag{3.71}$$

This solution is valid in the near-zone, with $x \to \infty$ corresponding to the overlap region rather than asymptotic infinity. To determine the behavior near asymptotic infinity one has to match to solutions of the far region. However, this has already been done when constructing the "up" solution. Thus the retarded solution near infinity is determined by

$$C^{\infty}_{\rm ret} = \frac{N x_0}{\alpha A(1-2h)} R^{\rm near}_{\rm in}(x_0) C^{\infty}_{\rm up}. \tag{3.72}$$

Using Eq. (3.54) for $C^{\infty}_{\rm up}$ gives

$$\begin{aligned} C^{\infty}_{\rm ret} = N x_0 \frac{1}{1-b} \frac{R^{\rm near}_{\rm in}(x_0)}{A} \\ \times (-1)^{-{\rm sign}(m)\, h} \frac{\Gamma(h-im)}{\Gamma(2h)} e^{\pi|m|} (im)^{h-1+im}. \end{aligned} \tag{3.73}$$

Using Eqs. (3.63) and (3.57) and simplifying gives

$$\begin{aligned} C^{\infty}_{\rm ret} = N x_0^h\, e^{3im/4} \left(\frac{2\epsilon}{x_0} + 1\right)^{i\left(\frac{\pi}{2} - m\right)} \frac{2h-1}{1-b} \frac{\Gamma(h-im)^2}{\Gamma(2h)^2} \\ \times (-1)^{-{\rm sign}(m)\, h} e^{\pi|m|} (im)^{h-1+im} (3im/2)^{h-1}\, \mathscr{W}, \end{aligned} \tag{3.74}$$

where $\mathscr{W}$ was defined in (3.69). Squaring and plugging in to (3.28) gives the infinity flux,

$$\begin{aligned} \dot{\mathcal{E}}_{\infty} = \frac{q^2}{24M^2} (3m^2 x_0/2)^{2{\rm Re}[h]} m^{-2} e^{\pi|m|} S\left(\tfrac{\pi}{2}\right)^2 \\ \times \left| \frac{2h-1}{1-b} \frac{\Gamma(h-im)^2}{\Gamma(2h)^2} \mathscr{W} \right|^2. \end{aligned} \tag{3.75}$$

Recall that b is given in Eq. (3.60) and $\mathscr{W}$ is given in Eq. (3.69). The energy flux to infinity scales as $x_0^{2\mathrm{Re}[h]}$, so that for the ISCO it scales as $\epsilon^{(4/3)\mathrm{Re}[h]}$. The dominant modes are when h has an imaginary part, in which case $\mathrm{Re}[h] = 1/2$ and $b \sim 1$ with oscillations. The modes with real h are subdominant with $b \ll 1$ and no oscillations at leading order.

3.3.10 Agreement with extremal calculation

Chapter 2 solved the physically distinct problem of the radiation from a particle orbiting at a radius $x_0 \ll 1$ in precisely extremal Kerr. Remarkably, our final answer (3.75) for the flux to infinity agrees *precisely* with the analogous answer (2.61) when we identify the x coordinates (3.4) in extremal and near-extremal Kerr.[6] In Chapter 2 the horizon flux was not explicitly given for the retarded solution, but performing the calculation shows perfect agreement as well. Near infinity we can also sensibly compare the detailed radiation pattern, which agrees as well: The asymptotic behavior of the retarded field is given by (3.74) together with (3.36) and $D^\infty = 0$, which differs from the expressions in Chapter 2 only by the phase $\exp[3im/4](2\epsilon/x_0 + 1)^{i(n/2-m)}$. This phase is of the form $\exp[imf(\epsilon)]$ and hence can be eliminated at any fixed ϵ by the redefinition $\phi \to \phi - f(\epsilon)$.

For real h the horizon flux (3.70) is in perfect agreement with the particle number flux (2.34). Using the Kerr/CFT dictionary, in Chapter 2, this flux was calculated independently in the CFT as the appropriate transition rate induced on the state of the system due to coupling to a source dual to the orbiting particle (Eq. (2.47)). Note,

[6] Chapter 2 uses the notation r for x and λ for q.

however, that the boundary conditions used for deriving (2.34) assumed Neumann falloff of the near solution (rather than the "up" falloff of (3.50)). The boundary conditions used here for the retarded solution were termed "leaky boundary conditions" in Chapter 2 because they allow radiation to leak out of the near region and reach future null infinity. However, as we saw in the previous section, for real h, the radiation that leaks to infinity here is subdominant and the CFT calculations of Chapter 2 still account for the flux down the horizon at leading order.

3.4 Gravitational Case

The problem of the gravitational radiation from a particle of mass m_0 orbiting on the near-extremal ISCO can be solved in a manner precisely analogous to the scalar calculation of Sec. 3.3. However, given the agreement in the scalar case with the analogous calculation of Chapter 2 (Sec. 3.3.10), we can instead obtain analytic expressions by postulating agreement in the gravitational case as well. The expression for the gravitational flux at infinity is given in Eq. (2.102) of Chapter 2. The flux at the horizon was not computed in Chapter 2, but it is a straightforward exercise to do so. Identifying these expressions using the x-coordinate radius of the particle produces expressions for the power radiated in our near-extremal ISCO problem. We confirm these expressions numerically.

We now present these results. In some formulae we use the variable $s = -2$ (the spin) to emphasize similarity to the scalar case $s = 0$. For each mode $\ell \geq 2$ and

$|m| \leq \ell$ the fluxes are given by

$$\dot{\mathcal{E}}_H = -\frac{m_0^2}{2^6 3^2 M^2}\frac{1}{|\mathcal{C}|^2}\, x_0\, e^{-\pi|m|}\frac{|\Gamma(h-im-s)|^2}{|\Gamma(2h)|^2}\left|\mathscr{M}_s + \frac{b_s}{1-b_s}\frac{\Gamma(1-h-im-s)}{\Gamma(1-2h)}\mathscr{W}_s\right|^2 \tag{3.76}$$

$$\dot{\mathcal{E}}_\infty = \frac{m_0^2}{2^5 3^3 M^2}(3m^2 x_0/2)^{2\mathrm{Re}[h]} m^{-2} e^{\pi|m|}\left|\frac{2h-1}{1-b_s}\frac{\Gamma(h-im-s)\Gamma(h-im+s)}{\Gamma(2h)^2}\mathscr{W}_s\right|^2, \tag{3.77}$$

where

$$b_s = \frac{\Gamma(1-2h)^2}{\Gamma(2h-1)^2}\frac{\Gamma(h-im-s)}{\Gamma(1-h-im-s)}\frac{\Gamma(h-im+s)}{\Gamma(1-h-im+s)}\left(\frac{3m^2x_0}{2}\right)^{2h-1} \tag{3.78}$$

$$\begin{aligned}\mathscr{M}_s = {} & 2\left[(h^2-h+6-im)S + 4(2i+m)S' - 4S''\right] M_{im-2,h-\frac{1}{2}}(3im/2) \\ & - (h-2+im)\left[(4+3im)S - 8iS'\right] M_{im-1,h-\frac{1}{2}}(3im/2)\end{aligned} \tag{3.79}$$

$$\begin{aligned}\mathscr{W}_s = {} & 2\left[(h^2-h+6-im)S + 4(2i+m)S' - 4S''\right] W_{im-2,h-\frac{1}{2}}(3im/2) \\ & + \left[(4+3im)S - 8iS'\right] W_{im-1,h-\frac{1}{2}}(3im/2)\,.\end{aligned} \tag{3.80}$$

$$|\mathcal{C}|^2 = [(-2+h)^2+m^2][(-1+h)^2+m^2][h^2+m^2][(1+h)^2+m^2]. \tag{3.81}$$

The spin-2 spheroidal harmonics $S(\theta)$ and their eigenvalues K are defined to be the regular solutions to

$$\left[\frac{\partial_\theta(\sin\theta\,\partial_\theta)}{\sin\theta} + K^s_{\ell m} - \frac{m^2+s^2+2ms\cos\theta}{\sin^2\theta} - \frac{m^2}{4}\sin^2\theta - ms\cos\theta\right] S^s_{\ell m} = 0, \tag{3.82}$$

normalized so that $\int \sin\theta d\theta S^2 = 1$. In Eqs. (3.79) and (3.80), a prime represents a θ-derivative and the harmonics are evaluated at the equator $\theta = \pi/2$. The spin-2 spheroidal harmonics and their eigenvalues are not native in *Mathematica*, but are straightforward to compute using (e.g.) the spectral method of [15]. We provide a notebook online [83] that implements this method and evaluates the complete analytic flux formulae.

Eq. (3.78) for b_s generalizes the scalar expression (3.52) for b, reducing to that expression when $s = 0$. Eqs. (3.79) and (3.80) for $\mathscr{M}_s$ and $\mathscr{W}_s$ generalize $\mathscr{M}$ and $\mathscr{W}$ in the sense that they play analogous roles in the expressions for the energy flux, but do not reduce to their scalar counterparts in any direct sense. The formula for $|\mathcal{C}|^2$ is the same as Eq. (3.23) of [55] (specialized to the modes appearing in our calculation); it accounts for relating spin ± 2 quantities in the Newman-Penrose formalism.

As in the scalar case, $b_s \ll 1$ for real h, while $b_s \sim 1$ (and is oscillatory) for complex h. The character of the fluxes is thus precisely analogous to the scalar case; we refer the reader to the text below (3.70) and (3.75) for discussion.

3.5 Numerical Results

In this section we describe two new numerical codes and the comparison of their results with our analytic flux formulae. It was necessary to construct these new codes as previously developed software did not work sufficiently close to extremality to allow for a clear comparison with the analytic results. Typically the maximum spin achievable in these older codes was around $\epsilon \simeq 10^{-3}$, equivalently $a \simeq 0.9999995M$ [82, 15]. The two new codes we present here mark significant improvements over previous technology, allowing us to work all the way down to $\epsilon = 10^{-13}$ or $a = 0.9999999999999999999999999995M$.

Our new codes feature three key improvements. First, the codes are implemented in *Mathematica*, which allows us to work beyond standard machine precision. Second, for the gravitational case we derive new, more accurate, asymptotic approximations used for boundary conditions. Third, again in the gravitational case, we employ a

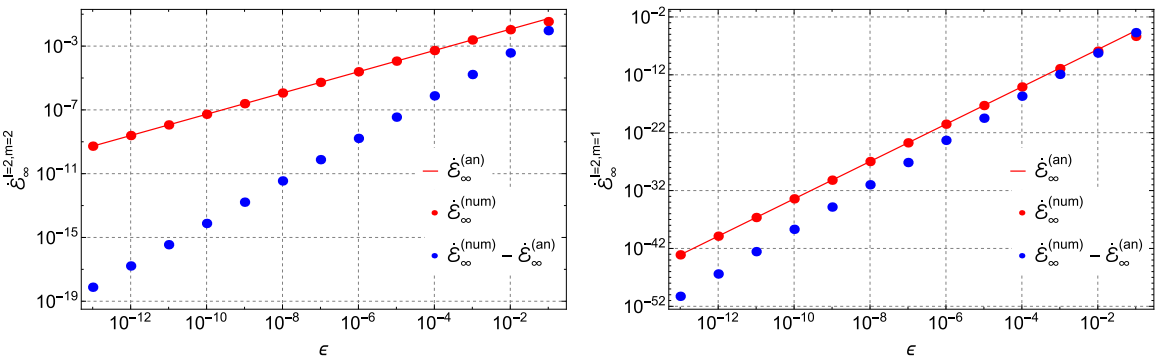

(a) $\ell = 2, m = 2$ (b) $\ell = 2, m = 1$

Figure 3.3: Energy flux to infinity for the 2-2 and 2-1 modes in the gravitational case. The analytic results and numerical results are denoted by $\dot{\mathcal{E}}_\infty^{(\mathrm{an})}$ and $\dot{\mathcal{E}}_\infty^{(\mathrm{num})}$, respectively. The 2-2 mode has $h \simeq 1/2 + 2.050928i$ and hence an exponent of $p = 2/3$, while the 2-1 mode has $h \simeq 2.419070$ and an exponent of $p \simeq 3.225427$. The 2-2 mode also has oscillations, too small to be seen on this scale but clearly visible in Fig. 3.4. Note that the results in this figure have been adimensionalized so that $\dot{\mathcal{E}}^{(\mathrm{here})} \equiv (M/m_0)^2 \dot{\mathcal{E}}$.

simpler matching procedure to construct inhomogeneous solutions to the Teukolsky equation than that presented in Ref. [15]. We briefly discuss these points in the following subsection before presenting the comparison between the numerical and analytic results in Sec. 3.5.2.

3.5.1 Numerical Implementation

The scalar problem was defined at the start of Sec. 3.3. The main task is to solve the spin-zero Teukolsky equation (3.14) with boundary conditions (3.19) corresponding to no incoming radiation. We use a reimplementation in Mathematica of the

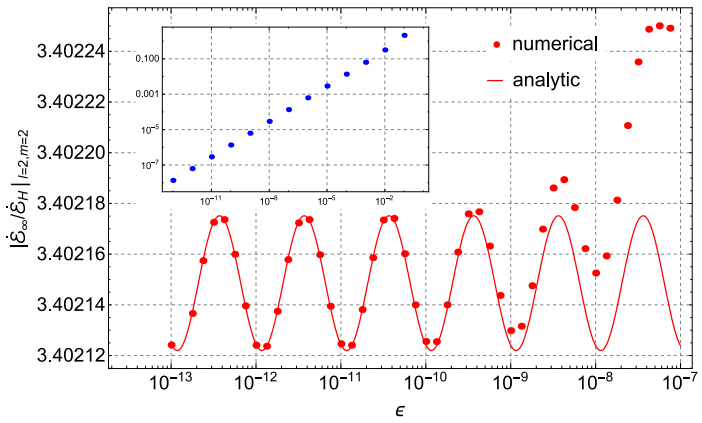

Figure 3.4: The ratio of the infinity flux to horizon flux for the 2-2 mode in the gravitational case. The oscillations occur in both the infinity and horizon fluxes, but are dominated by the $\epsilon^{2/3}$ scaling. The ratio removes the dominant scaling and makes the oscillations clear. The inset shows the absolute difference between the analytic and numerical results for the ratio of the fluxes and demonstrates that our numerical results are in good agreement with the analytic formula through to $\epsilon = 10^{-13}$.

algorithm presented in Ref. [82]. Briefly, the steps are as follows: (i) construct unit normalized boundary conditions for the homogeneous solutions far from the particle; (ii) using these boundary conditions, numerically integrate the field equation to get $R_{\ell m}$ and its derivative at the particle; (iii) compute weighting coefficients for the inhomogeneous solutions via the variations of parameters method. As our source contains a delta-function this reduces to a matching procedure at the particle's radius. We refer the reader to Ref. [82] for the explicit details of each of these steps.[7]

For gravitational perturbations we opt to solve the spin-two Teukolsky equation. In this scenario we cannot proceed exactly as in the scalar case as the 'long-ranged' potential of the Teukolsky equation makes it numerically challenging to avoid contamination from modes with incoming radiation. This is a well known problem which is neatly circumvented by transforming to a new variable as was first described by Sasaki and Nakamura [84]. Using the new variable the field equation has a 'short-ranged' potential and, as such, is better suited to numerical treatment. Once the Sasaki-Nakamura radial function and its derivatives are computed at the particle, we transform back to the Teukolsky radial function and continue, as in the scalar case, to construct the inhomogeneous solutions via matching. From the matching coefficients we then extract the radiated fluxes. A similar procedure was carried out by Hughes [15]. In addition to implementing our code in Mathematica, we make some important improvements as we outline now.

[7]We correct a mistake in the horizon-side boundary conditions in Ref. [82]. The arXiv version has been updated to give the correct recursion relation.

The Sasaki-Nakamura equation takes the form [84]

$$\frac{dX}{dr_*^2} - F(r)\frac{dX}{dr_*} - U(r)X(r) = 0, \tag{3.83}$$

where r_* is the tortoise coordinate defined by $dr_*/dr = (r^2 + a^2)/\Delta$ with $\Delta = r^2 - 2Mr + a^2$. The functions $F(r)$ and $U(r)$ are rather unwieldy and can be found in the Appendix B of Ref. [15]. Asymptotically, as the horizon and spatial infinity are approached, the 'outer' and 'inner' radial solutions behave as

$$X^{\infty}(r_* \to \infty) \sim e^{i\omega r_*}, \tag{3.84}$$

$$X^{H}(r_* \to -\infty) \sim e^{-i(\omega - m\Omega_H)r_*}, \tag{3.85}$$

respectively. In our numerical procedure we must work on a finite radial domain. Let us denote the boundaries of this domain by $r_{\rm in}$ and $r_{\rm out}$. In order to construct suitable boundary conditions at $r_{\rm in/out}$ we expand the above asymptotic forms with the following ansatz

$$X^{\infty} = e^{i\omega r_*} \sum_{k=0}^{k^{\infty}_{\rm max}} a_k^{\infty} (\omega r_{\rm out})^{-k}, \tag{3.86}$$

$$X^{H} = e^{-i(\omega - m\Omega_H)r_*} \sum_{k=0}^{k^{H}_{\rm max}} a_k^{H} (r_{\rm in} - r_+)^{k}. \tag{3.87}$$

The $a_k^{\infty/H}$ coefficients of these series expansions are determined by substituting the expansions into the Sasaki-Nakamura equation (3.83) and solving for the resulting recursion relations. Explicitly finding the recursion relations is one point where our algorithm differs from previous work. For example, the first three coefficients in Eq. (3.86) were explicitly computed in Ref. [15]; the first four coefficients were given Ref. [85]. Both the aforementioned works just set $a_0^H = 1$ and used only the first

term in the horizon expansion, i.e., $k^H_{\rm max} = 0$. We find that using just these few terms in the boundary condition expansions is insufficient for computations around rapidly rotating black holes. With our recursion relations we can compute arbitrary numbers of coefficients which allows us to place the numerical boundaries for the inner and outer solutions further from the horizon and closer to the edge of the wavezone, respectively.

The complicated form of the functions $F(r)$ and $U(r)$ in Eq. (3.83) makes solving for the recursion relations challenging, even with the assistance of computer algebra packages. Such recursion relations are not unique but the ones we identify have 13 and 14 terms for the infinity and horizon expansions, respectively. The recursion relations we compute are too lengthy to be displayed here but we make them available in electronic format online [83]. To check the recursion relations we set $a_0^{\infty/H} = 1$ (we are free to set this to any non-zero number as we are solving for the homogeneous solutions), compute a number of terms in the expansions, substitute the resulting expansion back into the homogeneous field equation (3.83) and check that is it satisfied. For the 2-2 mode with the particle on the ISCO and $a \lesssim 0.99M$ we find we can satisfy the field equation at $r_{\rm out} = 100M$ and $r_{\rm in} = r_+ + 10^{-2}M$ to over 100 significant digits with ease. As we increase the spin of the black hole the outer boundary doesn't need to move but we find we must move the inner boundary radius inwards so that by the time we reach $\epsilon = 10^{-13}$ we must place the inner boundary at $r_{\rm in} = r_+ + 10^{-15}M$ to achieve similar accuracy.

Lastly, we briefly mention an improvement in the practical application of the variations of parameters method used to construct the inhomogeneous solutions by

integrating the homogeneous solutions against the source. With this method it is necessary to compute the Wronskian of homogeneous solutions and in Ref. [15] this is calculated at a large radius. To achieve this a variant of Richardson extrapolation was used to accurately calculate the 'inner' homogeneous solution at large radii. This step is unnecessary as the Wronskian, defined with derivatives with respect to r_*, is a constant for all r and so can be calculated at any suitable radius. We find it convenient to calculate the Wronskian at the particle's orbital radius where we can calculate the homogeneous solutions to high accuracy via direct numerical integration of the field equation.

As a test of our new Sasaki-Nakamura code we compared our results for the fluxes against those of Ref. [15] for $a \leq 0.99M$, finding agreement to over 8 significant figures, which is consistent with the given error bars. We also compare against results of Ref. [86], which solves the Teukolsky equation as a series of special functions [84], finding 13 significant figures of agreement.

3.5.2 Comparison of results

In this section we compare the fluxes computed with our new numerical codes against our analytic flux formulae given by Eqs. (3.70) and (3.75) for the scalar case and Eqs. (3.76) and (3.77) for the gravitational case. The results for the scalar and gravitational cases are very similar and so we will concentrate on the physically more interesting gravitational case.

In making our calculations we need to evaluate the spin-weighted spheroidal-harmonics and their eigenvalues which are used in both the analytic formula and

ϵ	$\dot{\mathcal{E}}_\infty$	$\dot{\mathcal{E}}_H$	$\Delta_{\rm rel}\dot{\mathcal{E}}_\infty$	$\Delta_{\rm rel}\dot{\mathcal{E}}_H$
10^{-1}	$1.71745312 \times 10^{-2}$	$-3.11049626 \times 10^{-3}$	3.5×10^{-1}	6.0×10^{-1}
10^{-2}	$5.33839225 \times 10^{-3}$	$-1.43536969 \times 10^{-3}$	6.6×10^{-2}	1.5×10^{-1}
10^{-3}	$1.21422396 \times 10^{-3}$	$-3.50339388 \times 10^{-4}$	1.3×10^{-2}	3.2×10^{-2}
10^{-4}	$2.64399402 \times 10^{-4}$	$-7.74081267 \times 10^{-5}$	2.9×10^{-3}	6.8×10^{-3}
10^{-5}	$5.70914114 \times 10^{-5}$	$-1.67667887 \times 10^{-5}$	6.1×10^{-4}	1.5×10^{-3}
10^{-6}	$1.23059093 \times 10^{-5}$	$-3.61646072 \times 10^{-6}$	1.3×10^{-4}	3.2×10^{-4}
10^{-7}	$2.65150343 \times 10^{-6}$	$-7.79336251 \times 10^{-7}$	2.9×10^{-5}	6.8×10^{-5}
10^{-8}	$5.71261941 \times 10^{-7}$	$-1.67911892 \times 10^{-7}$	6.1×10^{-6}	1.5×10^{-5}
10^{-9}	$1.23075261 \times 10^{-7}$	$-3.61759396 \times 10^{-8}$	1.3×10^{-6}	3.2×10^{-6}
10^{-10}	$2.65157915 \times 10^{-8}$	$-7.79388978 \times 10^{-9}$	2.9×10^{-7}	6.8×10^{-7}
10^{-11}	$5.71265599 \times 10^{-9}$	$-1.67914365 \times 10^{-9}$	6.1×10^{-8}	1.5×10^{-7}
10^{-12}	$1.23075461 \times 10^{-9}$	$-3.61760597 \times 10^{-10}$	1.3×10^{-8}	3.2×10^{-8}
10^{-13}	$2.65158073 \times 10^{-10}$	$-7.79389645 \times 10^{-11}$	2.9×10^{-9}	6.8×10^{-9}

Table 3.1: Sample numerical results and their comparison with the analytic formula for the gravitational 2-2 mode. The second and third columns give the flux radiated to infinity and through the horizon, respectively. The fourth and fifth columns give the relative difference between the numerical results and the analytic formulae, i.e., $\Delta_{\rm rel}\dot{\mathcal{E}}_{\infty/H} = 1 - \dot{\mathcal{E}}^{\rm (num)}_{\infty/H}/\dot{\mathcal{E}}^{\rm (an)}_{\infty/H}$. Note that the data in columns two and three has been adimensionalized so that $\dot{\mathcal{E}}^{\rm (here)} \equiv (M/m_0)^2\dot{\mathcal{E}}$.

the numerical procedure. For the spin-0 harmonics we use Mathematica's inbuilt `SpheroidalPS` and `SpheroidalEigenvalue` functions. For the spin-2 harmonics we use the spectral decomposition method described in Appendix A of Ref. [15]. For ease of comparison we provide a Mathematica notebook online that evaluates the analytic flux formulae [83].

Our main results are presented in Figs. 3.3, 3.4 and Table 3.1 for the gravitational case. For the scalar case we give numerical data in Table 3.2. For small ϵ we find the numerical and analytic results agree, as expected. As an example, for the gravitational 2-2 mode we find, for the flux at infinity, that the relative difference between the analytically calculated flux, $\dot{\mathcal{E}}_\infty^{(\mathrm{an})}$, and numerically calculated flux, $\dot{\mathcal{E}}_\infty^{(\mathrm{num})}$, is around 6.6% for $\epsilon = 10^{-2}$. The agreement improves by $\epsilon = 10^{-13}$ to over 8 significant figures.

For all modes the horizon flux scales as $\epsilon^{2/3}$. On the other hand, the scaling of the energy flux radiated to infinity depends on the mode in question, going as ϵ^p where $p = 4/3\mathrm{Re}[h]$. For modes with $m \sim \ell$ the scaling exponent is $p = 2/3$ but for low m modes p is larger. Which modes are dominant or subdominant is illustrated in Fig. 3.1 for $\ell \leq 15$. For $\ell = 2$ this difference in scaling can be seen explicitly by comparing the two plots in Fig. 3.3. In addition to the leading order scaling, the horizon flux and the infinity flux for modes with $p = 2/3$ exhibit oscillations. Taking the ratio of the horizon and infinity fluxes removes this leading-order behavior and makes the oscillations clear, as we show in Fig. 3.4.

The excellent agreement we observe between our analytical and numerical results gives us confidence in both. In particular, numerical codes often struggle in such high-spin regimes and we envisage that our analytic formula will provide a valuable

ϵ	$\dot{\mathcal{E}}_\infty$	$\dot{\mathcal{E}}_H$	$\Delta_{\rm rel}\dot{\mathcal{E}}_\infty$	$\Delta_{\rm rel}\dot{\mathcal{E}}_H$
10^{-1}	$5.85189833 \times 10^{-4}$	$-3.34966656 \times 10^{-4}$	-7.4×10^{-1}	6.1×10^{-1}
10^{-2}	$1.06917341 \times 10^{-4}$	$-1.56686813 \times 10^{-4}$	-4.6×10^{-1}	1.5×10^{-1}
10^{-3}	$1.74509810 \times 10^{-5}$	$-3.84548334 \times 10^{-5}$	-1.2×10^{-1}	3.3×10^{-2}
10^{-4}	$3.48448909 \times 10^{-6}$	$-8.51021948 \times 10^{-6}$	-2.6×10^{-2}	7.2×10^{-3}
10^{-5}	$7.30812181 \times 10^{-7}$	$-1.84356886 \times 10^{-6}$	-5.6×10^{-3}	1.6×10^{-3}
10^{-6}	$1.57583045 \times 10^{-7}$	$-3.97754374 \times 10^{-7}$	-1.2×10^{-3}	3.3×10^{-4}
10^{-7}	$3.38175817 \times 10^{-8}$	$-8.56962339 \times 10^{-8}$	-2.6×10^{-4}	7.2×10^{-5}
10^{-8}	$7.28828188 \times 10^{-9}$	$-1.84681469 \times 10^{-8}$	-5.5×10^{-5}	1.6×10^{-5}
10^{-9}	$1.57315673 \times 10^{-9}$	$-3.97796344 \times 10^{-9}$	-1.2×10^{-5}	3.3×10^{-6}
10^{-10}	$3.37478969 \times 10^{-10}$	$-8.57211607 \times 10^{-10}$	-2.6×10^{-6}	7.2×10^{-7}
10^{-11}	$7.31738299 \times 10^{-11}$	$-1.84647008 \times 10^{-10}$	-5.6×10^{-7}	1.6×10^{-7}
10^{-12}	$1.56369119 \times 10^{-11}$	$-3.97866228 \times 10^{-11}$	-1.2×10^{-7}	3.4×10^{-8}
10^{-13}	$3.40087145 \times 10^{-12}$	$-8.57097932 \times 10^{-12}$	-2.6×10^{-8}	7.2×10^{-9}

Table 3.2: The same as Table 3.1 but for a particle carrying scalar charge orbiting at the ISCO. The data in columns two and three has been adimensionalized so that $\dot{\mathcal{E}}^{(\rm here)} \equiv (M/q)^2\dot{\mathcal{E}}$.

benchmark for future numerical work on rapidly rotating black holes.

Chapter 4

Slow Plunges into near-extreme Kerr black holes

4.1 Introduction

General relativity implies that the high-redshift region very near the horizon of a near maximally-spinning Kerr black hole is governed by an infinite-dimensional conformal symmetry [10, 11]. X-rays [5] and iron lines [7] from such regions have already been observed, and the future may hold yet higher precision observations. It is of interest to explore any potential observational consequences of the conformal symmetry. In Chapters 2 and 3, the conformal symmetry was exploited to compute gravity wave emission for an extreme-mass-ratio-inspiral within this near-horizon region. This approximates the signal from a stellar mass object orbiting near an extreme supermassive Kerr black hole and is potentially observable at eLISA [12, 13, 14]. Once such an object passes the innermost stable circular orbit (ISCO), it plunges into the

black hole. The plunge trajectory turns out to be related by a conformal map to the circular orbit. In this chapter we use the conformal map to compute the gravitational radiation produced during this post-ISCO plunge into a near-extreme Kerr black hole. This complements the computation in [19] of radiation produced during the post-ISCO plunge into a nonrotating Schwarzschild black hole.

In section 4.2 we set notation and briefly review the geometry of Kerr, near-horizon extreme Kerr (NHEK) and near-horizon near-extreme Kerr (near-NHEK). Section 4.3 gives the conformal map from a circular orbit of a pointlike 'star' in NHEK to a plunge trajectory in near-NHEK. In section 4.4, as a warmup to the gravity case, we couple a scalar field to the star. 4.4.1 computes the radiation production within near-NHEK using a bulk gravity analysis. 4.4.2 computes the same process using the techniques of two-dimensional conformal field theory (CFT). The results are shown to agree in subsection 4.4.3. In subsection 4.4.4 we turn to asymptotically flat near-extreme Kerr by reattaching the asymptotically flat region to near-NHEK. The resulting outgoing scalar radiation at flat future null infinity is computed. In 4.4.5 we derive the late-time quasinormal mode (QNM) decomposition. In section 4.5 all of these steps are repeated for the spin two case of gravitational radiation.

4.2 Kerr, NHEK and near-NHEK

The Kerr metric in Boyer-Lindquist coordinates reads ($G = \hbar = c = 1$):

$$ds^2 = -\frac{\Delta}{\hat{\rho}^2}\left(d\hat{t} - a\sin^2\theta d\hat{\phi}\right)^2 + \frac{\sin^2\theta}{\hat{\rho}^2}\left((\hat{r}^2+a^2)d\hat{\phi} - a d\hat{t}\right)^2 + \frac{\hat{\rho}^2}{\Delta}d\hat{r}^2 + \hat{\rho}^2 d\theta^2\,, \quad (4.1)$$

$$\Delta = \hat{r}^2 - 2M\hat{r} + a^2, \qquad \hat{\rho}^2 = \hat{r}^2 + a^2\cos^2\theta\,.$$

It is labeled by the mass M and angular momentum $J = aM$. The horizons are located at:

$$r_\pm = M \pm \sqrt{M^2 - a^2}\,. \tag{4.2}$$

The Hawking temperature, angular velocity of the horizon, and Bekenstein-Hawking entropy are:

$$T_H = \frac{r_+ - M}{4\pi M r_+}\,, \quad \Omega_H = \frac{a}{2M r_+}\,, \quad S_{BH} = 2\pi M r_+\,. \tag{4.3}$$

Extreme Kerr is characterized by $a = M$ so that angular momentum takes the maximal value $J = M^2$. Near extremality one has

$$\kappa \equiv \sqrt{1 - \left(\frac{a}{M}\right)^2} \ll 1\,. \tag{4.4}$$

In this case there is a long throat to the horizon of the black hole and we can derive a regular throat geometry by zooming in to the horizon (Appendix A). Defining

$$r = \frac{\hat{r} - r_+}{r_+}, \qquad t = \frac{\hat{t}}{2M}, \qquad \phi = \hat{\phi} - \frac{\hat{t}}{2M}\,, \tag{4.5}$$

the near-NHEK geometry [51] is obtained by scaling $r \sim \kappa$ to zero:

$$ds^2 = 2M^2\Gamma(\theta)\left[-r(r+2\kappa)dt^2 + \frac{dr^2}{r(r+2\kappa)} + d\theta^2 + \Lambda(\theta)^2(d\phi + (r+\kappa)dt)^2\right]\,, \tag{4.6}$$

where

$$\Gamma(\theta) = \frac{1+\cos^2\theta}{2}\,, \quad \Lambda(\theta) = \frac{2\sin\theta}{1+\cos^2\theta}\,. \tag{4.7}$$

The NHEK geometry [10] is obtained by scaling κ to zero first:

$$ds^2 = 2M^2\Gamma(\theta)\left[-R^2dT^2 + \frac{dR^2}{R^2} + d\theta^2 + \Lambda(\theta)^2(d\Phi + RdT)^2\right]\,. \tag{4.8}$$

4.3 Mapping from near-NHEK plunge to NHEK orbit

We wish to study radiation sourced by a particle that spirals off the ISCO in near-NHEK and plunges into the horizon. As shown in Appendix B this equatorial plunge orbit is given by:

$$t(r) = \frac{1}{2\kappa}\ln\frac{1}{r(r+2\kappa)} + t_0\,, \tag{4.9}$$

$$\phi(r) = \frac{3r}{4\kappa} + \frac{1}{2}\ln\frac{r}{r+2\kappa} + \phi_0\,, \tag{4.10}$$

and has energy and angular momentum (per unit rest mass):

$$e = 0\,, \qquad l = 2M/\sqrt{3}\,. \tag{4.11}$$

This orbit is very special in that it is a Killing flow. The corresponding Killing vector becomes manifest when we make the following transformation to NHEK [87, 88, 89, 90]:

$$\begin{aligned} T &= -e^{-\kappa t}\frac{r+\kappa}{\sqrt{r(r+2\kappa)}}\,, \\ R &= \frac{1}{\kappa}e^{\kappa t}\sqrt{r(r+2\kappa)}\,, \\ \Phi &= \phi - \frac{1}{2}\ln\frac{r}{r+2\kappa}\,. \end{aligned} \tag{4.12}$$

This is illustrated in Figure 4.1. The transformation takes the near-NHEK equatorial plunge geodesics (4.9, 4.10) to the equatorial circular orbits in NHEK:

$$R = R_0\,, \tag{4.13}$$

$$\Phi(T) = -\frac{3}{4}R_0\,T + \Phi_0\,, \tag{4.14}$$

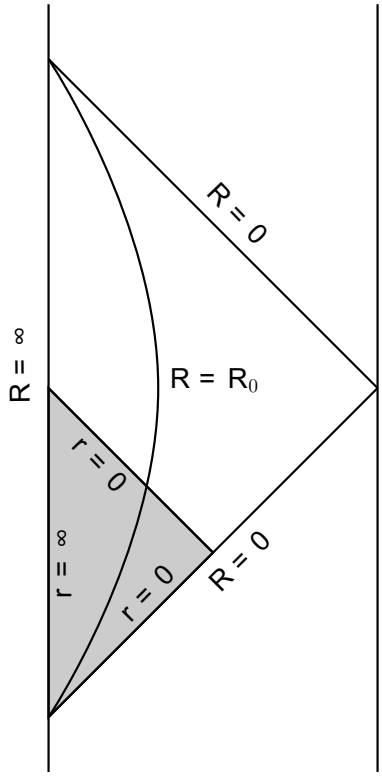

Figure 4.1: Penrose diagram of the throat geometry. The large wedge (bounded by $R = 0$ and $R = \infty$) is NHEK. The small shaded wedge (bounded by $r = 0$ and $r = \infty$) is near-NHEK. The line $R = R_0$ is the circular orbit in NHEK which in near-NHEK is seen to plunge into the future horizon at $r = 0$.

where,

$$R_0 = e^{\kappa t_0}/\kappa\,, \quad \Phi_0 = \phi_0 - 3/4\,. \tag{4.15}$$

Note that (4.13-4.14) is precisely what we would call an equatorial plunge trajectory in NHEK, that is, the geodesic with energy and angular momentum those of the marginally stable circular orbits of NHEK: $E = 0, L = 2M/\sqrt{3}$ (Appendix B).

The NHEK problem has a manifest Killing symmetry with respect to $\chi = \partial_T - (3/4)R_0\partial_\Phi$ and has been fully solved, both from the gravity and the CFT point of

view, in Chapter 2. In this chapter we will thus solve the near-NHEK plunge problem by performing the bulk diffeomorphism (4.12) on the gravity computation and the boundary conformal transformation,

$$T = -e^{-\kappa t}\,, \tag{4.16}$$

$$\Phi = \phi\,, \tag{4.17}$$

on the CFT computation of Chapter 2. We will see that the results remain in perfect agreement. Note that this conformal transformation is not among the $SL(2,R)$ isometries and hence this agreement tests the full infinite-dimensional conformal symmetry.

4.4 Scalar radiation from a plunging star

In this section we consider a massless scalar field Ψ coupled to a source $\mathcal{S}$ via the interaction:

$$S_I = -4\pi\lambda \int d^4x\sqrt{-g}\,\Psi(x)\mathcal{S}(x)\,, \tag{4.18}$$

where λ is a coupling constant. The source due to a pointlike 'star' on a geodesic $x^\mu_*(\tau)$ is the covariant delta function integrated along the worldline of the star:

$$\mathcal{S}(x) = -\int d\tau(-g)^{-1/2}\delta^{(4)}(x - x_*(\tau))\,. \tag{4.19}$$

In this case the wave equation becomes

$$\Box\,\Psi(x) = -4\pi\lambda \int d\tau(-g)^{-1/2}\delta^{(4)}(x - x_*(\tau))\,. \tag{4.20}$$

4.4.1 Gravity analysis

In this subsection we solve the wave equation (4.20) for the near-NHEK plunge and compute the flux across the future horizon. The solution for a particle on the geodesic (4.13-4.14) in NHEK with boundary conditions ingoing at the horizon and Neumann at the boundary is (Chapter 2, setting $\Phi_0 = 0$):

$$\Psi = \sum_{\ell,m} e^{im(\Phi+3R_0T/4)} S_\ell(\theta) R_{\ell m}(R)\,, \tag{4.21}$$

where S_ℓ are the spheroidal harmonics obeying

$$\frac{1}{\sin\theta}\partial_\theta(\sin\theta\,\partial_\theta S_\ell) + \left(K_\ell - \frac{m^2}{\sin^2\theta} - \frac{m^2}{4}\sin^2\theta\right) S_\ell = 0\,, \tag{4.22}$$

and $R_{\ell m}$ is given by:

$$R_{\ell m}(R) = \frac{1}{W}\left[X\,\Theta(R_0-R) W_{im,h-\frac{1}{2}}(-2i\Omega/R) + Z\,\Theta(R-R_0) M_{im,h-\frac{1}{2}}(-2i\Omega/R)\right]\,, \tag{4.23}$$

where $W_{k,\mu}$ and $M_{k,\mu}$ are Whittaker functions and

$$\begin{aligned}
\Omega &= -\frac{3}{4}mR_0\,,\\
h &= \frac{1}{2} + \sqrt{1/4 + K_\ell - 2m^2}\,,\\
X &= -\frac{\sqrt{3}\lambda R_0}{2M} S_\ell(\pi/2) M_{im,h-\frac{1}{2}}(3im/2)\,,\\
Z &= -\frac{\sqrt{3}\lambda R_0}{2M} S_\ell(\pi/2) W_{im,h-\frac{1}{2}}(3im/2)\,,\\
W &= 2i\Omega\frac{\Gamma(2h)}{\Gamma(h-im)}\,.
\end{aligned}$$

This solution has the asymptotic behaviors:

$$\Psi(R\to 0) = \sum_{\ell,m} e^{im(\Phi+3R_0T/4)}\, S_\ell(\theta)\,\frac{X}{W}(-2i\Omega)^{im}\, R^{-im} e^{-3imR_0/4R}\,, \tag{4.24}$$

$$\Psi(R\to\infty) = \sum_{\ell,m} e^{im(\Phi+3R_0T/4)}\, S_\ell(\theta)\,\frac{Z}{W}(-2i\Omega)^{h}\, R^{-h}\,. \tag{4.25}$$

As explained in section 4.3, the solution to the near-NHEK plunge problem, with the same boundary conditions, may be obtained by transforming the above NHEK solution using the transformation (4.12). That is to say, the Ψ given above, transformed via (4.12), will be the solution to the wave equation (4.20) in near-NHEK with a source due to a plunging particle on the trajectory (4.9-4.10).

Holding t, ϕ fixed, from the transformation (4.12) we see that

$$R \approx \sqrt{\frac{2}{\kappa}}\, e^{\kappa t}\, r^{1/2} \to 0 \qquad \text{for } r \to 0\,, \tag{4.26}$$

$$R \approx \frac{e^{\kappa t}}{\kappa}\, r \to \infty \qquad \text{for } r \to \infty\,, \tag{4.27}$$

and

$$e^{im(\Phi+3R_0T/4)}\,(r\to 0) = (2\kappa)^{im/2} e^{im\phi} r^{-im/2} \exp\left[-\frac{3imR_0}{4}\sqrt{\frac{\kappa}{2r}}\, e^{-\kappa t}\right], \tag{4.28}$$

$$e^{im(\Phi+3R_0T/4)}\,(r\to \infty) = e^{im\phi} \exp\left[-\frac{3imR_0}{4}\, e^{-\kappa t}\right]. \tag{4.29}$$

We thus find:

$$\Psi(r\to 0) = \sum_{\ell,m} \frac{X}{W} \kappa^{im} (-2i\Omega)^{im}\, e^{im\phi}\, S_\ell(\theta)\, r^{-im} e^{-im\kappa t} \times \\ \times \exp\left[-\frac{3imR_0}{2}\sqrt{\frac{\kappa}{2r}}\, e^{-\kappa t}\right], \tag{4.30}$$

$$\Psi(r\to \infty) = \sum_{\ell,m} \frac{Z}{W} \kappa^{h} (-2i\Omega)^{h}\, e^{im\phi}\, S_\ell(\theta)\, r^{-h} e^{-h\kappa t} \times \\ \times \exp\left[-\frac{3imR_0}{4}\, e^{-\kappa t}\right]. \tag{4.31}$$

In terms of the Fourier decomposition[1]:

$$\Psi(r\to 0) = \frac{1}{\sqrt{2\pi}}\int d\omega \sum_{\ell,m} I\, e^{-i\omega t}\, e^{im\phi}\, S_\ell(\theta) r^{-\frac{i}{2}(m+\omega/\kappa)}\,, \tag{4.32}$$

$$\Psi(r\to \infty) = \frac{1}{\sqrt{2\pi}}\int d\omega \sum_{\ell,m} N\, e^{-i\omega t}\, e^{im\phi}\, S_\ell(\theta) r^{-h}\,, \tag{4.33}$$

where

$$I = \frac{1}{\sqrt{2\pi}} 2^{\frac{i}{2}(m-\omega/\kappa)} \frac{X}{W} \kappa^{-1+\frac{i}{2}(m+\omega/\kappa)} (-2i\Omega)^{i\omega/\kappa} \Gamma(im - i\omega/\kappa)\,, \tag{4.34}$$

$$N = \frac{1}{\sqrt{2\pi}} 2^{h-i\omega/\kappa} \frac{Z}{W} \kappa^{h-1} (-2i\Omega)^{i\omega/\kappa} \Gamma(h - i\omega/\kappa)\,. \tag{4.35}$$

The Klein-Gordon particle number flux is defined as:

$$\mathcal{F} = \int \sqrt{-g} J^r\, d\theta d\phi\,, \quad J^\mu = \frac{i}{8\pi}\left(\Psi^*\nabla^\mu\Psi - \Psi\nabla^\mu\Psi^*\right)\,. \tag{4.36}$$

The near-NHEK solution (4.32-4.33) obeys ingoing boundary conditions at the horizon and Neumann at the boundary. Thus for real h the Klein-Gordon particle number flux vanishes at the boundary. Finally, the horizon flux, for $\omega > 0\,, m > 0$, is:

$$\mathcal{F}_{\ell m\omega} = \frac{M^2}{4\pi\kappa}\left|\frac{X}{W}\right|^2 \frac{m+\omega/\kappa}{m-\omega/\kappa} \frac{e^{-\pi\omega/\kappa}}{\sinh\pi(m-\omega/\kappa)} \tag{4.37}$$

$$\approx \frac{M^2}{2\pi\kappa}\left|\frac{X}{W}\right|^2 e^{-2\pi\omega/\kappa} e^{\pi m}\,, \tag{4.38}$$

where in the last line we have used $\kappa \ll 1$.

[1]The relevant Fourier transforms are:

$$F\left(e^{-im\kappa t}\exp\left[-\frac{3imR_0}{2}\sqrt{\frac{\kappa}{2r}}\,e^{-\kappa t}\right]\right) = \frac{1}{\sqrt{2\pi\kappa}}\left(\frac{2}{\kappa}\right)^{i\frac{m}{2}-i\frac{\omega}{2\kappa}}\left(\frac{3imR_0}{2}\right)^{-im+i\frac{\omega}{\kappa}}\Gamma\left(im - i\frac{\omega}{\kappa}\right) r^{i\frac{m}{2}-i\frac{\omega}{2\kappa}}\,.$$

$$F\left(e^{-h\kappa t}\exp\left[-\frac{3imR_0}{4}\,e^{-\kappa t}\right]\right) = \frac{1}{\sqrt{2\pi\kappa}}\left(\frac{3imR_0}{4}\right)^{-h+i\frac{\omega}{\kappa}}\Gamma\left(h - i\frac{\omega}{\kappa}\right)\,.$$

4.4.2 CFT analysis

In this subsection we derive the flux formula (4.38) from the CFT representation of gravity in near-NHEK as a 2D CFT at temperatures $T_L = 1/2\pi$, $T_R = \kappa/2\pi$ and an angular potential [51]. As shown in Chapter 2, the addition of a star to NHEK is dual to a certain deformation of the CFT. The latter is described by the deformation of the two-dimensional action S_{CFT}:

$$S = S_{CFT} + \sum_{\ell} \int d\Phi\, dT\, J_\ell(\Phi, T)\mathcal{O}_\ell(\Phi, T)\,, \tag{4.39}$$

where $\mathcal{O}_\ell$ are CFT operators with left and right weights h.[2] For a star on the orbit (4.13-4.14) it was shown that

$$J_\ell(\Phi, T) = \sum_m \frac{X}{W} C\, e^{im(\Phi + 3R_0 T/4)}\,, \tag{4.40}$$

where $C = (-2i\Omega)^{1-h}\Gamma(2h-1)/\Gamma(h-im)$. Since $\mathcal{O}_\ell$ carry left and right weights h it follows by conformal invariance of (4.39) that J_ℓ carry left and right weights $1-h$. As a result, the conformal transformation (4.16) gives:

$$J_\ell(\phi, t) = \kappa^{1-h} e^{(h-1)\kappa t} \sum_m \frac{X}{W} C\, e^{im(\phi - 3R_0 e^{-\kappa t}/4)}\,. \tag{4.41}$$

The Fourier decomposition is:

$$J_\ell(\phi, t) = \frac{1}{\sqrt{2\pi}} \int d\omega \sum_{\ell, m} J_{\ell m\omega}\, e^{-i\omega t}\, e^{im\phi}\,, \tag{4.42}$$

where

$$J_{\ell m\omega} = \frac{1}{\sqrt{2\pi}} \frac{X}{W} C\, \kappa^{-h} \left(\frac{3imR_0}{4}\right)^{h-1+i\omega/\kappa} \Gamma(1 - h - i\omega/\kappa)\,. \tag{4.43}$$

[2] To avoid index clutter we suppress here and in the following the ℓ subscript on h.

The deformed action (4.39) may then be written:

$$S = S_{CFT} + \frac{1}{\sqrt{2\pi}} \int d\omega \sum_{\ell,m} \int d\phi\, dt\, J_{\ell m\omega} e^{im\phi - i\omega t} \mathcal{O}_\ell(\phi, t)\,. \tag{4.44}$$

The time dependent sources pump both left and right energy into the CFT. The leading-order transition rate out of the thermal state is given by Fermi's golden rule [31, 52, 1]:

$$\mathcal{R} = \int d\omega \sum_{\ell,m} |J_{\ell m\omega}|^2 \int d\phi\, dt\, e^{-im\phi + i\omega t} G(\phi, t)\,, \tag{4.45}$$

where $G(\phi, t) = \langle \mathcal{O}^\dagger(\phi, t)\mathcal{O}(0,0)\rangle_{T_L,T_R}$ is the finite temperature two point function of the CFT. Using $T_L = \frac{1}{2\pi}$, $T_R = \frac{\kappa}{2\pi}$, for $\omega > 0\,, m > 0$ with the appropriate $i\epsilon$ prescription, the Fourier transform of the two point function is:

$$\begin{aligned} \mathcal{R}_{\ell m\omega} &= C_{\mathcal{O}}^2 \frac{1}{\Gamma(2h)^2} |J_{\ell m\omega}|^2 \kappa^{2h-1} e^{\pi\omega/\kappa} e^{\pi m} |\Gamma(h + i\omega/\kappa)|^2 |\Gamma(h + im)|^2 & (4.46)\\ &\approx C_{\mathcal{O}}^2 \frac{8\pi}{2^{2h}(2h-1)^2\kappa} \left|\frac{X}{W}\right|^2 e^{-2\pi\omega/\kappa} e^{\pi m}\,, & (4.47) \end{aligned}$$

where $C_{\mathcal{O}}^2$ is the operator normalization and in the last line we have used $\kappa \ll 1$.

4.4.3 Gravity/CFT matching

With the normalization found in Chapter 2,

$$C_{\mathcal{O}} = \frac{2^{h-1}(2h-1)}{2\pi} M\,, \tag{4.48}$$

we have the exact match of the gravity and CFT computations:

$$\mathcal{R}_{\ell m\omega} = \frac{M^2}{2\pi\kappa} \left|\frac{X}{W}\right|^2 e^{-2\pi\omega/\kappa} e^{\pi m} = \mathcal{F}_{\ell m\omega}\,. \tag{4.49}$$

4.4.4 Reattaching the asymptotically flat region

In the previous subsections we considered scalar radiation production in near-NHEK. Boundary conditions were imposed such that all radiation was (for real h) reflected off of the asymptotic throat boundary and ultimately falls into the future horizon. Here we reattach the asymptotically flat region and compute the outgoing radiation at future null infinity.

Consider the scalar field on Kerr expanded in modes:

$$\Psi = \frac{1}{\sqrt{2\pi}} \int d\hat{\omega} \sum_{\ell,m} e^{-i\hat{\omega}\hat{t}} e^{im\hat{\phi}} \hat{S}_\ell(\theta) \hat{R}_{\ell m\hat{\omega}}(\hat{r}) \,. \tag{4.50}$$

The wave equation separates into the spheroidal angular equation,

$$\frac{1}{\sin\theta}\partial_\theta(\sin\theta\,\partial_\theta \hat{S}_\ell) + \left(\hat{K}_\ell - \frac{m^2}{\sin^2\theta} - a^2\hat{\omega}^2\sin^2\theta\right)\hat{S}_\ell = 0\,, \tag{4.51}$$

and a radial equation which in the coordinates (4.6) reads:

$$r(r+\tau_H)\hat{R}''_{\ell m\hat{\omega}} + (2r+\tau_H)\hat{R}'_{\ell m\hat{\omega}} + V\hat{R}_{\ell m\hat{\omega}} = \hat{T}_{\ell m\hat{\omega}}\,, \tag{4.52}$$

with

$$V = \frac{(r_+\hat{\omega}r^2 + 2r_+\hat{\omega}r + n\tau_H/2)^2}{r(r+\tau_H)} + 2am\hat{\omega} - \hat{K}_\ell \,. \tag{4.53}$$

Here $\hat{K}_\ell$ is the separation constant and,

$$\tau_H \equiv \frac{r_+ - r_-}{r_+}\,, \qquad n \equiv 4M\frac{\hat{\omega} - m\Omega_H}{\tau_H}\,. \tag{4.54}$$

In the near extremal, near superradiant bound regime,

$$\tau_H \ll 1 \quad \text{and} \quad n\tau_H \ll 1\,, \tag{4.55}$$

we have to leading order:

$$\tau_H = 2\kappa\ ,\ 2r_+\hat{\omega} = 2a\hat{\omega} = m\ ,\ \hat{K}_\ell = K_\ell\ ,\ \hat{S}_\ell = S_\ell\ ,\ 2M\hat{\omega} - m = (n-m)\kappa\,. \tag{4.56}$$

Then, identifying

$$\omega = (n-m)\kappa\,, \tag{4.57}$$

we can match a near-NHEK solution containing the source with a far Kerr vacuum solution as follows. For $r \gg max(\tau_H, n\tau_H)$ equation (4.52) becomes the vacuum far equation in extreme Kerr and the solution that is purely outgoing at null infinity behaves as (Chapter 2):

$$\begin{aligned} \hat{R}^{far}_{\ell m\hat{\omega}}(r\to\infty) &= Q\,\frac{\Gamma(2-2h)}{\Gamma(1-h+im)}(im)^{h-1+im}\times \\ &\quad\times\left[1-\frac{(-im)^{2h-1}}{(im)^{2h-1}}\frac{\sin\pi(h+im)}{\sin\pi(h-im)}\right] r^{-1+im}e^{imr/2}\,, \end{aligned} \tag{4.58}$$

$$\hat{R}^{far}_{\ell m\hat{\omega}}(r\to 0) = P\,r^{h-1}+Q\,r^{-h}\,, \tag{4.59}$$

where

$$\frac{P}{Q} = -(-im)^{2h-1}\frac{\Gamma(2-2h)}{\Gamma(2h)}\frac{\Gamma(h-im)}{\Gamma(1-h-im)}\,. \tag{4.60}$$

For $r \ll 1$ equation (4.52) becomes the near-NHEK equation,

$$r(r+2\kappa)\hat{R}''_{\ell m\hat{\omega}} + 2(r+\kappa)\hat{R}'_{\ell m\hat{\omega}} + \left[\frac{(mr+n\kappa)^2}{r(r+2\kappa)} + m^2 - K_\ell\right]\hat{R}_{\ell m\hat{\omega}} = \hat{T}_{\ell m\hat{\omega}}\,, \tag{4.61}$$

with the source $\hat{T}_{\ell m\hat{\omega}}$ due to the plunging star on (4.9-4.10). In section 4.4.1 we found the solution to this equation with ingoing boundary conditions at the horizon and Neumann at the boundary of the throat (equations (4.32-4.33)). The latter implies no flux leaking outside the throat. However, here we wish to allow the necessary flux leak out in such a way that we can match the large r behavior of the solution to (4.61) with the small r behavior of $\hat{R}^{far}_{\ell m\hat{\omega}}$ in (4.59). This is done by adding to the solution of section 4.4.1 an ingoing at the horizon homogeneous solution of (4.61),

$$\hat{R}^{near}_{in} = r^{-in/2}\left(\frac{r}{2\kappa}+1\right)^{i(n/2-m)}{}_2F_1\left(h-im\,,1-h-im\,,1-in\,,-\frac{r}{2\kappa}\right)\,, \tag{4.62}$$

with the appropriate amplitude to match the Dirichlet mode of (4.59). Doing so fixes the amplitude Q according to:

$$Q = 2MN\left[1-(-2im\kappa)^{2h-1}\frac{\Gamma(1-2h)^2}{\Gamma(2h-1)^2}\frac{\Gamma(h-im)^2}{\Gamma(1-h-im)^2}\frac{\Gamma(h-i(n-m))}{\Gamma(1-h-i(n-m))}\right]^{-1}, \tag{4.63}$$

where N is given in (4.35). Plugging into equation (4.58) we obtain the waveform at future null infinity as a function of ℓ, m and $\hat{\omega}$:

$$\begin{aligned}\hat{R}^{far}_{\ell m\hat{\omega}}(r\to\infty) = {}& \frac{4\lambda}{\sqrt{6\pi}}(-1)^{-h}(2\kappa)^{h-1}(3R_0/4)^{i(n-m)}\times \\ & \times\frac{S_\ell(\pi/2)W_{im,h-\frac{1}{2}}\left(3im/2\right)(im)^{h-2+in}e^{\pi m}(1-2h)\Gamma(h-im)^2/\Gamma(2h)^2}{\frac{1}{\Gamma(h-i(n-m))}-(-2im\kappa)^{2h-1}\frac{\Gamma(1-2h)^2}{\Gamma(2h-1)^2}\frac{\Gamma(h-im)^2}{\Gamma(1-h-im)^2}\frac{1}{\Gamma(1-h-i(n-m))}}\times \\ & \times r^{-1+im}e^{imr/2}\,,\end{aligned} \tag{4.64}$$

for $m>0$.

4.4.5 Quasinormal mode decomposition

The waveform at future infinity as a function of time rather than frequency is obtained by plugging (4.64) into (4.50) and integrating over frequencies. It is well known that for appropriately late times the waveform is dominated by the quasinormal mode contribution, which is determined by the residues of $\hat{R}^{far}_{\ell m\hat{\omega}}(r\to\infty)$ at its poles. From (4.64) the poles are located where the denominator,

$$\mathcal{D}\equiv\frac{1}{\Gamma(h-i(n-m))}-(-2im\kappa)^{2h-1}\frac{\Gamma(1-2h)^2}{\Gamma(2h-1)^2}\frac{\Gamma(h-im)^2}{\Gamma(1-h-im)^2}\frac{1}{\Gamma(1-h-i(n-m))}\,, \tag{4.65}$$

vanishes. These QNMs of near extreme Kerr were first studied for the case $n\to\infty$ in [91] and more recently for $n=$ finite in [92]. Here we follow the latter because

this case gives the most long lived resonances. In order to have $\mathcal{D} = 0$, the two different terms need to be of the same magnitude as $\kappa \to 0$ which happens when $\Gamma(h - i(n-m))$ itself is close to a pole. Accordingly, we write the following ansatz for the QNM frequency:

$$n = m - i(N + h - \epsilon\eta)\,, \tag{4.66}$$

where $\epsilon \equiv (-2im\kappa)^{2h-1} \ll 1$ for real h, and $N = 0, 1, 2, \ldots$ is the overtone number which enumerates the different poles. Then we can approximate,

$$\Gamma(h - i(n-m)) = \Gamma(-N + \epsilon\eta) \approx \frac{(-1)^N}{N!\,\epsilon\,\eta}\,, \tag{4.67}$$

so that $\mathcal{D}$ near the QNM frequencies may be written as:

$$\mathcal{D} \approx \epsilon\,(-1)^N\,N!\;(\eta - \eta_{QNM})\;, \tag{4.68}$$

with

$$\eta_{QNM} = \frac{\Gamma(1-2h)^2}{\Gamma(2h-1)^2}\frac{\Gamma(h-im)^2}{\Gamma(1-h-im)^2}\frac{(-1)^N}{N!\,\Gamma(1-2h-N)}\,. \tag{4.69}$$

So all the poles in (4.64) are simple poles in the lower complex $\hat{\omega}$ plane located at:

$$\hat{\omega}_{N\ell m} = \frac{1}{2M}\left[m - i\kappa(N+h)\right]\,. \tag{4.70}$$

Then, by the residue theorem, the QNM contribution to the waveform at asymptotic flat infinity is given by:

$$\Psi^{far}(r \to \infty) = \sum_{N,\,\ell,\,m} c_{N\ell m}\, e^{-i\hat{\omega}_{N\ell m}\hat{t}}\, e^{im\hat{\phi}}\, S_\ell(\theta)\, r^{-1+im} e^{imr/2}\,, \tag{4.71}$$

where the amplitudes are

$$\begin{aligned} c_{N\ell m} \;=\; & \frac{\lambda}{\sqrt{3}M}\frac{(-1)^{N-h}}{N!}(2\kappa)^h(3R_0/4)^{N+h}S_\ell(\pi/2)W_{im,h-\frac{1}{2}}(3im/2)\times \\ & \times (im)^{N+2h-2+im}e^{\pi m}(1-2h)\Gamma(h-im)^2/\Gamma(2h)^2\,. \end{aligned} \tag{4.72}$$

Finally, performing the sum over N we find:

$$\begin{aligned}
&\Psi^{far}(r\to\infty)\\
&=\sum_{\ell,m}\frac{3^{h-\frac{1}{2}}\lambda}{2^h M}(-1)^{-h}e^{3im/4}S_\ell(\pi/2)W_{im,h-\frac{1}{2}}\left(3im/2\right)(im)^{2h-2+im}e^{\pi m}\times\\
&\qquad\times\frac{(1-2h)\Gamma(h-im)^2}{\Gamma(2h)^2}\exp\left[-i\frac{m-i\kappa h}{2M}(\hat{t}-\hat{t}_0)-\frac{3im}{4\kappa}e^{-\frac{\kappa}{2M}(\hat{t}-\hat{t}_0)}\right]\times\\
&\qquad\times e^{im(\hat{\phi}-\hat{\phi}_0)}S_\ell(\theta)\,r^{-1+im}e^{imr/2}\,,
\end{aligned}\tag{4.73}$$

where we have used that $R_0=\kappa^{-1}e^{\kappa\hat{t}_0/(2M)}\,,\hat{\phi}_0=\hat{t}_0/(2M)+3/4$. We note that this QNM waveform is valid starting at times,

$$\exp\left[-\frac{\kappa}{2M}(\hat{t}-\hat{t}_0)\right]\sim\kappa\,,\tag{4.74}$$

so that in (4.73) we have $\Psi^{far}\sim\kappa^h$.

4.5 Gravitational radiation from a plunging star

In this section we repeat the analysis for the realistic case of plunging stars coupled to gravity rather than scalars. It is conceptually similar but slightly more intricate computationally.

4.5.1 Gravity analysis

In Chapter 2 the solution to the Teukolsky equation describing gravitational wave generation in NHEK due to a particle on (4.13-4.14) was found to be:

$$\psi^{(-2)}=\sum_{\ell,m}e^{im(\Phi+3R_0T/4)}S_\ell(\theta)R_{\ell m}(R)\,,\tag{4.75}$$

where $\psi^{(-2)}$ is a Newman-Penrose component of the Weyl tensor, S_ℓ are the spin-weighted spheroidal harmonics obeying

$$\frac{1}{\sin\theta}\partial_\theta(\sin\theta\,\partial_\theta S_\ell)+\left(K_\ell-\frac{m^2+s^2+2ms\cos\theta}{\sin^2\theta}-\frac{m^2}{4}\sin^2\theta-ms\cos\theta\right)S_\ell=0\,, \tag{4.76}$$

and $R_{\ell m}$ is:

$$R_{\ell m}(R)=\frac{1}{R_0^{-2s}W}\left[\mathcal{X}\,\Theta(R_0-R)\mathcal{W}(R)+\mathcal{Z}\,\Theta(R-R_0)\mathcal{M}(R)\right]+a_2\delta(R-R_0)\,, \tag{4.77}$$

with

$$\begin{aligned}
\mathcal{M}(R) &= R^{-s}\,M_{im+s,h-\frac{1}{2}}\left(-2i\Omega/R\right)\,,\\
\mathcal{W}(R) &= R^{-s}\,W_{im+s,h-\frac{1}{2}}\left(-2i\Omega/R\right)\,,\\
W &= 2i\Omega\frac{\Gamma(2h)}{\Gamma(h-im-s)}\,,\\
\mathcal{X} &= R_0\mathcal{M}'(R_0)(2sa_2-a_1-2a_2)+\mathcal{M}(R_0)(a_0-2sa_1-2sa_2+4s^2a_2-a_2V_s(R_0))\,,\\
\mathcal{Z} &= \mathcal{X}(\mathcal{M}\to\mathcal{W})\,,\\
V_s(R) &= 2m^2-K_\ell+s(s+1)+\frac{2\Omega(m-is)}{R}+\frac{\Omega^2}{R^2}\,,\\
a_0 &= \frac{m_0R_0^3}{16\sqrt{3}M^5}\left(40S+3imS-\frac{9}{8}m^2S+6mS'-16iS'-8S''\right)\,,\\
a_1 &= \frac{m_0R_0^3}{16\sqrt{3}M^5}\left(8iS'-3imS-16S\right)\,,\\
a_2 &= \frac{m_0R_0^3}{16\sqrt{3}M^5}2S\,.
\end{aligned}$$

Here S, S', S'' denote $S_\ell(\pi/2), S'_\ell(\pi/2), S''_\ell(\pi/2)$ respectively and $s=-2$ is understood. This solution obeys ingoing boundary conditions at the horizon and Neumann

at the boundary:

$$\begin{aligned}\psi^{(-2)}(R\to 0) &= \sum_{\ell,m} e^{im(\Phi+3R_0T/4)}\,S_\ell(\theta)\times \\ &\qquad \times\frac{\mathcal{X}}{R_0^4 W}(-2i\Omega)^{im-2}\,R^{-im+4}e^{-3imR_0/4R}\,, \qquad (4.78)\\ \psi^{(-2)}(R\to\infty) &= \sum_{\ell,m} e^{im(\Phi+3R_0T/4)}\,S_\ell(\theta)\times \\ &\qquad \times\frac{\mathcal{Z}}{R_0^4 W}(-2i\Omega)^{h}\,R^{-h+2}\,. \qquad (4.79)\end{aligned}$$

As in the scalar case, the solution to the Teukolsky equation in near-NHEK with a source due to a plunging particle on (4.9-4.10) and with the same boundary conditions, may be obtained by transforming the above NHEK solution via equations (4.12). However, a minor additional step is in order here. In NHEK the solution above describes metric perturbations according to $\psi^{(-2)} = (1-i\cos\theta)^4\delta\psi_4$ with the Weyl scalar $\psi_4 \equiv C_{\mu\nu\rho\sigma}n^\mu\bar{m}^\nu n^\rho\bar{m}^\sigma$ defined with respect to the NHEK Kinnersley tetrad

$$\begin{aligned}L^\mu &= \left(\frac{1}{R^2},1,0,-\frac{1}{R}\right)\,,\\ N^\mu &= \frac{1}{2M^2(1+\cos^2\theta)}\left(1,-R^2,0,-R\right)\,, \qquad (4.80)\\ M^\mu &= \frac{1}{\sqrt{2}M(1+i\cos\theta)}\left(0,0,1,\frac{i(1+\cos^2\theta)}{2\sin\theta}\right)\,.\end{aligned}$$

The transformation (4.12) takes this NHEK Kinnersley tetrad to a near-NHEK tetrad in which the spin coefficient $\epsilon \neq 0$ but in which l and n are still aligned along the repeated principal null directions of the Weyl tensor. Thus to get to the near-NHEK

Kinnersley tetrad,

$$\begin{aligned} l^\mu &= \left(\frac{1}{r(r+2\kappa)}, 1, 0, -\frac{r+\kappa}{r(r+2\kappa)}\right) , \\ n^\mu &= \frac{1}{2M^2(1+\cos^2\theta)} \left(1, -r(r+2\kappa), 0, -(r+\kappa)\right) , \\ m^\mu &= \frac{1}{\sqrt{2}M(1+i\cos\theta)} \left(0, 0, 1, \frac{i(1+\cos^2\theta)}{2\sin\theta}\right) , \end{aligned} \tag{4.81}$$

the transformation (4.12) needs to be followed by a (Class III) rotation $l \to (R/r)l\,, n \to (r/R)n$ which rotates,

$$\psi^{(-2)} \to \kappa^2 e^{-2\kappa t} \frac{r}{r+2\kappa}\, \psi^{(-2)} \,. \tag{4.82}$$

We do this primarily for later convenience when matching to the standard Kerr Teukolsky equation separated in the Kinnersley tetrad.

Using equations (4.26-4.29) followed by a Fourier transform we get:

$$\psi^{(-2)}(r\to 0) = \frac{1}{\sqrt{2\pi}} \int d\omega \sum_{\ell,m} \mathcal{I}\, e^{-i\omega t}\, e^{im\phi}\, S_\ell(\theta) r^{-\frac{i}{2}(m+\omega/\kappa)+2} \,, \tag{4.83}$$

$$\psi^{(-2)}(r\to \infty) = \frac{1}{\sqrt{2\pi}} \int d\omega \sum_{\ell,m} \mathcal{N}\, e^{-i\omega t}\, e^{im\phi}\, S_\ell(\theta) r^{-h+2} \,, \tag{4.84}$$

where

$$\mathcal{I} = \frac{1}{\sqrt{2\pi}} 2^{\frac{i}{2}(m-\omega/\kappa)} \frac{\mathcal{X}}{R_0^4 W} \kappa^{-1+\frac{i}{2}(m+\omega/\kappa)} (-2i\Omega)^{i\omega/\kappa} \Gamma(-2+im-i\omega/\kappa) \,, \tag{4.85}$$

$$\mathcal{N} = \frac{1}{\sqrt{2\pi}} 2^{h-i\omega/\kappa} \frac{\mathcal{Z}}{R_0^4 W} \kappa^{h-1} (-2i\Omega)^{i\omega/\kappa} \Gamma(h-i\omega/\kappa) \,. \tag{4.86}$$

For $\omega > 0, m > 0$, the graviton number flux at the horizon, to leading order in κ, is [55]:

$$\begin{aligned} \mathcal{F}_{\ell m\omega} &= \frac{8M^{10}}{\pi\kappa} \left|\frac{\mathcal{X}}{R_0^4 W}\right|^2 \frac{e^{-2\pi\omega/\kappa}}{|\mathcal{C}|^2} e^{\pi m} \,, \\ |\mathcal{C}|^2 &\equiv \left((K_\ell - m^2)^2 + m^2\right)\left((K_\ell - m^2 - 2)^2 + 9m^2\right) \,. \end{aligned} \tag{4.87}$$

4.5.2 Gravity/CFT matching

The source corresponding to the NHEK problem, as obtained from the leading term of the appropriate Hertz potential at the boundary, is given by (Chapter 2):

$$J_\ell(\Phi,T)=\sum_m \frac{4}{\mathcal{C}}\frac{\mathcal{X}}{R_0^{-2s}W}\frac{(-2i\Omega)^{1-h}\Gamma(2h-1)}{\Gamma(h-im-s)}\,e^{im(\Phi+3R_0T/4)}\,. \tag{4.88}$$

Now $\mathcal{O}_\ell$ carry weights [93] $h_R=h\,,h_L=h-s$ so that conformal invariance implies J_ℓ carry right weight $1-h$ and left weight $1-h+s$. Thus as in the scalar case, after the conformal transformation we find $J_\ell(\phi,t)$ given as in (4.42) with:

$$J_{\ell m\omega}=\frac{2^{3-h-i\omega/\kappa}}{\sqrt{2\pi}\,\mathcal{C}}\kappa^{-h}\frac{\mathcal{X}}{R_0^{-2s}W}(-2i\Omega)^{i\omega/\kappa}\Gamma(1-h-i\omega/\kappa)\frac{\Gamma(2h-1)}{\Gamma(h-im-s)}\,. \tag{4.89}$$

Using the above together with the operator normalization from Chapter 2,

$$C_{\mathcal{O}}=\frac{2^{h-1}M^5}{2\pi}\frac{\sqrt{\Gamma(2h+4)\Gamma(2h)}}{\Gamma(2h-1)}\,, \tag{4.90}$$

and plugging into Fermi's golden rule reproduces, to leading order in κ, the rate (4.87).

4.5.3 Reattaching the asymptotically flat region

Consider the full Teukolsky equation in Kerr for $\hat{\psi}^{(-2)}\equiv(\hat{r}-ia\cos\theta)^4\delta\hat{\psi}_4$ expanded in modes:

$$\hat{\psi}^{(-2)}=\frac{1}{\sqrt{2\pi}}\int d\hat{\omega}\sum_{\ell,m}e^{-i\hat{\omega}\hat{t}}e^{im\hat{\phi}}\hat{S}_\ell(\theta)\hat{R}_{\ell m\hat{\omega}}(\hat{r})\,. \tag{4.91}$$

In the near extremal, near superradiant regime (4.55), given the relations (4.56-4.57), we can match, across the entrance to the throat, an ingoing at the horizon solution of

the near-NHEK equation containing the source with a far Kerr vacuum solution that is purely outgoing at null infinity. The desired far solution is given by (Chapter 2):

$$\begin{aligned}\hat{R}^{far}_{\ell m\hat{\omega}}(r\to\infty) &= Q\,\frac{\Gamma(2-2h)}{\Gamma(1-h+im-s)}(im)^{h-1+im-s}\times \\ &\quad\times\left[1-\frac{(-im)^{2h-1}}{(im)^{2h-1}}\frac{\sin\pi(h+im)}{\sin\pi(h-im)}\right]r^{-1+im-2s}e^{imr/2}\,, \qquad (4.92)\\ \hat{R}^{far}_{\ell m\hat{\omega}}(r\to 0) &= P\,r^{h-1-s}+Q\,r^{-h-s}\,, \qquad (4.93)\end{aligned}$$

where

$$\frac{P}{Q}=-(-im)^{2h-1}\frac{\Gamma(2-2h)}{\Gamma(2h)}\frac{\Gamma(h-im+s)}{\Gamma(1-h-im+s)}\,. \qquad (4.94)$$

To match this with a solution of the near-NHEK equation,

$$\begin{aligned}&r(r+2\kappa)\hat{R}''_{\ell m\hat{\omega}}+2(s+1)(r+\kappa)\hat{R}'_{\ell m\hat{\omega}} \qquad (4.95)\\ &+\left[\frac{(mr+n\kappa)^2-2is(r+\kappa)(mr+n\kappa)}{r(r+2\kappa)}+2ism+m^2+s(s+1)-K_\ell\right]\hat{R}_{\ell m\hat{\omega}}=\hat{T}_{\ell m\hat{\omega}}\,,\end{aligned}$$

where the source $\hat{T}_{\ell m\hat{\omega}}$ is due to the plunging particle on (4.9-4.10), we need only adjust the Neumann boundary conditions of the solution found in section 4.5.1 to the leaky boundary conditions given in (4.93). This is done by adding an ingoing at the horizon homogeneous solution of (4.95),

$$\hat{R}^{near}_{in}=r^{-in/2-s}\left(\frac{r}{2\kappa}+1\right)^{i(n/2-m)-s}{}_2F_1\left(h-im-s\,,1-h-im-s\,,1-in-s\,,-\frac{r}{2\kappa}\right)\,, \qquad (4.96)$$

with the appropriate amplitude to match the Dirichlet mode of (4.93). Doing so we find (note that $\hat{\psi}^{(-2)}=M^6\psi^{(-2)}$):

$$\begin{aligned}&Q=2M^7\mathcal{N}\Bigg[1- \qquad (4.97)\\ &-(-2im\kappa)^{2h-1}\frac{\Gamma(1-2h)^2}{\Gamma(2h-1)^2}\frac{\Gamma(h-im-s)\Gamma(h-im+s)}{\Gamma(1-h-im-s)\Gamma(1-h-im+s)}\frac{\Gamma(h-i(n-m))}{\Gamma(1-h-i(n-m))}\Bigg]^{-1}\,,\end{aligned}$$

where $\mathcal{N}$ is given in (4.86). Plugging into equation (4.92) we obtain the full frequency domain solution at asymptotic flat infinity (for $m > 0$):

$$\begin{aligned}\hat{R}^{far}_{\ell m\hat{\omega}}(r\to\infty) = \frac{m_0 M^2}{6\sqrt{6\pi}}(-1)^{-h}(2\kappa)^{h-1}(3R_0/4)^{i(n-m)} \times \\ \times \frac{\gamma\,(im)^{h+in}e^{\pi m}(2h-1)\Gamma(2+h-im)\Gamma(-2+h-im)/\Gamma(2h)^2}{\frac{1}{\Gamma(h-i(n-m))} - (-2im\kappa)^{2h-1}\frac{\Gamma(1-2h)^2}{\Gamma(2h-1)^2}\frac{\Gamma(2+h-im)\Gamma(-2+h-im)}{\Gamma(3-h-im)\Gamma(-1-h-im)}\frac{1}{\Gamma(1-h-i(n-m))}} \times \\ \times\, r^{3+im}e^{imr/2}\,, \end{aligned} \tag{4.98}$$

where

$$\begin{aligned}\gamma \;=\; & 2\left[(h^2-h+6-im)S + 4(2i+m)S' - 4S''\right]W_{im-2,h-\frac{1}{2}}(3im/2) \\ & + \left[(4+3im)S - 8iS'\right]W_{im-1,h-\frac{1}{2}}(3im/2)\,. \end{aligned} \tag{4.99}$$

4.5.4 Quasinormal mode decomposition

As in the scalar case, the QNMs are determined by the zeros of the denominator in (4.98),

$$\begin{aligned}\mathcal{D} \;=\; & \frac{1}{\Gamma(h-i(n-m))} - \\ & -(-2im\kappa)^{2h-1}\frac{\Gamma(1-2h)^2}{\Gamma(2h-1)^2}\frac{\Gamma(2+h-im)\Gamma(-2+h-im)}{\Gamma(3-h-im)\Gamma(-1-h-im)}\frac{1}{\Gamma(1-h-i(n-m))}\,. \end{aligned} \tag{4.100}$$

This implies that the QNM frequencies are again as in (4.70) where $\mathcal{D}$ gives simple poles as in (4.68) with,

$$\eta_{QNM} = \frac{\Gamma(1-2h)^2}{\Gamma(2h-1)^2}\frac{\Gamma(2+h-im)\Gamma(-2+h-im)}{\Gamma(3-h-im)\Gamma(-1-h-im)}\frac{(-1)^N}{N!\,\Gamma(1-2h-N)}\,. \tag{4.101}$$

The QNM contribution to the waveform at asymptotic flat infinity is:

$$\begin{aligned}
&\psi^{(-2)}_{far}(r\to\infty)\\
&=\sum_{\ell,m}\frac{3^{h-\frac{3}{2}}m_0M}{2^{h+3}}(-1)^{-h}e^{3im/4}\,\gamma\,(im)^{2h+im}e^{\pi m}\times\\
&\qquad\times\frac{(2h-1)\Gamma(2+h-im)\Gamma(-2+h-im)}{\Gamma(2h)^2}\times\\
&\qquad\times\exp\left[-i\frac{m-i\kappa h}{2M}(\hat{t}-\hat{t}_0)-\frac{3im}{4\kappa}e^{-\frac{\kappa}{2M}(\hat{t}-\hat{t}_0)}\right]\times\\
&\qquad\times e^{im(\hat{\phi}-\hat{\phi}_0)}S_\ell(\theta)\,r^{3+im}e^{imr/2}\,,
\end{aligned}\tag{4.102}$$

where γ is given in (4.99).

Chapter 5

Fast plunges into Kerr black holes

5.1 Introduction

Properties of diffeomorphisms in general relativity imply that gravitational dynamics near the horizons of rapidly-rotating Kerr black holes (BHs) are constrained by an infinite-dimensional conformal symmetry [10, 11]. We refer to this as the 'weak' Kerr/CFT correspondence. It enables powerful analytic techniques developed in the study of two-dimensional conformal field theory (CFT) to be employed in the analysis of the near-horizon gravitational dynamics. The conjectured 'strong' Kerr/CFT correspondence (see [33, 34] for reviews) is that quantum gravity in the near-horizon region of such BHs is dual to a (warped) two-dimensional conformal field theory. This conjecture is relevant for the study of the quantum puzzles surrounding black holes. However, for some interesting questions strong Kerr/CFT is not needed. In particular weak Kerr/CFT is sufficient for questions which arise in observational astronomy [5, 7, 6].

One such question refers to gravitational radiation production by extreme-mass-ratio-inspirals (EMRIs) into near-extremal Kerr BHs. These systems are binaries which consist of a small compact object inspiralling into a much larger BH and are important candidates for direct gravitational wave (GW) detection by eLISA [12, 13, 14]. They are the focus of this thesis. For certain initial conditions, such as those furnished by separation events of binary systems passing near a supermassive BH, EMRIs consist of two stages [24, 19]: (i) a long quasi-circular inspiral followed by (ii) a quick plunge into the black hole from the innermost stable circular orbit (ISCO) at the edge of the accretion disk. For nearly extremal black holes, both near-ISCO circular orbits and the post-ISCO plunge take place deep in the near horizon region where Kerr/CFT predicts the extra conformal symmetry. More precisely, the latest part of stage (i) takes place in the near-horizon extreme Kerr (NHEK) geometry while the entire stage (ii) takes place in the near-horizon near-extreme Kerr (near-NHEK) geometry. Global $SL(2,R)$ conformal symmetry and local Virasoro conformal symmetry have been utilized in Chapters 2 and 4 to calculate the corresponding emitted gravitational waves during a near-ISCO circular orbit and the post-ISCO plunge, respectively. The analysis was entirely analytic – see [94, 95] for recent and compatible numerical analyses of this problem.[1]

Despite the fact that radiation reaction circularizes trajectories rather efficiently, most astrophysical relevant EMRIs are expected to have such large initial eccentricities that more than 50% of all observable EMRIs will end with plunges from

[1]The $SL(2,R)$ isometries have also been exploited in recent studies of BH magnetospheres [96, 97, 98] in order to find new analytical solutions to the equations of force-free electrodynamics in the extreme Kerr background.

a moderately eccentric last stable orbit [99]. Thus in this chapter we extend the analysis of Chapter 4, where only the special post-ISCO plunge was analyzed, and compute analytically the radiative signature of a new family of trajectories we call "fast plunges". These plunges are trajectories with arbitrary (near-)NHEK orbital energy which start at some finite time from the (near-)NHEK boundary. This is in contrast with the special post-ISCO plunge of [3] which comes in from the near-NHEK boundary in the infinite past. The fact that the fast plunges are soluble is again a direct consequence of the conformal symmetry: we show that they are related by conformal mapping to the circular orbit of Chapter 2. In this chapter we study a simplified version of the problem, replacing gravitational perturbations with a scalar field. The analysis is, however, readily generalizable to the linearized gravity case.

The holographic dual of the gravity problem with the geodesic particle on a circular orbit sourcing a bulk field may be understood as follows. The dual field theory is a CFT which is subject to an external driving source for the operator dual to the bulk field. The source is driving the system at a frequency given by the orbital frequency of the geodesic particle and induces a constant transition rate out of the initial state which matches exactly the bulk particle number flux down the BH horizon (Chapter 2). The holographic dual of the plunge problem has a richer dynamical evolution involving a quantum quench of the CFT that injects energy into the system which is subsequently thermalized and equilibrated. On the gravity side, the approach to equilibrium is characterized at late times by the quasinormal modes. As in Chapter 4, in this chapter we will only consider holographically the very high frequency limit, that is to say, we will only consider timescales which are much shorter than that of

the quench. In this case, we can again think of the CFT as being driven continuously by an external source throughout the entire period under study. The corresponding transition rates may then be obtained by conformal transformations in the CFT and we will see that the results remain in perfect agreement with the gravity calculations.

This chapter is organized as follows. In section 5.2 we analyze the fast NHEK plunge. In 5.2.1 we present the plunge trajectory and the mapping which takes it to a circular orbit. In 5.2.2 we use this mapping to compute the radiation emitted in the plunge. In 5.2.3 we perform the dual conformal field theory computation, and show the two agree. In 5.2.4 we reattach the asymptotically flat region and determine the radiation at future null infinity. In section 5.3 we repeat the above steps for the fast near-NHEK plunge.

5.2 Radiation from the fast NHEK plunge

The Kerr metric in Boyer-Lindquist coordinates is given by

$$ds^2 = -\frac{\Delta}{\hat{\rho}^2}\left(d\hat{t} - a\sin^2\theta\, d\hat{\phi}\right)^2 + \frac{\sin^2\theta}{\hat{\rho}^2}\left((\hat{r}^2+a^2)d\hat{\phi} - a\, d\hat{t}\right)^2 + \frac{\hat{\rho}^2}{\Delta}d\hat{r}^2 + \hat{\rho}^2 d\theta^2 \ , \quad (5.1)$$

where

$$\Delta = \hat{r}^2 - 2M\hat{r} + a^2 \ , \qquad \hat{\rho}^2 = \hat{r}^2 + a^2\cos^2\theta \ , \quad (5.2)$$

and is characterized by the BH mass M and angular momentum $J = aM$. The outer/inner horizons are situated at $r_\pm = M \pm \sqrt{M^2 - a^2}$. For extremal BHs $a = M$ and the NHEK geometry may be obtained by making the coordinate transformation

$$r = \frac{\hat{r} - r_+}{\epsilon\, r_+} \ , \qquad t = \frac{\epsilon\,\hat{t}}{2M} \ , \qquad \phi = \hat{\phi} - \frac{\hat{t}}{2M} \ , \quad (5.3)$$

and taking the limit $\epsilon \to 0$, keeping r, t finite. This effectively zooms into the near horizon region and yields the non-singular NHEK metric [10]:

$$ds^2 = 2M^2\Gamma(\theta)\left[-r^2dt^2 + \frac{dr^2}{r^2} + d\theta^2 + \Lambda(\theta)^2(d\phi + rdt)^2\right] , \tag{5.4}$$

where

$$\Gamma(\theta) = \frac{1+\cos^2\theta}{2} , \qquad \Lambda(\theta) = \frac{2\sin\theta}{1+\cos^2\theta} . \tag{5.5}$$

5.2.1 Trajectory & mapping

Consider the equatorial plunging trajectories of small (test) compact objects in NHEK with energy and angular momentum (per unit rest mass) given by

$$e = \frac{4M}{\sqrt{3}R_0} , \qquad l = \frac{2M}{\sqrt{3}} , \tag{5.6}$$

for arbitrary $R_0 > 0$. The solution for this trajectory is a fast NHEK plunge:

$$\begin{aligned} t(r) &= \frac{1}{r}\sqrt{1+R_0 r} , \\ \phi(r) &= \frac{3}{4}\sqrt{1+R_0 r} + \ln\frac{\sqrt{1+R_0 r}-1}{\sqrt{1+R_0 r}+1} + \Phi_0 . \end{aligned} \tag{5.7}$$

The mapping

$$\begin{aligned} T &= -\frac{r^2 t}{r^2t^2-1} , \\ R &= \frac{r^2t^2-1}{r} , \\ \Phi &= \phi + \ln\frac{rt+1}{rt-1} , \end{aligned} \tag{5.8}$$

maps the $rt \geq 1$ part of the NHEK patch (5.4) to the $RT \leq -1$ part of another NHEK patch (see Figure 5.1),

$$ds^2 = 2M^2\Gamma(\theta)\left[-R^2dT^2 + \frac{dR^2}{R^2} + d\theta^2 + \Lambda(\theta)^2(d\Phi + RdT)^2\right] . \tag{5.9}$$

The fast plunge trajectory (5.7) is mapped under (5.8) to

$$\begin{aligned} R &= R_0 \ , \\ \Phi &= -\frac{3}{4} R_0 T + \Phi_0 \ . \end{aligned} \tag{5.10}$$

The above, being a circular orbit, is a much simpler problem which has been solved, both in gravity and the CFT, in Chapter 2. Below we will use the transformation (5.8) in order to solve for the radiation produced during the fast plunge (5.7).

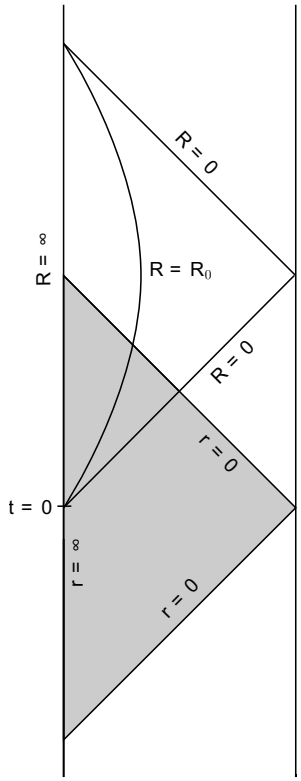

Figure 5.1: Penrose diagram with the fast NHEK plunge. Both upper (bounded by $R = 0$ and $R = \infty$) and lower (bounded by $r = 0$ and $r = \infty$, shaded) wedges are NHEK. The line $R = R_0$ is a circular orbit in the upper wedge. In the shaded wedge it plunges from the boundary $r = \infty$ at $t = 0$ into the future horizon $r = 0$.

5.2.2 Gravity analysis

Consider a star carrying scalar charge. The action for this system is given by

$$S = -\frac{1}{2}\int d^4x\sqrt{-g}\left[(\partial\Psi)^2 + 8\pi\lambda\Psi\mathcal{S}\right] \ , \tag{5.11}$$

where λ is a coupling constant and

$$\mathcal{S}(x) = -\int d\tau(-g)^{-1/2}\delta^{(4)}(x - x_*(\tau)) \ , \tag{5.12}$$

is the source term, with $x_*(\tau)$ the trajectory (5.7).

The solution for a star in a circular orbit in NHEK (5.10), with ingoing boundary condition at the horizon and Neumann at infinity, is (Chapter 2, setting $\Phi_0 = 0$):

$$\Psi = \sum_{\ell,m} e^{im(\Phi+3R_0T/4)}S_\ell(\theta)R^{(c)}_{\ell m}(R) \ , \tag{5.13}$$

where S_ℓ are NHEK spheroidal harmonics obeying

$$\frac{1}{\sin\theta}\partial_\theta(\sin\theta\partial_\theta S_\ell) + \left(K_\ell - \frac{m^2}{\sin^2\theta} - \frac{m^2}{4}\sin^2\theta\right)S_\ell = 0 \ , \tag{5.14}$$

and

$$R^{(c)}_{\ell m} = \frac{1}{W_\Omega}\left[X\,\Theta(R_0 - R)W_{im,h-1/2}\left(-2i\Omega/R\right) + Z\,\Theta(R - R_0)M_{im,h-1/2}\left(-2i\Omega/R\right)\right] . \tag{5.15}$$

In the above $W_{k,\mu}$, $M_{k,\mu}$ are Whittaker functions and

$$\begin{aligned}
\Omega &= -\frac{3mR_0}{4} \ , \\
h &= \frac{1}{2} + \sqrt{\frac{1}{4} + K_\ell - 2m^2} \ , \\
X &= -\frac{\sqrt{3}\lambda R_0}{2M}S_\ell\left(\pi/2\right)M_{im,h-1/2}\left(3im/2\right) \ , \\
Z &= -\frac{\sqrt{3}\lambda R_0}{2M}S_\ell\left(\pi/2\right)W_{im,h-1/2}\left(3im/2\right) \ , \\
W_\Omega &= 2i\Omega\frac{\Gamma(2h)}{\Gamma(h - im)} \ .
\end{aligned} \tag{5.16}$$

We will now compute the radiation produced by a star plunging into the black hole on the trajectory (5.7). As shown in section 5.2.1, this orbit is related to a circular orbit by (5.8). We use this mapping to generate the solution for fast plunge radiation directly from (5.13). It is important to note that the boundary condition of no incoming radiation from the past horizon in (5.4) implies no incoming radiation from the past horizon in (5.9), since for $rt < 1$ in (5.4) $\Psi = 0$ (see Figure 5.1).

Solution at the boundary. For fixed t, ϕ and $r \to \infty$

$$\begin{aligned} R &\approx r\,t^2 \to \infty \,, \\ T &\approx -\frac{1}{t} \,, \\ \Phi &\approx \phi \,. \end{aligned} \tag{5.17}$$

Using

$$M_{im,h-1/2}\,(-2i\Omega/R)\big|_{R\to\infty} \;\to\; (-2i\Omega)^h R^{-h} \,, \tag{5.18}$$

we obtain

$$R^{(c)}_{\ell m}\Big|_{r\to\infty} \;\approx\; \frac{Z}{W_\Omega}(-2i\Omega)^h t^{-2h} r^{-h} \,, \tag{5.19}$$

Putting this together, the solution (5.13) near the boundary is

$$\Psi|_{r\to\infty} = \Theta(t) \sum_{\ell,m} e^{im\left(\phi - \frac{3R_0}{4t}\right)} S_\ell(\theta) \left[\frac{Z}{W_\Omega}(-2i\Omega)^h\right] t^{-2h} r^{-h} \,, \tag{5.20}$$

where the Heaviside Θ-function is added since $\Psi(t<0) = 0$. In terms of the Fourier decomposition

$$\Psi|_{r\to\infty} = \frac{1}{\sqrt{2\pi}} \int d\omega \sum_{\ell,m} e^{i(m\phi - \omega t)} S_\ell(\theta)\, R^\infty_{\ell m\omega}(r) \,, \tag{5.21}$$

we find

$$R^{\infty}_{\ell m\omega} = \sqrt{\frac{2}{\pi}}\left[\frac{Z}{W_\Omega}(-2i\Omega)^h\right]\left(\frac{3mR_0}{4\omega}\right)^{1/2-h} ie^{i\pi h}\cos(2\pi h)\,K_{2h-1}\left(\sqrt{3mR_0\omega}\right)\,r^{-h}\,, \tag{5.22}$$

where K_ν is the modified Bessel function of the second kind and we take $\omega > 0$ and real $h < 1$ for simplicity.

Solution at future horizon. For $r \to 0$ with fixed $v \equiv t - 1/r$ and ϕ,

$$\begin{aligned} R &\approx 2v\,, \\ T &\approx -\frac{1}{2v}\,, \\ \Phi &\approx \phi + \ln\frac{2}{rv}\,. \end{aligned} \tag{5.23}$$

The solution near the horizon, for $v > 0$, is given by

$$\Psi_{hor} = \sum_{\ell,m} e^{im\phi}S_\ell(\theta)\left(\frac{2}{rv}\right)^{im} e^{-\frac{3imR_0}{8v}}R^{(c)}_{\ell m}(2v)\,, \tag{5.24}$$

while $\Psi(v<0) = 0$. In terms of the Fourier decomposition

$$\Psi_{hor} = \frac{1}{\sqrt{2\pi}}\int d\omega \sum_{\ell,m} e^{i(m\phi-\omega t)}S_\ell(\theta)\,R^{hor}_{\ell m\omega}(r)\,, \tag{5.25}$$

$$R^{hor}_{\ell m\omega} = \left(\frac{2}{r}\right)^{im} e^{i\frac{\omega}{r}}\frac{X}{W_\Omega}\frac{1}{\sqrt{2\pi}}\int_0^\infty dv\, e^{i\omega v}v^{-im}e^{-\frac{3imR_0}{8v}}W_{im,h-1/2}\left(\frac{3imR_0}{4v}\right) \tag{5.26}$$

where in (5.26) we consider the high frequency limit $\omega R_0 \gg 1$, so only the $v < R_0/2$ part contributes to the Fourier transform. The integral in (5.26) can be directly evaluated, then approximated using $\omega R_0 \gg 1$ to yield, for $\omega, m > 0$ and real $h < 1$,

$$\begin{aligned} R^{hor}_{\ell m\omega} &= \left(\frac{2}{r}\right)^{im} e^{i\frac{\omega}{r}}\frac{X}{W_\Omega}\frac{1}{\sqrt{2\pi}}\,i\,e^{\frac{\pi m}{2}}\,\omega^{-\frac{1}{2}+im}\sqrt{3mR_0}\,K_{2h-1}\left(\sqrt{3mR_0\omega}\right) \\ &\approx \frac{i}{2}\frac{X}{W_\Omega}2^{im}\,(3mR_0\omega)^{\frac{1}{4}}\,\omega^{-1+im}\,e^{\frac{\pi m}{2}}\,e^{-\sqrt{3mR_0\omega}}\,r^{-im}\,e^{i\frac{\omega}{r}}\,. \end{aligned} \tag{5.27}$$

The particle number flux down the horizon, as obtained by integrating the Klein-Gordon current $J^\mu = \frac{i}{8\pi}(\Psi^*\nabla\Psi - \Psi\nabla\Psi^*)$, is given for $\omega R_0 \gg 1$ by

$$\mathcal{F}_{\ell m\omega} = -\int \sqrt{-g} J^r d\theta d\phi \approx \frac{M^2}{8\pi}\left|\frac{X}{W_\Omega}\right|^2 \sqrt{\frac{3mR_0}{\omega}} e^{\pi m} e^{-2\sqrt{3mR_0\omega}} \ . \tag{5.28}$$

5.2.3 CFT analysis

Holographically, the introduction of a geodesic particle in the NHEK bulk may be understood as a particular deformation of the boundary CFT via an external driving source

$$S = S_{CFT} + \sum_\ell \int J_\ell(\Phi, T)\mathcal{O}_\ell(\Phi, T) d\Phi dT \ . \tag{5.29}$$

Here $\mathcal{O}_\ell$ are CFT operators with left and right weights h and for the circular orbit (5.10) it was shown in Chapter 2 that the source is given by

$$J_\ell = \sum_m \frac{X}{W_\Omega}(-2i\Omega)^{1-h}\frac{\Gamma(2h-1)}{\Gamma(h-im)} e^{im\Phi - i\Omega T} \ . \tag{5.30}$$

It follows from conformal invariance of (5.29) that J_ℓ carry left and right weights $1-h$. The transformation (5.8) induces the following $SL(2,R)$ conformal transformation on the boundary

$$\begin{aligned} T &= -\frac{1}{t} \ , \\ \Phi &= \phi \ . \end{aligned} \tag{5.31}$$

The transformed sources corresponding to the fast plunging star are therefore given by

$$J_\ell(\phi, t) = \Theta(t) t^{2h-2} \sum_m \frac{X}{W_\Omega}(-2i\Omega)^{1-h}\frac{\Gamma(2h-1)}{\Gamma(h-im)} e^{im\phi + i\Omega/t} \ , \tag{5.32}$$

and the step function $\Theta(t)$ is added because the quench is performed at $t = 0$ (see figure 5.1). As explained in the introduction, in this thesis we will only consider the high frequency limit $\omega R_0 \gg 1$ which allows us to apply Fermi's golden rule and compare the constant transition rate out of the vacuum with the particle number flux (5.28). In this limit, in terms of the Fourier decomposition, the sources are, for $\omega, m > 0$ and real $h < 1$,

$$\begin{aligned} J_\ell(\phi, t) &= \frac{1}{\sqrt{2\pi}} \int d\omega \sum_m J_{\ell m\omega} e^{i(m\phi - \omega t)} \ , \\ J_{\ell m\omega} &= \frac{X}{W_\Omega} \frac{\Gamma(2h-1)}{\Gamma(h-im)} (3mR_0\omega)^{1/4} (2\omega)^{-h} \ e^{\frac{i\pi h}{2} - \sqrt{3mR_0\omega}} \ . \end{aligned} \tag{5.33}$$

The transition rate out of the vacuum state is given by Fermi's golden rule [31, 52]

$$\mathcal{R} = \int d\omega \sum_{\ell,m} |J_{\ell m\omega}|^2 \int d\phi \, dt \, e^{i(\omega t - m\phi)} G(\phi, t) \ , \tag{5.34}$$

where $G(\phi, t) = \langle \mathcal{O}^\dagger(\phi, t) \mathcal{O}(0, 0) \rangle_{T_L}$ is the two point function of the CFT with left temperature $T_L = 1/(2\pi)$ and an angular potential [51]. Performing the integrals over t, ϕ with the appropriate $i\epsilon$ prescription and the operator normalization $C_\mathcal{O} = 2^{h-1}(2h-1)M/(2\pi)$ found in Chapter 2, we find perfect agreement with the bulk flux computation:

$$\mathcal{R}_{\ell m\omega} = \frac{M^2}{8\pi} \left| \frac{X}{W_\Omega} \right|^2 \sqrt{\frac{3mR_0}{\omega}} e^{\pi m} e^{-2\sqrt{3mR_0\omega}} = \mathcal{F}_{\ell m\omega} \ . \tag{5.35}$$

5.2.4 Gluing to asymptotically flat region

In section 5.2.2 we computed a particular solution for the scalar field with Neumann (reflecting) boundary conditions at the boundary of NHEK. Here we reattach the asymptotically flat region of extreme Kerr while allowing radiation to leak outside of NHEK, imposing a boundary condition of purely outgoing waves at future null

infinity in the full Kerr spacetime (keeping $\Psi = 0$ at the past horizon). We give only partial details of the matched asymptotic expansions procedure; for more details, see Chapter 2.

We expand the scalar field on extreme Kerr in Boyer-Lindquist coordinate (5.1) modes:

$$\Psi = \frac{1}{\sqrt{2\pi}} \int d\hat{\omega} \sum_{\ell,m} e^{i(m\hat{\phi}-\hat{\omega}\hat{t})}\, \hat{S}_\ell(\theta)\, \hat{R}_{\ell m\hat{\omega}}(\hat{r}) \ , \tag{5.36}$$

where $\hat{S}_\ell(\theta)$ are extreme Kerr spheroidal harmonics and $\hat{R}_{\ell m\hat{\omega}}(\hat{r})$ are radial wavefunctions. Modes penetrate the near-horizon region only if their frequency is close to the superradiant bound

$$\omega = 2M\hat{\omega} - m \ll 1 \ . \tag{5.37}$$

In this case, to leading order in ω, the extreme Kerr spheroidal harmonics identify with those of NHEK, $\hat{S}_\ell(\theta) = S_\ell(\theta)$. The radial wavefunction admits two useful approximations. The *near-horizon* region $r \ll 1$ corresponds to NHEK: the solution of section 5.2.2 is valid there. In the *far* region $r \gg \omega$ the radial equation simplifies, allowing again a solution in terms of Whittaker functions. For our choice of boundary conditions, the far region solution behaves asymptotically as

$$\begin{aligned}
\hat{R}^{far}_{\ell m\hat{\omega}}(r\to\infty) &= Q\,\frac{\Gamma(2-2h)}{\Gamma(1-h+im)}\,(im)^{h-1+im}\,\times \\
&\quad \times\left[1-\frac{(-im)^{2h-1}\sin\pi(h+im)}{(im)^{2h-1}\sin\pi(h-im)}\right] r^{-1+im}\,e^{imr/2} \ , \\
\hat{R}^{far}_{\ell m\hat{\omega}}(r\to 0) &= Q\left[r^{-h}-(-im)^{2h-1}\,\frac{\Gamma(2-2h)\Gamma(h-im)}{\Gamma(2h)\Gamma(1-h-im)}\,r^{h-1}\right] \ ,
\end{aligned} \tag{5.38}$$

where Q is a coefficient determined by the matching condition.

Gluing the asymptotically flat region is done by matching of asymptotic expansions in the near and far regions. In the near region the desired solution is found by adding to the particular solution of section 5.2.2 the ingoing homogeneous solution $R_{hom} = W_{im,h-1/2}\,(-2i\omega/r)$, with the appropriate amplitude $\mathcal{C}$, such that the horizon boundary conditions are not spoiled but radiation is allowed to leak outside the NHEK boundary. The matching condition then determines the constants $Q, \mathcal{C}$ and fixes the wavefunction uniquely. In particular, the waveform at infinity, for $m > 0$, $\omega > 0$ and real $h < 1$, is given by

$$\begin{aligned}\hat{R}_{\ell m\hat{\omega}}(r\to\infty) = \frac{\lambda}{\pi}\sqrt{\frac{R_0}{2\pi}}\; 2^h\, i e^{i\pi h}\, \sin(4\pi h)\; e^{\pi m/2}\; m^{h+im-3/2}\;\times \\ \times\, S_\ell(\pi/2)\, W_{im,h-1/2}(3im/2)\,\frac{\Gamma(1-2h)}{\Gamma(2h-1)}\Gamma(h-im)^2\,\omega^{h-1/2}\,K_{2h-1}\left(\sqrt{3mR_0\omega}\right)\times \\ \times\left[1-(-2i\omega)^{2h-1}(-im)^{2h-1}\frac{\Gamma(1-2h)^2\Gamma(h-im)^2}{\Gamma(2h-1)^2\Gamma(1-h-im)^2}\right]^{-1} r^{-1+im}e^{imr/2}\,. \end{aligned} \tag{5.39}$$

5.3 Radiation from the fast near-NHEK plunge

The near-NHEK geometry may be obtained by starting with a near-extremal Kerr BH characterized by

$$a = M\sqrt{1-(\kappa\epsilon)^2}\,, \tag{5.40}$$

making the coordinate transformation (5.3) and taking the limit $\epsilon \to 0$. This yields the nonsingular near-horizon metric near-NHEK [51]

$$ds^2 = 2M^2\Gamma(\theta)\left[-r(r+2\kappa)dt^2 + \frac{dr^2}{r(r+2\kappa)} + d\theta^2 + \Lambda(\theta)^2(d\phi+(r+\kappa)dt)^2\right] \tag{5.41}$$

5.3.1 Trajectory & mapping

Fast near-NHEK plunges with energy and angular momentum (per unit rest mass)

$$e = \frac{2M\kappa}{\sqrt{3}R_0} \ , \qquad l = \frac{2M}{\sqrt{3}} \ , \tag{5.42}$$

for arbitrary $R_0 > 0$, are given by

$$\begin{aligned} t(r) &= \frac{1}{2\kappa} \ln \frac{r + \kappa(1+R_0) + \sqrt{\kappa}\sqrt{2R_0 r + \kappa(1+R_0)^2}}{r + \kappa(1+R_0) - \sqrt{\kappa}\sqrt{2R_0 r + \kappa(1+R_0)^2}} \ , \\ \phi(r) &= \frac{3}{4\sqrt{\kappa}} \sqrt{2R_0 r + \kappa(1+R_0)^2} \\ &+ \frac{1}{2} \ln \frac{R_0 r + \kappa(1+R_0) - \sqrt{\kappa}\sqrt{2R_0 r + \kappa(1+R_0)^2}}{R_0 r + \kappa(1+R_0) + \sqrt{\kappa}\sqrt{2R_0 r + \kappa(1+R_0)^2}} + \Phi_0 \ . \end{aligned} \tag{5.43}$$

The transformation

$$\begin{aligned} T &= -\frac{\sqrt{r(r+2\kappa)}\sinh\kappa t}{\sqrt{r(r+2\kappa)}\cosh\kappa t - (r+\kappa)} \ , \\ R &= \frac{1}{\kappa}\left[\sqrt{r(r+2\kappa)}\cosh\kappa t - (r+\kappa)\right] \ , \\ \Phi &= \phi - \frac{1}{2}\ln\frac{\sqrt{r(r+2\kappa)} - (r+\kappa)\cosh\kappa t + \kappa\sinh\kappa t}{\sqrt{r(r+2\kappa)} - (r+\kappa)\cosh\kappa t - \kappa\sinh\kappa t} \ , \end{aligned} \tag{5.44}$$

maps the $\kappa t + \ln\sqrt{r/(r+2\kappa)} \geq 0$ part of the near-NHEK geometry (5.41) to the $T+1/R \leq -1$ part of the geometry (5.9). The fast plunge trajectory (5.43) is mapped under (5.44) to the circular NHEK orbit (5.10) (see Figure 5.2).

5.3.2 Gravity analysis

Consider a fast near-NHEK plunging scalar-charged star with trajectory (5.43). This system is described by the action (5.11) with source term (5.12). The solution in the case of a circular orbit in NHEK (5.10), as found in Chapter 2, was given in section 5.2.2. Here, we compute the radiation produced by the fast near-NHEK plunge (5.43),

using the mapping (5.44). Performing this transformation on the solution (5.13) gives the desired solution here (setting $\Phi_0 = 0$). As in the fast NHEK plunge, the condition of no-incoming radiation from the past horizon in (5.41) implies no-incoming radiation from the past horizon in (5.9) (see Figure 5.2).

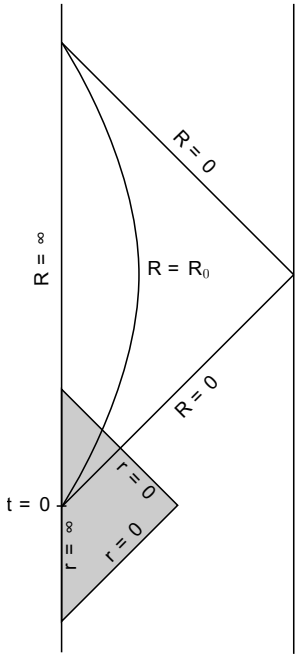

Figure 5.2: Penrose diagram with the fast near-NHEK plunge. The upper (bounded by $R = 0$ and $R = \infty$) wedge is NHEK. The lower (bounded by $r = 0$ and $r = \infty$) shaded wedge is near-NHEK. The line $R = R_0$ is a circular orbit in the upper wedge. In the shaded wedge it plunges from the boundary $r = \infty$ at $t = 0$ into the near-NHEK future horizon $r = 0$.

Solution at the boundary. For fixed t, ϕ and $r \to \infty$

$$\begin{aligned} R &\approx \frac{2r}{\kappa} \sinh^2 \frac{\kappa t}{2} \to \infty \,, \\ T &\approx -\coth \frac{\kappa t}{2} \,, \\ \Phi &\approx \phi \,. \end{aligned} \tag{5.45}$$

Putting this together and using (5.18), the solution near the boundary, for $t > 0$, is

$$\Psi|_{r\to\infty} = \left[\left(\frac{\kappa}{2}\right)^h \frac{Z}{W_\Omega} (-2i\Omega)^h \right] \frac{1}{\sqrt{2\pi}} \int d\omega \sum_{\ell,m} N_{\ell m\omega}\, e^{i(m\phi-\omega t)} S_\ell(\theta)\, r^{-h} \,, \tag{5.46}$$

with

$$N_{\ell m\omega} = \frac{1}{\sqrt{2\pi}} \int_0^\infty dt\, e^{i\omega t}\, e^{-\frac{3imR_0}{4}\coth\frac{\kappa t}{2}} \left(\sinh\frac{\kappa t}{2}\right)^{-2h} \,. \tag{5.47}$$

Solution at future horizon. For $r \to 0$ with fixed $v \equiv \kappa t + \ln\sqrt{r/(r+2\kappa)}$ and ϕ,

$$\begin{aligned} R &\approx e^v - 1 \,, \\ T &\approx -\frac{1}{1-e^{-v}} \,, \\ \Phi &\approx \phi - \ln(1-e^{-v}) - \ln\sqrt{\frac{r}{2\kappa}} \,. \end{aligned} \tag{5.48}$$

The solution near the horizon, for $v > 0$, is given by

$$\Psi_{hor} = \sum_{\ell,m} e^{im\phi} S_\ell(\theta) \left(\frac{r}{2\kappa}\right)^{-\frac{im}{2}} \left(1-e^{-v}\right)^{-im} e^{-\frac{3imR_0}{4(1-e^{-v})}} R^{(c)}_{\ell m}(e^v - 1) \,. \tag{5.49}$$

In terms of the Fourier decomposition

$$\begin{aligned} \Psi_{hor} &= \frac{1}{\sqrt{2\pi}} \int d\omega \sum_{\ell,m} e^{i(m\phi-\omega t)} S_\ell(\theta)\, R^{hor}_{\ell m\omega}(r) \,, \\ R^{hor}_{\ell m\omega} &= \left(\frac{r}{2\kappa}\right)^{-\frac{i}{2}\left(\frac{\omega}{\kappa}+m\right)} \frac{X}{W_\Omega} \frac{\kappa^{-1}}{\sqrt{2\pi}} \int_0^\infty dv\, e^{i\frac{\omega}{\kappa}v} \left(1-e^{-v}\right)^{-im} e^{-\frac{3imR_0}{4(1-e^{-v})}} W_{im,h-1/2}\left(\frac{3imR_0}{2(e^v-1)}\right) \,, \end{aligned}$$

where as in (5.26) we consider the high frequency limit $\omega/\kappa \gg 1$ and disregard the $v > \ln(1+R_0)$ part of the Fourier integral. The remaining integral above may be evaluated approximately using $\omega/\kappa \gg 1$ to obtain, for $\omega, m > 0$ and real $h < 1$,

$$R^{hor}_{\ell m\omega} \approx \frac{i}{2}\frac{X}{W_\Omega} 2^{\frac{i}{2}\left(\frac{\omega}{\kappa}+m\right)} \left(\frac{6mR_0\omega}{\kappa}\right)^{1/4} \omega^{-1+im}\,\kappa^{\frac{i}{2}\left(\frac{\omega}{\kappa}-m\right)}\, e^{\frac{\pi m}{2}}\, e^{-\sqrt{\frac{6mR_0\omega}{\kappa}}}\, r^{-\frac{i}{2}\left(\frac{\omega}{\kappa}+m\right)} .$$

The particle number flux down the horizon is thus given, for $\omega/\kappa \gg 1$, by

$$\mathcal{F}_{\ell m\omega} \approx \frac{M^2}{4\pi}\left|\frac{X}{W_\Omega}\right|^2 \sqrt{\frac{3mR_0}{2\omega\kappa}}\, e^{\pi m}\, e^{-2\sqrt{\frac{6mR_0\omega}{\kappa}}} . \tag{5.50}$$

5.3.3 CFT analysis

The transformation (5.44) induces the following conformal transformation on the boundary

$$\begin{aligned} T &= -\coth\frac{\kappa t}{2} , \\ \Phi &= \phi . \end{aligned} \tag{5.51}$$

Note that this is not one of the global $SL(2,R)$ transformations, instead it is one of the local Virasoro symmetries of Kerr/CFT. After this conformal transformation the CFT source (5.30) becomes

$$J_\ell(\phi,t) = \Theta(t)\left(\frac{\kappa}{2}\right)^{1-h}\left(\sinh\frac{\kappa t}{2}\right)^{2h-2}\sum_m \frac{X}{W_\Omega}(-2i\Omega)^{1-h}\frac{\Gamma(2h-1)}{\Gamma(h-im)}\, e^{im\phi+i\Omega\coth\frac{\kappa t}{2}} \tag{5.52}$$

The Fourier decomposition in the $\omega/\kappa \gg 1$ limit, for $\omega, m > 0$ and real $h < 1$, is

$$\begin{aligned} J_\ell(\phi,t) &= \frac{1}{\sqrt{2\pi}}\int d\omega \sum_m J_{\ell m\omega} e^{i(m\phi-\omega t)} , \\ J_{\ell m\omega} &\approx \frac{X}{W_\Omega}\frac{\Gamma(2h-1)}{\Gamma(h-im)}\left(\frac{6mR_0\omega}{\kappa}\right)^{1/4}(2\omega)^{-h}\, e^{\frac{i\pi h}{2}-\sqrt{\frac{6mR_0\omega}{\kappa}}} . \end{aligned} \tag{5.53}$$

The transition rate out of the vacuum state, given by Fermi's golden rule (5.34) with $G(\phi,t)=\langle\mathcal{O}^\dagger(\phi,t)\mathcal{O}(0,0)\rangle_{T_L,T_R}$ the two point function of the CFT at $T_L=\frac{1}{2\pi}$, $T_R=\frac{\kappa}{2\pi}$ and an angular potential. Performing the integrals, we find for $\omega/\kappa\gg 1$,

$$\mathcal{R}_{\ell m\omega}=\frac{M^2}{4\pi}\left|\frac{X}{W_\Omega}\right|^2\sqrt{\frac{3mR_0}{2\omega\kappa}}e^{\pi m}e^{-2\sqrt{\frac{6mR_0\omega}{\kappa}}}=\mathcal{F}_{\ell m\omega}\ . \tag{5.54}$$

which establishes perfect agreement with the bulk gravity computation.

5.3.4 Gluing to asymptotically flat region

To compute radiation at future null infinity, we reattach the asymptotically flat region of the full near-extremal Kerr to our near-NHEK and glue solutions via matched asymptotic expansions. This is done in a similar manner to that described in section 5.2.4 for exactly extremal Kerr. Details of the procedure may be found in [3]; here we will directly state the final result.

We expand the scalar field in Kerr as in (5.36). Via the dimensionless Hawking temperature $\tau_H=(r_+-r_-)/r_+$ and horizon angular velocity $\Omega_H=a/(2Mr_+)$, we define a rescaled near-superradiant frequency

$$n\equiv 4M\,\frac{\hat{\omega}-m\Omega_H}{\tau_H}\ . \tag{5.55}$$

We can then perform matched asymptotic expansions for $\max(\tau_H,n\tau_H)\ll 1$. The waveform at future null infinity, for $m>0$, is given by

$$\begin{aligned}\hat{R}_{\ell m\hat{\omega}}(r\to\infty)=&\frac{\lambda}{\pi}R_0^h\,2^{2-3h}\,3^{h-1/2}\,\tau_H^{h-1}\,\sin(2\pi h)\,e^{\pi m/2}\,m^{2h+im-2}\times\\&\times S_\ell(\pi/2)\,W_{im,h-1/2}(3im/2)\,\frac{\Gamma(1-2h)}{\Gamma(2h-1)}\Gamma(h-im)^2\,\mathcal{N}\times\\&\times\left[1-(-im\tau_H)^{2h-1}\frac{\Gamma(1-2h)^2\Gamma(h-im)^2}{\Gamma(2h-1)^2\Gamma(1-h-im)^2}\frac{\Gamma(h-i(n-m))}{\Gamma(1-h-i(n-m))}\right]^{-1}\times\\&\times r^{-1+im}e^{imr/2}\,,\end{aligned} \tag{5.56}$$

where $\mathcal{N}$ is the integral (5.47):

$$\mathcal{N} = \frac{1}{\sqrt{2\pi}} \int_0^\infty dy\, e^{i(n-m)y}\, e^{-\frac{3imR_0}{4}\coth\frac{y}{2}} \left(\sinh\frac{y}{2}\right)^{-2h} \quad . \tag{5.57}$$

Bibliography

[1] A. P. Porfyriadis and A. Strominger, "Gravity waves from the Kerr/CFT correspondence," *Phys. Rev.* **D90** (2014), no. 4 044038, [arXiv:1401.3746].

[2] S. E. Gralla, A. P. Porfyriadis, and N. Warburton, "Particle on the Innermost Stable Circular Orbit of a Rapidly Spinning Black Hole," *Phys. Rev.* **D92** (2015), no. 6 064029, [arXiv:1506.08496].

[3] S. Hadar, A. P. Porfyriadis, and A. Strominger, "Gravity Waves from Extreme-Mass-Ratio Plunges into Kerr Black Holes," *Phys. Rev.* **D90** (2014), no. 6 064045, [arXiv:1403.2797].

[4] S. Hadar, A. P. Porfyriadis, and A. Strominger, "Fast plunges into Kerr black holes," *JHEP* **07** (2015) 078, [arXiv:1504.07650].

[5] J. E. McClintock, R. Shafee, R. Narayan, R. A. Remillard, S. W. Davis, and L.-X. Li, "The Spin of the Near-Extreme Kerr Black Hole GRS 1915+105," *Astrophys. J.* **652** (2006) 518–539, [astro-ph/0606076].

[6] L. Gou, J. E. McClintock, R. A. Remillard, J. F. Steiner, M. J. Reid, J. A. Orosz, R. Narayan, M. Hanke, and J. García, "Confirmation Via the Continuum-Fitting Method that the Spin of the Black Hole in Cygnus X-1 is Extreme," *Astrophys. J.* **790** (2014), no. 1 29, [arXiv:1308.4760].

[7] L. W. Brenneman and C. S. Reynolds, "Constraining Black Hole Spin Via X-ray Spectroscopy," *Astrophys. J.* **652** (2006) 1028–1043, [astro-ph/0608502].

[8] C. S. Reynolds, "Measuring Black Hole Spin using X-ray Reflection Spectroscopy," *Space Sci. Rev.* **183** (2014), no. 1-4 277–294, [arXiv:1302.3260].

[9] L. Brenneman, "Measuring Supermassive Black Hole Spins in Active Galactic Nuclei," arXiv:1309.6334.

[10] J. M. Bardeen and G. T. Horowitz, "The Extreme Kerr throat geometry: A Vacuum analog of $AdS_2 \times S^2$," *Phys. Rev.* **D60** (1999) 104030, [hep-th/9905099].

[11] M. Guica, T. Hartman, W. Song, and A. Strominger, "The Kerr/CFT Correspondence," *Phys. Rev.* **D80** (2009) 124008, [arXiv:0809.4266].

[12] L. S. Finn and K. S. Thorne, "Gravitational waves from a compact star in a circular, inspiral orbit, in the equatorial plane of a massive, spinning black hole, as observed by LISA," *Phys. Rev.* **D62** (2000) 124021, [gr-qc/0007074].

[13] J. R. Gair, L. Barack, T. Creighton, C. Cutler, S. L. Larson, E. S. Phinney, and M. Vallisneri, "Event rate estimates for LISA extreme mass ratio capture sources," *Class. Quant. Grav.* **21** (2004) S1595–S1606, [gr-qc/0405137].

[14] eLISA. http://www.elisascience.org.

[15] S. A. Hughes, "The Evolution of circular, nonequatorial orbits of Kerr black holes due to gravitational wave emission," *Phys. Rev.* **D61** (2000), no. 8 084004, [gr-qc/9910091]. [Erratum: Phys. Rev.D90,no.10,109904(2014)].

[16] S. A. Hughes, "Evolution of circular, nonequatorial orbits of Kerr black holes due to gravitational wave emission. II. Inspiral trajectories and gravitational wave forms," *Phys. Rev.* **D64** (2001) 064004, [gr-qc/0104041]. [Erratum: Phys. Rev.D88,no.10,109902(2013)].

[17] Y. Mino, "Perturbative approach to an orbital evolution around a supermassive black hole," *Phys. Rev.* **D67** (2003) 084027, [gr-qc/0302075].

[18] T. Hinderer and E. E. Flanagan, "Two timescale analysis of extreme mass ratio inspirals in Kerr. I. Orbital Motion," *Phys. Rev.* **D78** (2008) 064028, [arXiv:0805.3337].

[19] S. Hadar and B. Kol, "Post-ISCO Ringdown Amplitudes in Extreme Mass Ratio Inspiral," *Phys. Rev.* **D84** (2011) 044019, [arXiv:0911.3899].

[20] Y. Pan, A. Buonanno, R. Fujita, E. Racine, and H. Tagoshi, "Post-Newtonian factorized multipolar waveforms for spinning, non-precessing black-hole binaries," *Phys. Rev.* **D83** (2011) 064003, [arXiv:1006.0431]. [Erratum: Phys. Rev.D87,no.10,109901(2013)].

[21] N. Yunes, A. Buonanno, S. A. Hughes, Y. Pan, E. Barausse, M. C. Miller, and W. Throwe, "Extreme Mass-Ratio Inspirals in the Effective-One-Body Approach: Quasi-Circular, Equatorial Orbits around a Spinning Black Hole," *Phys. Rev.* **D83** (2011) 044044, [arXiv:1009.6013]. [Erratum: Phys. Rev.D88,no.10,109904(2013)].

[22] Z. Zhang, N. Yunes, and E. Berti, "Accuracy of the post-Newtonian approximation. II. Optimal asymptotic expansion of the energy flux for quasicircular, extreme mass-ratio inspirals into a Kerr black hole," *Phys. Rev.* **D84** (2011) 024029, [arXiv:1103.6041].

[23] M. Sasaki and H. Tagoshi, "Analytic black hole perturbation approach to gravitational radiation," *Living Rev. Rel.* **6** (2003) 6, [gr-qc/0306120].

[24] P. Amaro-Seoane, J. R. Gair, M. Freitag, M. Coleman Miller, I. Mandel, C. J. Cutler, and S. Babak, "Astrophysics, detection and science applications of intermediate- and extreme mass-ratio inspirals," *Class. Quant. Grav.* **24** (2007) R113–R169, [astro-ph/0703495].

[25] L. Blanchet, "Gravitational Radiation from Post-Newtonian Sources and Inspiralling Compact Binaries," *Living Rev. Rel.* **17** (2014) 2, [arXiv:1310.1528].

[26] L. Barack, "Gravitational self force in extreme mass-ratio inspirals," *Class. Quant. Grav.* **26** (2009) 213001, [arXiv:0908.1664].

[27] E. Poisson, A. Pound, and I. Vega, "The Motion of point particles in curved spacetime," *Living Rev. Rel.* **14** (2011) 7, [arXiv:1102.0529].

[28] E. E. Flanagan and T. Hinderer, "Transient resonances in the inspirals of point particles into black holes," *Phys. Rev. Lett.* **109** (2012) 071102, [arXiv:1009.4923].

[29] A. Strominger and C. Vafa, "Microscopic origin of the Bekenstein-Hawking entropy," *Phys. Lett.* **B379** (1996) 99–104, [hep-th/9601029].

[30] J. M. Maldacena and A. Strominger, "Black hole grey body factors and d-brane spectroscopy," *Phys. Rev.* **D55** (1997) 861–870, [hep-th/9609026].

[31] J. M. Maldacena and A. Strominger, "Universal low-energy dynamics for rotating black holes," *Phys. Rev.* **D56** (1997) 4975–4983, [hep-th/9702015].

[32] J. M. Maldacena, "The Large N limit of superconformal field theories and supergravity," *Int. J. Theor. Phys.* **38** (1999) 1113–1133, [hep-th/9711200]. [Adv. Theor. Math. Phys.2,231(1998)].

[33] I. Bredberg, C. Keeler, V. Lysov, and A. Strominger, "Cargese Lectures on the Kerr/CFT Correspondence," *Nucl. Phys. Proc. Suppl.* **216** (2011) 194–210, [arXiv:1103.2355].

[34] G. Compere, "The Kerr/CFT correspondence and its extensions: a comprehensive review," *Living Rev. Rel.* **15** (2012) 11, [arXiv:1203.3561].

[35] J. D. Brown and M. Henneaux, "Central Charges in the Canonical Realization of Asymptotic Symmetries: An Example from Three-Dimensional Gravity," *Commun. Math. Phys.* **104** (1986) 207–226.

[36] A. P. Porfyriadis and F. Wilczek, "Effective Action, Boundary Conditions, and Virasoro Algebra for AdS_3," arXiv:1007.1031.

[37] Y. Matsuo, T. Tsukioka, and C.-M. Yoo, "Another Realization of Kerr/CFT Correspondence," *Nucl. Phys.* **B825** (2010) 231–241, [arXiv:0907.0303].

[38] Y. Matsuo, T. Tsukioka, and C.-M. Yoo, "Yet Another Realization of Kerr/CFT Correspondence," *Europhys. Lett.* **89** (2010) 60001, [arXiv:0907.4272].

[39] J. Rasmussen, "Isometry-preserving boundary conditions in the Kerr/CFT correspondence," *Int. J. Mod. Phys.* **A25** (2010) 1597–1613, [arXiv:0908.0184].

[40] D. M. Hofman and A. Strominger, "Chiral Scale and Conformal Invariance in 2D Quantum Field Theory," *Phys. Rev. Lett.* **107** (2011) 161601, [arXiv:1107.2917].

[41] S. El-Showk and M. Guica, "Kerr/CFT, dipole theories and nonrelativistic CFTs," *JHEP* **12** (2012) 009, [arXiv:1108.6091].

[42] W. Song and A. Strominger, "Warped AdS3/Dipole-CFT Duality," *JHEP* **05** (2012) 120, [arXiv:1109.0544].

[43] I. Bena, M. Guica, and W. Song, "Un-twisting the NHEK with spectral flows," *JHEP* **03** (2013) 028, [arXiv:1203.4227].

[44] S. Detournay, T. Hartman, and D. M. Hofman, "Warped Conformal Field Theory," *Phys. Rev.* **D86** (2012) 124018, [arXiv:1210.0539].

[45] M. Guica, "Decrypting the warped black strings," *JHEP* **11** (2013) 025, [arXiv:1305.7249].

[46] A. J. Amsel, G. T. Horowitz, D. Marolf, and M. M. Roberts, "No Dynamics in the Extremal Kerr Throat," *JHEP* **09** (2009) 044, [arXiv:0906.2376].

[47] D. E. Berenstein, R. Corrado, W. Fischler, and J. M. Maldacena, "The Operator product expansion for Wilson loops and surfaces in the large N limit," *Phys. Rev.* **D59** (1999) 105023, [hep-th/9809188].

[48] V. Balasubramanian, P. Kraus, A. E. Lawrence, and S. P. Trivedi, "Holographic probes of anti-de Sitter space-times," *Phys. Rev.* **D59** (1999) 104021, [hep-th/9808017].

[49] U. H. Danielsson, E. Keski-Vakkuri, and M. Kruczenski, "Vacua, propagators, and holographic probes in AdS / CFT," *JHEP* **01** (1999) 002, [hep-th/9812007].

[50] I. R. Klebanov and E. Witten, "AdS / CFT correspondence and symmetry breaking," *Nucl. Phys.* **B556** (1999) 89–114, [hep-th/9905104].

[51] I. Bredberg, T. Hartman, W. Song, and A. Strominger, "Black Hole Superradiance From Kerr/CFT," *JHEP* **04** (2010) 019, [arXiv:0907.3477].

[52] S. S. Gubser, "Absorption of photons and fermions by black holes in four-dimensions," *Phys. Rev.* **D56** (1997) 7854–7868, [hep-th/9706100].

[53] T. Azeyanagi, D. M. Hofman, W. Song, and A. Strominger, "The Spectrum of Strings on Warped $AdS_3 \times S^3$," *JHEP* **04** (2013) 078, [arXiv:1207.5050].

[54] G. Compère, W. Song, and A. Strominger, "Chiral Liouville Gravity," *JHEP* **05** (2013) 154, [arXiv:1303.2660].

[55] S. A. Teukolsky and W. H. Press, "Perturbations of a rotating black hole. III - Interaction of the hole with gravitational and electromagnet ic radiation," *Astrophys. J.* **193** (1974) 443–461.

[56] S. Chandrasekhar, *The Mathematical Theory of Black Holes*. Oxford University Press, New York, 1983.

[57] S. A. Teukolsky, "Rotating black holes - separable wave equations for gravitational and electromagnetic perturbations," *Phys. Rev. Lett.* **29** (1972) 1114–1118.

[58] S. A. Teukolsky, "Perturbations of a rotating black hole. 1. Fundamental equations for gravitational electromagnetic and neutrino field perturbations," *Astrophys. J.* **185** (1973) 635–647.

[59] P. L. Chrzanowski, "Vector Potential and Metric Perturbations of a Rotating Black Hole," *Phys. Rev.* **D11** (1975) 2042–2062.

[60] R. M. Wald, "Construction of Solutions of Gravitational, Electromagnetic, Or Other Perturbation Equations from Solutions of Decoupled Equations," *Phys. Rev. Lett.* **41** (1978) 203–206.

[61] O. J. C. Dias, H. S. Reall, and J. E. Santos, "Kerr-CFT and gravitational perturbations," *JHEP* **08** (2009) 101, [arXiv:0906.2380].

[62] T. Hartman, W. Song, and A. Strominger, "Holographic Derivation of Kerr-Newman Scattering Amplitudes for General Charge and Spin," *JHEP* **03** (2010) 118, [arXiv:0908.3909].

[63] S. L. Detweiler, "Black Holes and Gravitational Waves. I. Circular Orbits About a Rotating Hole," *Astrophys. J.* **225** (1978) 687–693.

[64] W. H. Press and S. A. Teukolsky, "Perturbations of a Rotating Black Hole. II. Dynamical Stability of the Kerr Metric," *Astrophys. J.* **185** (1973) 649–674.

[65] E. W. Leaver, "An Analytic representation for the quasi normal modes of Kerr black holes," *Proc. Roy. Soc. Lond.* **A402** (1985) 285–298.

[66] E. Berti, V. Cardoso, and M. Casals, "Eigenvalues and eigenfunctions of spin-weighted spheroidal harmonics in four and higher dimensions," *Phys. Rev.* **D73** (2006) 024013, [gr-qc/0511111]. [Erratum: Phys. Rev.D73,109902(2006)].

[67] A. Le Tiec, "The overlap of numerical relativity, perturbation theory and post-Newtonian theory in the binary black hole problem," *International Journal of Modern Physics D* **23** (Sept., 2014) 30022, [arXiv:1408.5505].

[68] A. Buonanno and T. Damour, "Effective one-body approach to general relativistic two-body dynamics," *Phys. Rev. D* **59** (Apr., 1999) 084006, [gr-qc/9811091].

[69] V. E. Hubeny, "Overcharging a black hole and cosmic censorship," *Phys. Rev. D* **59** (Mar., 1999) 064013, [gr-qc/9808043].

[70] T. Jacobson and T. P. Sotiriou, "Overspinning a Black Hole with a Test Body," *Physical Review Letters* **103** (Oct., 2009) 141101, [arXiv:0907.4146].

[71] A. Ori and K. S. Thorne, "Transition from inspiral to plunge for a compact body in a circular equatorial orbit around a massive, spinning black hole," *Phys. Rev. D* **62** (Dec., 2000) 124022, [gr-qc/0003032].

[72] M. Kesden, "Transition from adiabatic inspiral to plunge into a spinning black hole," *Phys. Rev. D* **83** (May, 2011) 104011, [arXiv:1101.3749].

[73] E. Barausse, V. Cardoso, and G. Khanna, "Test bodies and naked singularities: Is the self-force the cosmic censor?," *Phys. Rev. Lett.* **105** (2010) 261102, [arXiv:1008.5159].

[74] E. Barausse, V. Cardoso, and G. Khanna, "Testing the cosmic censorship conjecture with point particles: The effect of radiation reaction and the self-force," *Phys. Rev. D* **84** (Nov., 2011) 104006, [arXiv:1106.1692].

[75] M. Colleoni and L. Barack, "Overspinning a Kerr black hole: The effect of the self-force," *Phys. Rev. D* **91** (May, 2015) 104024, [arXiv:1501.07330].

[76] P. L. Chrzanowski, "Applications of metric perturbations of a rotating black hole - Distortion of the event horizon," *Phys. Rev. D* **13** (Feb., 1976) 806–818.

[77] H. Yang, F. Zhang, A. Zimmerman, D. A. Nichols, E. Berti, and Y. Chen, "Branching of quasinormal modes for nearly extremal Kerr black holes," *Phys. Rev. D* **87** (Feb., 2013) 041502, [arXiv:1212.3271].

[78] H. Yang, A. Zimmerman, A. Zenginoğlu, F. Zhang, E. Berti, and Y. Chen, "Quasinormal modes of nearly extremal Kerr spacetimes: Spectrum bifurcation and power-law ringdown," *Phys. Rev. D* **88** (Aug., 2013) 044047, [arXiv:1307.8086].

[79] A. A. Starobinskij, "Amplification of waves reflected from a rotating "black hole".," *Zhurnal Eksperimentalnoi i Teoreticheskoi Fiziki* **64** (1973) 48–57.

[80] A. A. Starobinskij and S. M. Churilov, "Amplification of electromagnetic and gravitational waves scattered by a rotating black hole.," *Zhurnal Eksperimentalnoi i Teoreticheskoi Fiziki* **65** (1973) 3–11.

[81] J. M. Bardeen, W. H. Press, and S. A. Teukolsky, "Rotating Black Holes: Locally Nonrotating Frames, Energy Extraction, and Scalar Synchrotron Radiation," *Astrophys. J.* **178** (Dec., 1972) 347–370.

[82] N. Warburton and L. Barack, "Self force on a scalar charge in Kerr spacetime: circular equatorial orbits," *Phys.Rev.* **D81** (2010) 084039, [arXiv:1003.1860].

[83] N. Warburton. http://www.nielswarburton.net.

[84] M. Sasaki and T. Nakamura, "Gravitational Radiation From a Kerr Black Hole. 1. Formulation and a Method for Numerical Analysis," *Prog.Theor.Phys.* **67** (1982) 1788.

[85] A. G. Shah, J. L. Friedman, and T. S. Keidl, "EMRI corrections to the angular velocity and redshift factor of a mass in circular orbit about a Kerr black hole," *Phys.Rev.* **D86** (2012) 084059, [arXiv:1207.5595].

[86] W. Throwe, S. A. Hughes, and S. Drasco. in preparation.

[87] J. M. Maldacena, J. Michelson, and A. Strominger, "Anti-de Sitter fragmentation," *JHEP* **02** (1999) 011, [hep-th/9812073].

[88] M. Spradlin and A. Strominger, "Vacuum states for AdS(2) black holes," *JHEP* **11** (1999) 021, [hep-th/9904143].

[89] A. J. Amsel, G. T. Horowitz, D. Marolf, and M. M. Roberts, "No Dynamics in the Extremal Kerr Throat," *JHEP* **09** (2009) 044, [arXiv:0906.2376].

[90] O. J. C. Dias, H. S. Reall, and J. E. Santos, "Kerr-CFT and gravitational perturbations," *JHEP* **08** (2009) 101, [arXiv:0906.2380].

[91] S. L. Detweiler, "Black Holes And Gravitational Waves. III. The Resonant Frequencies Of Rotating Holes," *Astrophys. J.* **239** (1980) 292–295.

[92] S. Hod, "Slow relaxation of rapidly rotating black holes," *Phys. Rev.* **D78** (2008) 084035, [arXiv:0811.3806].

[93] T. Hartman, W. Song, and A. Strominger, "Holographic Derivation of Kerr-Newman Scattering Amplitudes for General Charge and Spin," *JHEP* **03** (2010) 118, [arXiv:0908.3909].

[94] A. Taracchini, A. Buonanno, G. Khanna, and S. A. Hughes, "Small mass plunging into a Kerr black hole: Anatomy of the inspiral-merger-ringdown waveforms," *Phys. Rev.* **D90** (2014), no. 8 084025, [arXiv:1404.1819].

[95] A. Nagar, E. Harms, S. Bernuzzi, and A. Zenginoğlu, "The antikick strikes back: recoil velocities for nearly-extremal binary black hole mergers in the test-mass limit," *Phys. Rev.* **D90** (2014), no. 12 124086, [arXiv:1407.5033].

[96] A. Lupsasca, M. J. Rodriguez, and A. Strominger, "Force-Free Electrodynamics around Extreme Kerr Black Holes," *JHEP* **12** (2014) 185, [arXiv:1406.4133].

[97] F. Zhang, H. Yang, and L. Lehner, "Towards an understanding of the force-free magnetosphere of rapidly spinning black holes," *Phys. Rev.* **D90** (2014), no. 12 124009, [arXiv:1409.0345].

[98] A. Lupsasca and M. J. Rodriguez, "Exact Solutions for Extreme Black Hole Magnetospheres," *JHEP* **07** (2015) 090, [arXiv:1412.4124].

[99] L. Barack and C. Cutler, "LISA capture sources: Approximate waveforms, signal-to-noise ratios, and parameter estimation accuracy," *Phys. Rev.* **D69** (2004) 082005, [gr-qc/0310125].

[100] R. Geroch, "Limits of spacetimes," *Communications in Mathematical Physics* **13** (Sept., 1969) 180–193.

[101] T. Jacobson, "Where is the extremal Kerr ISCO?," *Classical and Quantum Gravity* **28** (Sept., 2011) 187001, [arXiv:1107.5081].

Appendix A

Near-Horizon Limits and Symmetries

In this appendix we review the NHEK limits and how their enhanced symmetry naturally assigns a conformal weight h to certain solutions of the wave equation. While all of this material has appeared in some form in the literature, the references vary in their choices of notation, coordinate patch, and symmetry algebra basis. We present the relevant results here with choices suited to our calculation.

A.1 Far limit

A convenient form for the Kerr exterior metric in BL coordinates is

$$ds^2 = -\frac{\Delta}{\rho^2}\left(dt - a\sin^2\theta d\phi\right)^2 + \frac{\sin^2\theta}{\rho^2}\left((r^2+a^2)d\phi - adt\right)^2 + \frac{\rho^2}{\Delta}dr^2 + \rho^2 d\theta^2, \tag{A.1}$$

where $\Delta = r^2 - 2Mr + a^2$ and $\rho^2 = r^2 + a^2\cos^2\theta$. Setting $a = M$ (equivalently $\epsilon = 0$) gives extremal Kerr. More formally, we could introduce an auxiliary parameter δ by

$$\epsilon = \sqrt{1 - (a/M)^2} = \bar{\epsilon}\delta \tag{A.2}$$

for some fixed $\bar{\epsilon}$. Letting $\delta \to 0$ at fixed BL coordinates produces extremal Kerr. In the language of Geroch [100], we use the BL coordinates to identify metrics at different values of δ.

A.2 Near-horizon limit

We are free, however, to identify the metrics differently. If we still use (A.2) but instead hold fixed

$$\bar{x} = \frac{x}{\delta} = \frac{r - r_+}{r_+}\delta^{-1}, \quad \bar{t} = \frac{t}{2M}\delta, \quad \bar{\phi} = \phi - \frac{t}{2M}, \tag{A.3}$$

then letting $\delta \to 0$ gives

$$\begin{aligned} ds^2 = 2M^2\Gamma(\theta)\Big\{ &- \bar{x}(\bar{x} + 2\bar{\epsilon})d\bar{t}^2 + \frac{d\bar{x}^2}{\bar{x}(\bar{x} + 2\bar{\epsilon})} \\ &+ d\theta^2 + \Lambda^2(\theta)[d\bar{\phi} + (\bar{x} + \bar{\epsilon})d\bar{t}]^2\Big\}, \end{aligned} \tag{A.4}$$

where $\Gamma(\theta) = (1 + \cos^2\theta)/2$ and $\Lambda(\theta) = 2\sin\theta/(1 + \cos^2\theta)$. This is the "near-NHEK" metric [51]. This limit is expected to be useful for near-extremal, near-horizon physics. It corresponds to the lowest "crack" in the throats diagram, Fig. 3.2.

It is also the near-horizon metric in the more pedestrian sense that it agrees with near-extremal Kerr near the horizon. That is to say, Eq. (A.4) may also be obtained by using the coordinates (A.3) with $\delta = 1$ and using $x \ll 1$ in the metric components,

keeping to leading order in each component. The redefinition of the ϕ coordinate in (A.3) is essential for the resulting metric to be non-singular, making these "good" near-horizon coordinates.

Consider a scalar field Φ in non-extremal Kerr ($\epsilon > 0$) with the usual harmonic t and ϕ dependence. Expressing in the scaled coordinates (A.3) gives

$$\Phi \sim e^{-i\omega t} e^{im\phi} = e^{-i\bar{\omega}\bar{t}} e^{im\bar{\phi}}, \tag{A.5}$$

where we define

$$\bar{\omega} = \frac{2M\omega - m}{\delta}. \tag{A.6}$$

If we have a family of scalar fields, one for each ϵ, then for this family to have a good near-horizon limit ω must approach $m/(2M)$ linearly with ϵ. (Recall that $1/(2M)$ is the extremal limit of the horizon angular velocity.) For a circular orbit of angular velocity Ω we have $\omega = m\Omega$. Thus for the associated mode functions to have a good near-horizon limit, Ω must approach the extremal horizon frequency linearly with ϵ.

For the ISCO, $\Omega - 1/(2M) \sim \epsilon^{2/3}$ and hence $\bar{\omega} \sim \delta^{-1/3}$. The n defined in the text (3.16) corresponds to $\bar{\omega}/\bar{\epsilon}$ with $\delta = 1$, explaining $n \sim \epsilon^{-1/3}$ as $\epsilon \to 0$ (3.24). The coordinate position of the ISCO also diverges in this limit, since $x_0 \sim \epsilon^{2/3}$ and hence $\bar{x} \sim \delta^{-1/3}$. Thus from the near-NHEK point of view, the ISCO orbits infinitely far away and infinitely fast. This is the physical origin of the infinitely oscillating phases and the need for large-n asymptotics.

A.3 Intermediate (ISCO) limit

In order to avoid these difficulties one could instead define an alternate limit by keeping (A.2) but replacing (A.3) with

$$\tilde{x} = \frac{r - r_+}{r_+}\delta^{-2/3}, \quad \tilde{t} = \frac{t}{2M}\delta^{2/3}, \quad \tilde{\phi} = \phi - \frac{t}{2M}, \tag{A.7}$$

which will keep the ISCO radius and frequency finite. In this limit the metric becomes

$$ds^2 = 2M^2\Gamma\left\{ -\tilde{x}^2 d\tilde{t}^2 + \frac{d\tilde{x}^2}{\tilde{x}^2} + d\theta^2 + \Lambda^2[d\tilde{\phi} + \tilde{x}d\tilde{t}]^2 \right\}, \tag{A.8}$$

where Γ and Λ are given below (A.4). This metric agrees with the near metric (A.4) when $\bar{x} \gg \bar{\epsilon}$ and with the far metric (extremal Kerr) when $x \ll 1$. It too can be derived the pedestrian way, that is to say, Eq. (A.8) may also be obtained by using the coordinates (A.3) with $\delta = 1$ and using $\epsilon \ll x \ll 1$ in the metric components, keeping to leading order in each component. The ISCO limit is thus intermediate between the near and far regions, corresponding to the middle region in the throats diagram, Fig. 3.2.

Eq. (A.8) is a non-singular spacetime; in fact it is *diffeomorphic* to (A.4). Eq. (A.8) is generally called "NHEK" or"Poincare NHEK" and it is the form originally discovered in [10] as a limit of precisely extremal Kerr. This metric also approximates the near-horizon region of precisely extremal black hole in the pedestrian sense. Poincare NHEK and near-NHEK cover different patches of the maximally extended spacetime.

Despite its adaptation to the ISCO, the limit (A.7) does not appear to be useful in calculating the radiation from a particle orbiting there. Since the metric does not agree with near-extreme Kerr at the horizon or at infinity, it cannot be used to impose boundary conditions at either place. We have found it more useful to include the ISCO

region in our "near" region in the main body for the purposes of calculation, defined as $x \ll 1$ without deciding between $x \sim \epsilon$ (the near-horizon region) and $x \sim \epsilon^{2/3}$ (the intermediate region). Note that the ISCO is *not* in our region of overlap, since that region has $x \gg \epsilon^{2/3}$ (as well as $x \ll 1$). Correspondingly, the wave equation associated with the ISCO limit, that is the NHEK wave equation, does not appear explicitly in our calculation. Note however the connection to the extremal calculation of Chapter 2, discussed in the Introduction and in Section 3.3.10 of Chapter 3, which involved solving explicitly the NHEK wave equation.

A.4 Symmetry Group and Conformal Weights

The NHEK spacetime has an enhanced $SL(2,R) \times U(1)$ isometry group. The explicit form of the Killing fields depends on the coordinates and the choice of basis. We will be agnostic to both, and simply name the Killing fields H_0, $H_\pm$ and W_0, demanding only the $SL(2,R)$ commutation relations $[H_0, H_\pm] = \mp H_\pm$, $[H_+, H_-] = 2H_0$ and the $U(1)$ generator W_0 commuting with everything.

For any complex number h and integer m, an infinite-dimensional representation $\{\psi_{h,m,k}\}$ with $k \geq 0$ may be constructed as follows. The member $\psi_{h,m,0}$ should satisfy the highest-weight condition,

$$\mathcal{L}_{H_+}\psi_{h,m,0} = 0 \tag{A.9a}$$

$$\mathcal{L}_{H_0}\psi_{h,m,0} = h\psi, \tag{A.9b}$$

together with $\mathcal{L}_{W_0}\psi_{h,m,0} = im\psi$. The remaining members of the representation are

formed by repeated application of H_-,

$$\psi_{h,m,k} = (\mathcal{L}_{H_-})^k \psi_{h,m,0}. \tag{A.10}$$

Here $\mathcal{L}$ is the Lie derivative. Since $SL(2,R)$ is not compact, this tower does not terminate and the representation is infinite-dimensional.

Solutions to the wave equation may be organized in representations of the isometry group. For simplicity, we work in the case of a scalar field Φ and drop circumflexes in order to be agnostic between the coordinates (A.4) and (A.8). Adopting the decomposition

$$\Phi = Q(x,t)S(\theta)e^{im\phi}, \tag{A.11}$$

with S satisfying the angular equation (3.22), the wave equation implies:

$$\left[\mathcal{L}_{H_0}(\mathcal{L}_{H_0} - 1) - \mathcal{L}_{H_-}\mathcal{L}_{H_+}\right]\Phi = (K - 2m^2)\Phi. \tag{A.12}$$

The operator on the LHS is the Casimir of $SL(2,R)$; thus Φ is an eigenstate of the Casimir with eigenvalue $K - 2m^2$. If Φ is also highest-weight (A.9) then this becomes

$$h(h-1) + 2m^2 - K = 0, \tag{A.13}$$

which is solved by

$$h = \frac{1}{2} \pm \sqrt{K - 2m^2 + \frac{1}{4}}. \tag{A.14}$$

(In the text we define h to be the plus branch of (A.14). The minus branch appears as $1 - h$ in (e.g.) (3.33).) The highest-weight condition thus replaces the second-order differential equation (A.12) with two first-order equations (A.9a) and (A.9b). Once the highest-weight solution is found by solving these equations, further solutions

arise from its descendants via (A.10). In this way one constructs an infinite tower of solutions for each $\{K, m\}$ angular mode. It is generally believed that these comprise a complete basis for solutions of the wave equation. Our near equation (3.31) is the radial near-NHEK wave equation for the ansatz $\Phi = R(x)e^{-i(n-m)\epsilon t}S(\theta)e^{im\phi}$. Therefore, the near solutions $R^{\text{near}}(x)e^{-i(n-m)\epsilon t}S(\theta)e^{im\phi}$ must be expressible as linear combinations of the members of the highest weight representations labelled by (A.14).

A.5 Where is the extremal Kerr ISCO?

Having introduced three inequivalent limits and discussed their properties, we conclude with a discussion of the "location" of the extremal Kerr ISCO, an innocent question with an amusingly complicated answer.

The far limit produces the extremal Kerr exterior and the ISCO exits the domain, approaching $r = M$ ($x = 0$). Correspondingly, every equatorial (prograde) circular orbit in extremal Kerr is stable. If we complete the domain by including the horizon (e.g. taking the limit at fixed Doran coordinate), then the ISCO approaches the horizon generators [101].

The near-horizon limit produces near-NHEK (A.4) and the ISCO also exits the domain, approaching $\bar{x}_0 \to \infty$. Correspondingly, there are no stable circular orbits in near-NHEK [3].

The intermediate limit produces NHEK (A.8) and ISCO achieves a finite coordinate value $\tilde{x}_0 = 2^{1/3}$. Is this, then, the location of the ISCO? No: redefining (A.7) by $\tilde{x} \to c\tilde{x}$ and $\tilde{t} \to \tilde{t}/c$ for a number c, we produce the same limiting metric (A.8) but find that the ISCO instead approached $\tilde{x}_0 = c \times 2^{1/3}$. We can therefore put the ISCO

anywhere we want. Within (A.8) itself this can be seen as the fact that $\tilde{x} \to c\tilde{x}$ and $\tilde{t} \to \tilde{t}/c$ is a symmetry—the "dilation" member of the enhanced $SL(2,R)$ symmetry group. This symmetry maps circular orbits to circular orbits, making all circular orbits physically equivalent within NHEK.[1] In particular, they are all marginally stable [3], like the ISCO.

Where is the extremal Kerr ISCO? It's on the horizon in the far limit, at infinity in the near-horizon limit, and in the intermediate limit, it is everywhere!

[1] The position of the ISCO gains meaning only through matching to the external region (far limit), which breaks the $SL(2,R)$ symmetries.

Appendix B

Equatorial geodesic equations in NHEK-like metric

Consider a NHEK-like metric:

$$ds^2 = 2M^2\Gamma(\theta)\left[-N^2dt^2 + \frac{dr^2}{N^2} + d\theta^2 + \Lambda(\theta)^2(d\phi + N^\phi dt)^2\right], \tag{B.1}$$

where N^2, N^ϕ are functions of r only. Confining ourselves to the equatorial plane, $\theta = \pi/2$, the two constants of motion associated with the Killing fields ∂_t and ∂_ϕ, namely the energy and angular momentum (per unit rest mass) E and L, suffice to describe the geodesics. The timelike equatorial geodesics, parameterized by proper time τ, are given by:

$$\frac{dt}{d\tau} = \frac{E + LN^\phi}{M^2N^2}, \tag{B.2}$$

$$\frac{d\phi}{d\tau} = \frac{L}{4M^2} - N^\phi \cdot \frac{E + LN^\phi}{M^2N^2}, \tag{B.3}$$

and for the radial motion:

$$\Sigma^2\left(\frac{dr}{d\tau}\right)^2 = V(r), \tag{B.4}$$

with $\Sigma^2 = M^2/N^2$ and,

$$V(r) = \frac{4E^2 + 8ELN^\phi - 4M^2N^2 + 4L^2(N^\phi)^2 - L^2N^2}{4M^2N^2}\,. \tag{B.5}$$

For a circular orbit at some radius r we need $V(r) = 0$ and $V'(r) = 0$. These equations can be solved to give E and L in terms of the circle radius but circular orbits don't necessarily exist for all values of r. Moreover, not all circular orbits are stable. Stability requires $V''(r) \leq 0$.

B.1 near-NHEK

For near-NHEK:

$$N^2 = r(r+2\kappa)\,, \quad N^\phi = r + \kappa\,. \tag{B.6}$$

Circular orbits, satisfying $V(r) = 0$ and $V'(r) = 0$, exist for $3r^2 + 6\kappa r - \kappa^2 > 0$ and have:

$$E = \mp\frac{2M\kappa^2}{\sqrt{3r^2 + 6\kappa r - \kappa^2}}\,, \tag{B.7}$$

$$L = \pm\frac{2M(r+\kappa)}{\sqrt{3r^2 + 6\kappa r - \kappa^2}}\,, \tag{B.8}$$

where the upper (lower) sign refers to direct (retrograde) orbits. Among those, stable ones should also have $V''(r) \leq 0$ which is equivalent to:

$$\frac{8\kappa^2}{r(r+2\kappa)(3r^2 + 6\kappa r - \kappa^2)} \leq 0\,. \tag{B.9}$$

Thus in near-NHEK ISCO is at $r = \infty$. Since ISCO is a marginally stable orbit, we choose the plunging orbit with E and L those of ISCO (direct orbit):

$$E = 0\,, \qquad L = \frac{2M}{\sqrt{3}}\,. \tag{B.10}$$

Plugging these values into equations (B.2–B.4) we can integrate them to find the expressions for the plunge trajectory in near-NHEK:

$$t(r) = \frac{1}{2\kappa}\ln\frac{1}{r(r+2\kappa)} + t_0\,, \tag{B.11}$$

$$\phi(r) = \frac{3r}{4\kappa} + \frac{1}{2}\ln\frac{r}{r+2\kappa} + \phi_0\,. \tag{B.12}$$

B.2 NHEK

For NHEK:

$$N^2 = r^2\,, \quad N^\phi = r\,. \tag{B.13}$$

Circular orbits, satisfying $V(r) = 0$ and $V'(r) = 0$, exist at all $r > 0$ and they all have:

$$E = 0\,, \tag{B.14}$$

$$L = \pm\frac{2M}{\sqrt{3}}\,. \tag{B.15}$$

Moreover, all of them are marginally stable with $V''(r) = 0$. So there is no single *innermost* stable circular orbit (ISCO) in NHEK. Since these are marginally stable orbits the solution to the equatorial geodesic equations with $E = 0, L = 2M/\sqrt{3}$ may be called a (direct) plunge trajectory in NHEK. Plugging these values into equations (B.2–B.4) we can integrate them to find the expressions for the plunge trajectory in NHEK:

$$r(t) = r_0\,, \tag{B.16}$$

$$\phi(t) = -\frac{3}{4}r_0\,t + \phi_0\,. \tag{B.17}$$